Independent optical excitation of distinct neural populations

Nathan C Klapoetke[1–5], Yasunobu Murata[4,5], Sung Soo Kim[6], Stefan R Pulver[6], Amanda Birdsey-Benson[4,5], Yong Ku Cho[1–5], Tania K Morimoto[1–5], Amy S Chuong[1–5], Eric J Carpenter[7], Zhijian Tian[8], Jun Wang[8], Yinlong Xie[8], Zhixiang Yan[8], Yong Zhang[8], Brian Y Chow[9], Barbara Surek[10], Michael Melkonian[10], Vivek Jayaraman[6], Martha Constantine-Paton[4,5], Gane Ka-Shu Wong[7,8,11] & Edward S Boyden[1–5]

Optogenetic tools enable examination of how specific cell types contribute to brain circuit functions. A long-standing question is whether it is possible to independently activate two distinct neural populations in mammalian brain tissue. Such a capability would enable the study of how different synapses or pathways interact to encode information in the brain. Here we describe two channelrhodopsins, Chronos and Chrimson, discovered through sequencing and physiological characterization of opsins from over 100 species of alga. Chrimson's excitation spectrum is red shifted by 45 nm relative to previous channelrhodopsins and can enable experiments in which red light is preferred. We show minimal visual system–mediated behavioral interference when using the variant CsChrimson in neurobehavioral studies in *Drosophila melanogaster*. Chronos has faster kinetics than previous channelrhodopsins yet is effectively more light sensitive. Together these two reagents enable two-color activation of neural spiking and downstream synaptic transmission in independent neural populations without detectable cross-talk in mouse brain slice.

Microbial opsins, which are light-driven ion pumps and light-gated ion channels that can be genetically expressed in excitable cells, enable the optical activation or inhibition of the electrical activity of defined neuron types, axonal pathways or brain regions with millisecond resolution[1–6]. There exists an unmet need to independently drive pairs of light-driven ion channels with different colors of light, which would enable the independent activation of different cell populations. Many groups have used channelrhodopsins with peak wavelength sensitivity to green light in conjunction with channelrhodopsins with peak wavelength sensitivity to blue light to achieve differential spiking with yellow light[7–10], but residual neural spiking cross-talk in response to blue light stimulation remains due to the intrinsic blue absorption by the retinal chromophore[11,12]. This fundamental limitation means it is currently not possible to achieve robust, temporally precise independent two-color spiking using a red-shifted channelrhodopsin alongside channelrhodopsin-2 (ChR2) in mammalian brain tissue. Previous efforts to further red-shift opsins and reduce blue light sensitivity through mutagenesis have empirically proven difficult, with spectra remaining little red shifted beyond that of the first reported green-peaked channelrhodopsin, VChR1 (refs. 9,13,14). Similarly, efforts to further increase the blue light sensitivity of ChR2 have resulted in much slower channelrhodopsins[15–17], which elicit low-temporal-precision spiking in response to light pulses of up to 1 s or longer.

One potential strategy for achieving independent two-color excitation is engineering differences in blue light sensitivity between blue and red light–drivable channelrhodopsins. Then a low blue irradiance could drive precisely timed spikes with the blue light–drivable channelrhodopsin while eliciting only subthreshold depolarizations (not causing synaptic release) in neurons expressing the red light–drivable channelrhodopsin. To achieve these goals, we turned to the natural world, performing *de novo* transcriptome sequencing of 127 species of alga.

Chronos is a new blue and green light–drivable channelrhodopsin with kinetics faster than those of previous channelrhodopsins as well as high light sensitivity. Chrimson is a new red light–drivable channelrhodopsin with spectra that are red shifted 45 nm more than those of previous channelrhodopsins. Together, Chronos and Chrimson allow independent two-color spike driving of, and synaptic release from, distinct neural populations in mouse brain slice. In addition, Chronos represents an excellent general-use channelrhodopsin. Chrimson may enable temporally precise experiments requiring red light, such as deep tissue

[1]The MIT Media Laboratory, Synthetic Neurobiology Group, Massachusetts Institute of Technology (MIT), Cambridge, Massachusetts, USA. [2]Department of Biological Engineering, MIT, Cambridge, Massachusetts, USA. [3]MIT Center for Neurobiological Engineering, MIT, Cambridge, Massachusetts, USA. [4]Department of Brain and Cognitive Sciences, MIT, Cambridge, Massachusetts, USA. [5]MIT McGovern Institute for Brain Research, MIT, Cambridge, Massachusetts, USA. [6]Janelia Farm Research Campus, Howard Hughes Medical Institute, Ashburn, Virginia, USA. [7]Department of Biological Sciences, University of Alberta, Edmonton, Alberta, Canada. [8]Beijing Genomics Institute-Shenzhen, Shenzhen, China. [9]Department of Bioengineering, University of Pennsylvania, Philadelphia, Pennsylvania, USA. [10]Institute of Botany, Cologne Biocenter, University of Cologne, Cologne, Germany. [11]Department of Medicine, University of Alberta, Edmonton, Alberta, Canada. Correspondence should be addressed to E.S.B. (esb@media.mit.edu) or G.K.-S.W. (gane@ualberta.ca).

RECEIVED 23 SEPTEMBER 2013; ACCEPTED 10 JANUARY 2014; PUBLISHED ONLINE 9 FEBRUARY 2014; CORRECTED AFTER PRINT 28 AUGUST 2014; ADDENDUM PUBLISHED AFTER PRINT 28 AUGUST 2014; DOI:10.1038/NMETH.2836

targeting, or scenarios in which blue light is visually distracting. To the latter end, we demonstrate brain stimulation through the cuticle of *Drosophila* and reduction in visual system–triggered responses during optogenetic experiments. These tools may also serve as protein backbones for building future optogenetic tools with novel capabilities.

RESULTS

Discovering novel channelrhodopsins via *de novo* sequencing

In recent years, a number of channelrhodopsins have been engineered for neuroscientific applications[18], derived from four channelrhodopsin genes from *Chlamydomonas reinhardtii* or *Volvox carteri*. However, all known natural channelrhodopsins have blue-green (430- to 550-nm) spectral peaks[13,14,18,19], and engineered red-shifted channelrhodopsins such as C1V1 (ref. 9) and ReaChR[14] have peak wavelength sensitivity to green light (~545 nm) and a similar spectrum to VChR1 (ref. 7). Furthermore, existing channelrhodopsins exhibit an inverse relationship between two desired properties: high light sensitivity and fast kinetics[18]. We therefore sought to overcome these limitations by exploring the genetic diversity of natural channelrhodopsins.

We *de novo*–sequenced 127 algal transcriptomes[20] and identified 61 channelrhodopsin homologs, which we subsequently synthesized and screened for photocurrents in HEK293 cells via whole-cell patch clamp (**Supplementary Figs. 1–4** and **Supplementary Table 1**). Of these, we selected opsins with novel characteristics for further characterization in cultured neurons (**Fig. 1** and **Supplementary Table 2**), focusing primarily on photocurrent, wavelength sensitivity, kinetics and trafficking (**Fig. 1** and **Supplementary Figs. 5–9**). To avoid selection bias, we cotransfected all opsins into neurons with a secondary tdTomato plasmid, and we selected cells solely according to the presence of cytosolic tdTomato expression (**Supplementary Fig. 5a**,**b**). This unbiased selection method was applied throughout the paper in all culture experiments unless otherwise indicated.

We assessed wavelength sensitivity and photocurrent amplitude, using ChR2 for blue (470 nm) comparison and $C1V1_{TT}$ (ref. 9) for green (530 nm) and far-red (660 nm) comparison (**Fig. 1a–d**). Of the 20 opsins screened in neurons, we found 4 previously unknown channelrhodopsins, one each from the species *Chloromonas oogama* (CoChR), *Chloromonas subdivisa* (CsChR), *Stigeoclonium helveticum* (ShChR) and *Scherffelia dubia* (SdChR) that bore either significantly higher blue photocurrents than ChR2 ($P < 0.001$; ANOVA with Dunnett's *post hoc* test used for all multiway comparisons; **Fig. 1c**) or significantly higher green photocurrents than $C1V1_{TT}$ ($P < 0.001$; **Fig. 1b**). Additionally, we discovered the first reported yellow-peaked channelrhodopsin, CnChR1 from the species *Chlamydomonas noctigama*. CnChR1 had 660-nm far-red light photocurrents of 674 ± 120 pA ($n = 11$ cells; values throughout are mean ± s.e.m.), which are significantly higher (~30×, $P < 0.0001$; **Fig. 1a**,**d**) than those of $C1V1_{TT}$. Owing to its spectral sensitivity, we nicknamed this molecule 'Chrimson'. With a spectral peak at 590 nm, Chrimson is 45 nm more red shifted than previously known channelrhodopsins (**Fig. 1e** and **Supplementary Figs. 5d**,**e** and **9**).

Kinetic parameters and spiking performance

The ability to optically evoke spikes necessitates that channelrhodopsins possess not only photocurrents sufficient to depolarize the neuron cell membrane above its spike threshold, but also on-, off- and recovery kinetics fast enough to precisely control spike timing and fidelity[18,21]. Previously published green and red light–drivable channelrhodopsins have relatively slow off-kinetics, which limits their utility for high-frequency neural activation[14,18]. We characterized the kinetic properties of opsins with green photocurrents comparable to or higher than those of $C1V1_{TT}$ and found that only CsChR and ShChR had faster turn-on, turn-off and recovery kinetics (**Fig. 1f–h**). With a turn-on of 2.3 ± 0.3 ms ($n = 8$ cells) and a turn-off of 3.6 ± 0.2 ms ($n = 7$ cells), the *S. helveticum* channelrhodopsin ShChR possesses the fastest reported kinetics to date (**Supplementary Fig. 3**): we therefore nicknamed this molecule 'Chronos'.

We assessed Chronos's green light (530-nm) spiking fidelities at various irradiances and frequencies in cultured neurons (**Fig. 2a–c** and **Supplementary Figs. 10** and **11**). As expected from its fast kinetic properties, Chronos-mediated optical spiking replicated electrically driven spiking between 5 and 60 Hz (**Supplementary Fig. 11**). In contrast, CsChR reliably drove spikes only up to 20 Hz, and $C1V1_{TT}$ could not reliably drive spikes above 10 Hz even at the highest expression level (**Supplementary Figs. 10** and **11**). It has previously been noted that slow off-kinetics or poor recovery kinetics of channelrhodopsins can cause depolarization block or reduce photocurrents over sustained pulse trains[18]. Consistent with this observation, the spike failures we observed at high frequencies for CsChR and $C1V1_{TT}$ primarily occurred later in the pulse train (**Supplementary Fig. 10e**).

We next examined red light (625-nm)-evoked spiking fidelities. Consistent with the earlier photocurrent screening, Chrimson was the only opsin screened capable of red light–driven spiking with 5-ms pulses (**Fig. 2d**): these irradiances and pulse widths resulted in Chronos depolarizations of less than 1.5 mV (**Supplementary Fig. 12g**). However, Chrimson's slow kinetics of current decay after the cessation of light, or τ_{off}, of 21.4 ± 1.1 ms ($n = 11$ cells), in conjunction with its poor recovery kinetics, caused depolarization block and channelrhodopsin inactivation at frequencies exceeding 10 Hz (**Fig. 2e** and **Supplementary Fig. 12a–d**). We therefore optimized these parameters via mutagenesis, and we identified the K176R mutant, denoted as ChrimsonR, which sped up the off-kinetics to 15.8 ± 0.4 ms ($n = 5$ cells) without altering the red-shifted action spectrum (**Fig. 2f** and **Supplementary Fig. 12e**,**f**). This kinetics improvement enabled fast, reliable red light–driven spiking at frequencies of at least 20 Hz in both cultured neurons and acute cortical slice (**Fig. 2e** and **Supplementary Fig. 13**), comparable to the blue light spiking performance of the commonly used ChR2(H134R)[18,22]. We additionally found ChrimsonR to be capable of reliably eliciting spikes in cortical slice using >20-ms pulses of far-red light (735 nm) (**Supplementary Fig. 13**), which may be useful for *in vivo* scenarios in which deep-tissue light penetration, or lack of visual drive, is desired by the experimenter.

Use of CsChrimson in *Drosophila*

Although optogenetic tools have become widely used in mammalian behavioral experiments, such tools have found more limited use in *Drosophila* experiments[23–27], possibly owing to strong innate behavioral artifacts induced by stimulation light reaching photosensitive regions[28] and poor cuticle penetration of blue light[29]. Optogenetics has therefore typically been used (i) in constrained circumstances in which light is delivered to

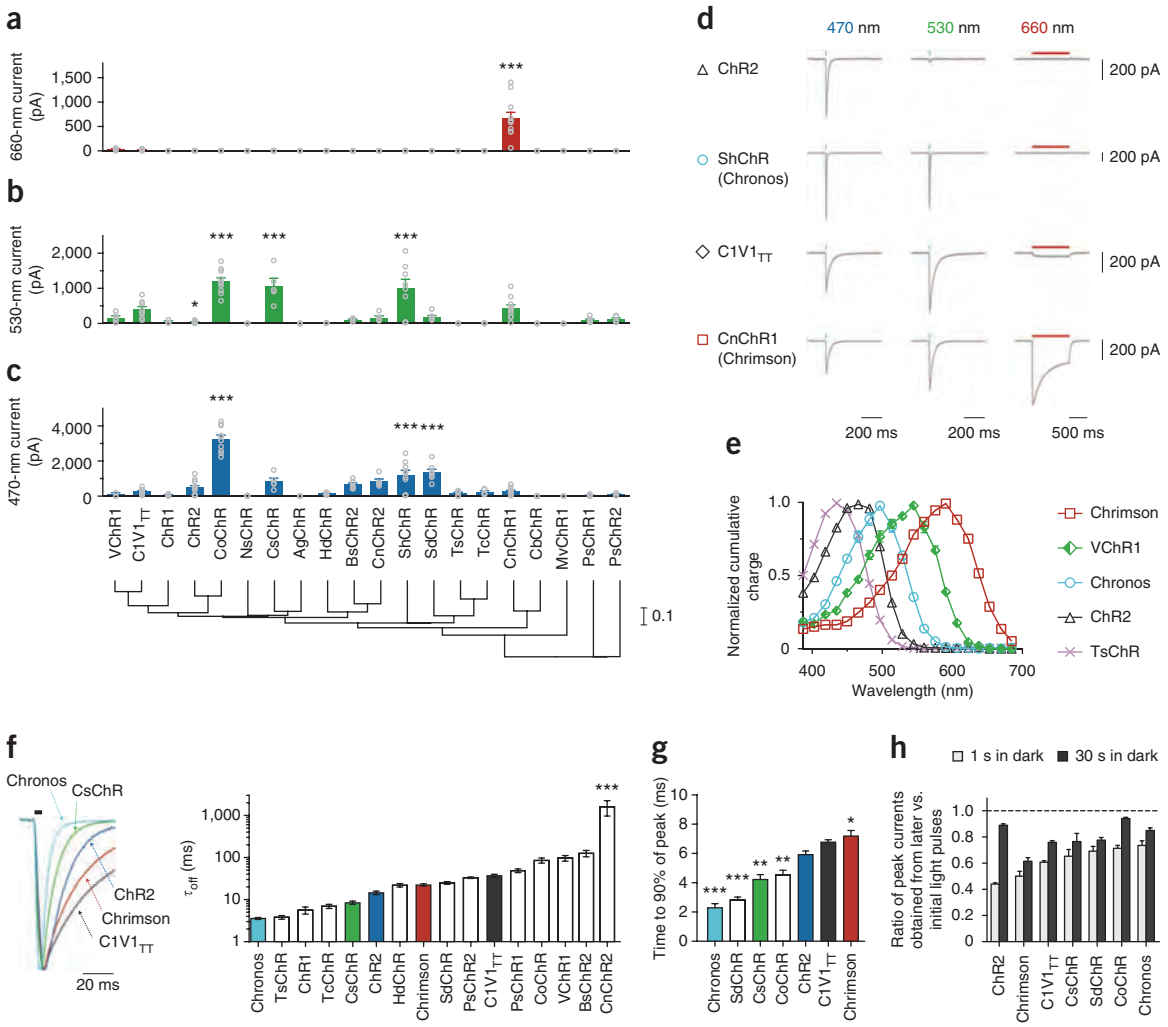

Figure 1 | Novel channelrhodopsin spectral classes discovered through algal transcriptome sequencing. (**a**–**c**) Maximum photocurrents in cultured neurons transfected with the different opsin-GFP fusions in response to far-red (660-nm), green (530-nm) and blue (470-nm) light; blue and green photon fluxes were matched, with illumination conditions defined as follows: 1-s pulse at 10 mW/mm^2 for red, 5-ms pulse at 3.66 mW/mm^2 for green and 5-ms pulse at 4.23 mW/mm^2 for blue. Individual cell photocurrents are plotted as gray circles and overlaid on the population bar graph. See **Supplementary Figure 6** for additional individual cell data. Bottom, phylogeny tree of the channelrhodopsins tested, based on transmembrane helix alignments. The scale indicates the number of substitutions per site. (**d**) Representative voltage-clamp traces in cultured neurons as measured under the screening conditions in **a**–**c** (the long red light pulse was used to ensure we did not miss any red-sensitive channelrhodopsins in our screen). (**e**) Channelrhodopsin action spectra (HEK293 cells; n = 6–8 cells; measured using equal photon fluxes, ~2.5 × 10^{21} photons/s/m^2). (**f**–**h**) Channelrhodopsin kinetic properties as measured in cultured neurons (see also **Supplementary Figs. 7** and **8**). Off-kinetics (**f**) were measured under the conditions in **a**–**c**; on-kinetics (**g**) and recovery kinetics (**h**) were measured with a 1-s pulse at 5 mW/mm^2. All opsins were illuminated near their respective peak wavelength, which was either blue or green for all opsins except Chrimson, which was characterized at 625 nm (n = 5–12 cells for all kinetic comparisons). τ_{off}, monoexponential fit of photocurrent decay. Peak current recovery ratios in **h** were determined from three 1-s light pulses, with the first pulse response used as the baseline for peak current recovery ratio calculations for both the second (1 s in dark after first pulse) and third pulse response (30 s in dark after second pulse). *P < 0.05, **P < 0.01, ***P < 0.001; ANOVA with Dunnett's *post hoc* test, with ChR2 as the reference in **c**,**f**,**g**, and C1V1$_{TT}$ as the reference in **a**,**b**. Exact P values and n values are in **Supplementary Table 2**. Plotted data are mean ± s.e.m. Opsins and the species they derive from are defined in the Online Methods.

peripheral organs while being blocked from reaching the eyes[25], (ii) in blind flies[23] or (iii) for cases in which undesired side effects of visible light stimulation do not substantially affect experimental interpretation[30]. Other technologies such as thermogenetics are often used despite their much slower time course[31,32]. We conjectured that red light activation with Chrimson, which is ~45 nm more red shifted than ReaChR[14,29] (**Supplementary Fig. 9**), would extend the reach of optogenetic tools to *Drosophila* behavioral experiments with reduced light-induced behavioral artifact and improved cuticle penetration.

We first used the *Drosophila* larval neuromuscular junction (NMJ) to examine the reliability of light-triggered action potentials in fly axons expressing CsChrimson. Larval muscles have passive membrane properties, so excitatory junction potentials (EJPs) at the larval NMJ accurately reflect spiking in motor axons[31]. In CsChrimson-expressing larvae, both 470-nm and 617-nm light triggered EJPs, even at short (1- to 2-ms) light-pulse durations and low intensities (0.06–0.14 mW/mm^2). In response to light-pulse durations over 2 ms, CsChrimson activation triggered long-lasting barrages of EJPs (**Fig. 3a**,**b**). Long-wavelength red light

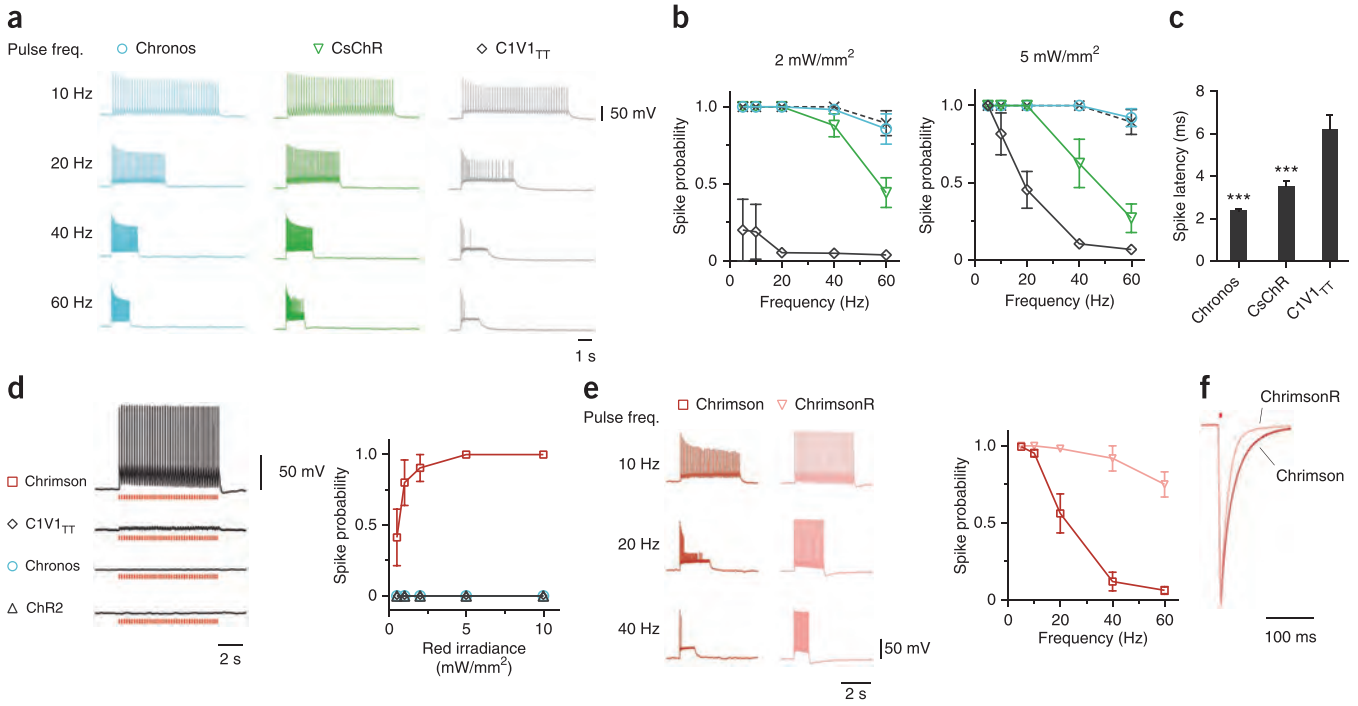

Figure 2 | Comparison of optical spiking in cultured neurons expressing different channelrhodopsins. (**a**–**c**) Green light–driven spiking fidelity. All green light spiking protocols used a train of 40 pulses, 2-ms pulse width, at 530 nm and at the indicated power (n = 5–8 cells for each opsin). (**a**) Representative green light–driven spiking traces at the indicated frequencies at 5 mW/mm^2. (**b**) Green light–driven spike probability over a range of frequencies. The dashed line is the electrical spiking control from Chronos-expressing neurons (this control comprised a train of 40 pulses at the indicated frequencies; each current-injection pulse was 5 ms long and was varied from 200 to 800 pA depending on each neuron's spike threshold). (**c**) Spike latencies (time between the light-pulse onset and the spike peak) calculated for 5-Hz trains at 5 mW/mm^2. (**d**–**f**) Comparison of spiking driven by red light (625 nm). (**d**) Representative current-clamp traces of red light response and spike fidelity (n = 5–8 cells for each opsin; 5-ms pulses, 5 Hz, 5 mW/mm^2). (**e**) Comparison of wild-type Chrimson and Chrimson K176R mutant (ChrimsonR) high-frequency red light spiking (n = 10 and 4 cells, respectively; 40-pulse train, 2-ms pulse width, 5 mW/mm^2). (**f**) Representative off-kinetics traces for Chrimson and ChrimsonR. ***P < 0.001; P = 0.0007 for CsChR and P < 0.0001 for Chronos; ANOVA with Dunnett's *post hoc* test with C1V1$_{TT}$ as reference. Plotted data are mean ± s.e.m.

(720 nm) also triggered EJPs (**Fig. 3c**); however, high-intensity light (1 mW/mm^2) and long light-pulse durations (40–160 ms) were required for robust activation of the NMJ (**Fig. 3d**,**e**). As a control, we tested a commonly used first-generation ChR2-expressing transgenic fly (ref. 33) and examined responses to 470-nm and 617-nm light pulses. As in previous work, 470-nm light triggered EJPs in ChR2-expressing animals, but only after relatively long light pulses (16 ms); 617-nm light pulses did not trigger EJPs in ChR2 animals (**Supplementary Fig. 14**).

In adult flies, we expressed CsChrimson in sweet taste receptor cells (using the Gr64f-Gal4 line to drive its expression in the proboscis and legs[34]) and measured the proboscis extension reflex (PER) elicited by light stimulation at different wavelengths and intensities (**Supplementary Video 1** and **Supplementary Fig. 15**). At 470 nm and 617 nm, PERs were robust at very low light intensities (0.02 mW/mm^2 and 0.015 mW/mm^2, respectively; **Fig. 3f**). Flies also responded to 720-nm light at an intensity substantially lower than that required in the larvae (0.07 mW/mm^2, 10 ms; **Fig. 3f** and **Supplementary Video 2**). 720 nm is believed to be outside of the fly photoreceptor light-absorption spectra[35,36]; we therefore hypothesized that CsChrimson could be used without inducing visually driven behavioral artifacts. However, control flies showed a clear startle response to 720-nm stimuli in darkness (**Fig. 3h** and **Supplementary Video 3**). Nevertheless, we reasoned that the saliency of 720-nm light would drop if it were presented along with other visual stimuli at a wavelength well within the sensitivity of photoreceptors, as might be expected during visual behavior experiments in adult flies. As expected, the startle response was efficiently inhibited when we introduced flowing blue random dots during 720-nm stimulation (reduction from 93.2% nonzero startle responses, out of 44 valid trials in darkness, to 22.2% out of 45 in a circular arena displaying flowing dots; see Online Methods for statistics), and the PER of Gr64f-Gal4/Chrimson-expressing flies was preserved (**Fig. 3g** and **Supplementary Videos 4** and **5**). With a far red–shifted activation spectrum, CsChrimson also allows direct brain stimulation without removing the cuticle while animals freely behave. We expressed CsChrimson in a set of antennal lobe projection neurons (PNv-1 using the VT03194-Gal4 driver line) innervating the V glomerulus, which is known to respond to CO_2 and induces an avoidance response when activated[37]. In this nonvisual paradigm, flies in a circular arena reliably avoided quadrants lit by weak red light (617 nm, 0.015 mW/mm^2; **Supplementary Fig. 16** and **Supplementary Video 6**; paired t-test: P = 0.007; see Online Methods), whereas wild-type flies did not show a response (P = 0.502).

Principles of two-color independent neural excitation

The fundamental limitation in creating an independent two-color channelrhodopsin pair is that all opsins can be driven to some extent by blue light. Additionally, neuron-to-neuron variation in opsin expression and optical scattering and absorption in tissue suggest that a large difference in effective blue light sensitivity

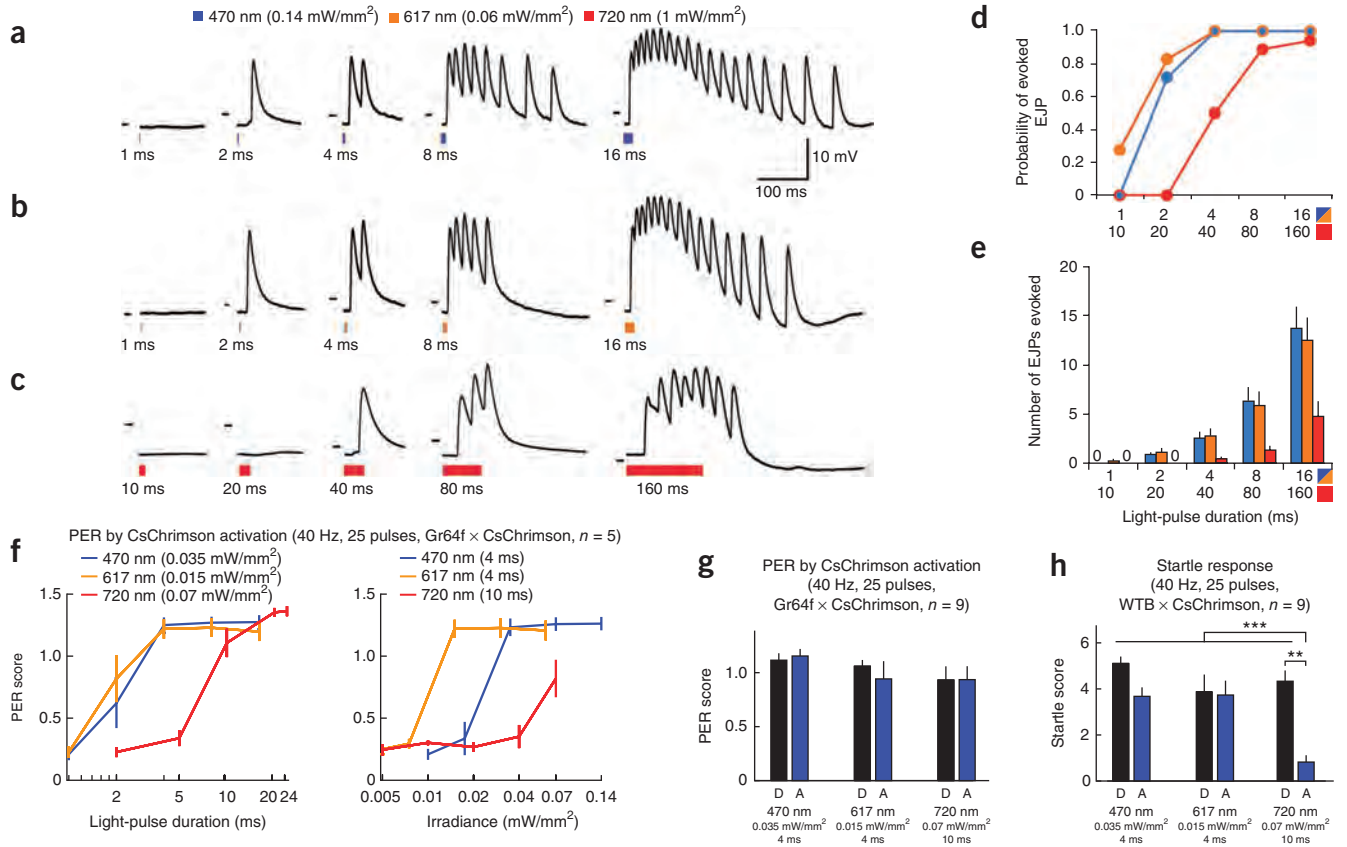

Figure 3 | CsChrimson evokes action potentials in larval *Drosophila* motor neurons and triggers stereotyped behavior in adult *Drosophila*. (**a**–**c**) Intracellular recordings from m6 muscles in 3rd instar larvae expressing CsChrimson in motor neurons. Responses to 470-nm, 617-nm and 720-nm light pulses of indicated power and increasing duration are shown. Dashes in each subpanel indicate –50 mV. (**d**) Probability of light-evoked excitatory junction potentials (EJPs) after pulses of 1, 2, 4, 8 or 16 ms in response to 470-nm and 617-nm light and after pulses of 10, 20, 40, 80 or 160 ms in response to 720-nm light. $n = 6$ muscles in 3 animals for all larvae experiments. (**e**) Mean number of EJPs evoked in response to light pulses. (**f**–**h**) Behavioral response of adult flies to light ($n = 5$ flies in each case). (**f**) Proboscis extension reflex (PER) of flies (pUAS-CsChrimson-mVenus in attP18/*w*⁻;*Gr64f-GAL4*/+;*Gr64f-GAL4*/+, shown as Gr64f × CsChrimson) in response to 25 pulses of lights at 470 nm, 617 nm and 720 nm (see Online Methods for PER scoring). (**g**) PER of Gr64f × CsChrimson flies to pulsed light in darkness (D) or in a visual arena with flowing blue random dots (A). (**h**) Startle response of control flies (pUAS-CsChrimson-mVenus in attP18/+;+/+;+/+, shown as WTB × CsChrimson) to visual stimuli as in **g**. The startle score is the number of moving legs after stimulation. ***$P < 0.001$, **$P < 0.01$. Error bars, s.e.m.

between blue and red-shifted channelrhodopsins, in addition to a large spectral separation, is required to guarantee robust, independent spiking in mammalian brain tissue. We here systematically explored channelrhodopsins' blue light sensitivity in cultured neurons, where, unlike in intact brain tissue, it is possible to precisely control light power.

In evaluating potential blue partners, we first examined the importance of fast channelrhodopsin kinetics. When Chrimson is exposed to blue light levels as dim as 0.1 mW/mm^2 over long durations, as a slow-to-activate blue channelrhodopsin might require, charge integration can result in action potentials (**Fig. 4a**). However, the on-kinetics of Chronos are roughly three times faster than those of ChR2 and ten times faster than those of Chrimson across all blue irradiances tested (**Fig. 4d**), which suggests it may be possible to activate Chronos without substantially activating Chrimson.

Thus, we examined expression variation in Chrimson cells (**Fig. 4b**), as this variance will translate into some cells exhibiting larger blue light depolarizations than others. We found cross-talk of up to 25 mV at typical blue light powers used for ChR2 excitation (1 mW/mm^2, 470 nm, 5-ms pulse). Given Chronos's high photocurrent (**Fig. 1c**), high light sensitivity (**Fig. 4c**) and fast on- and off-kinetics (**Figs. 1f**,**g** and **4d**), we examined whether these properties would translate into spiking at low blue irradiances. Chronos reliably drove 100% spiking at light powers as low as 0.05 mW/mm^2 and maintained this fidelity over two orders of magnitude to 20 mW/mm^2 (**Fig. 4e**,**f**). When we determined the minimum irradiance threshold to achieve 100% spiking (MIT_{100}), Chronos had a consistently lower MIT_{100} than ChR2 for similar GFP fluorescence levels (**Fig. 4f** and **Supplementary Fig. 17**), a result suggesting that Chronos's high effective light sensitivity is not due to higher expression and that Chronos can robustly mediate light-sensitive control of neural spiking across a range of expression levels (**Fig. 4f**) without altering neural excitability (**Fig. 4g**). These properties make Chronos an ideal blue candidate to be combined with Chrimson.

Validation of two-color excitation in brain slices

To determine acceptable blue and red irradiances to selectively drive Chronos and Chrimson without spiking cross-talk, we first examined the powers at which 470-nm and 625-nm LEDs could drive spiking in Chronos and Chrimson neurons as well as the

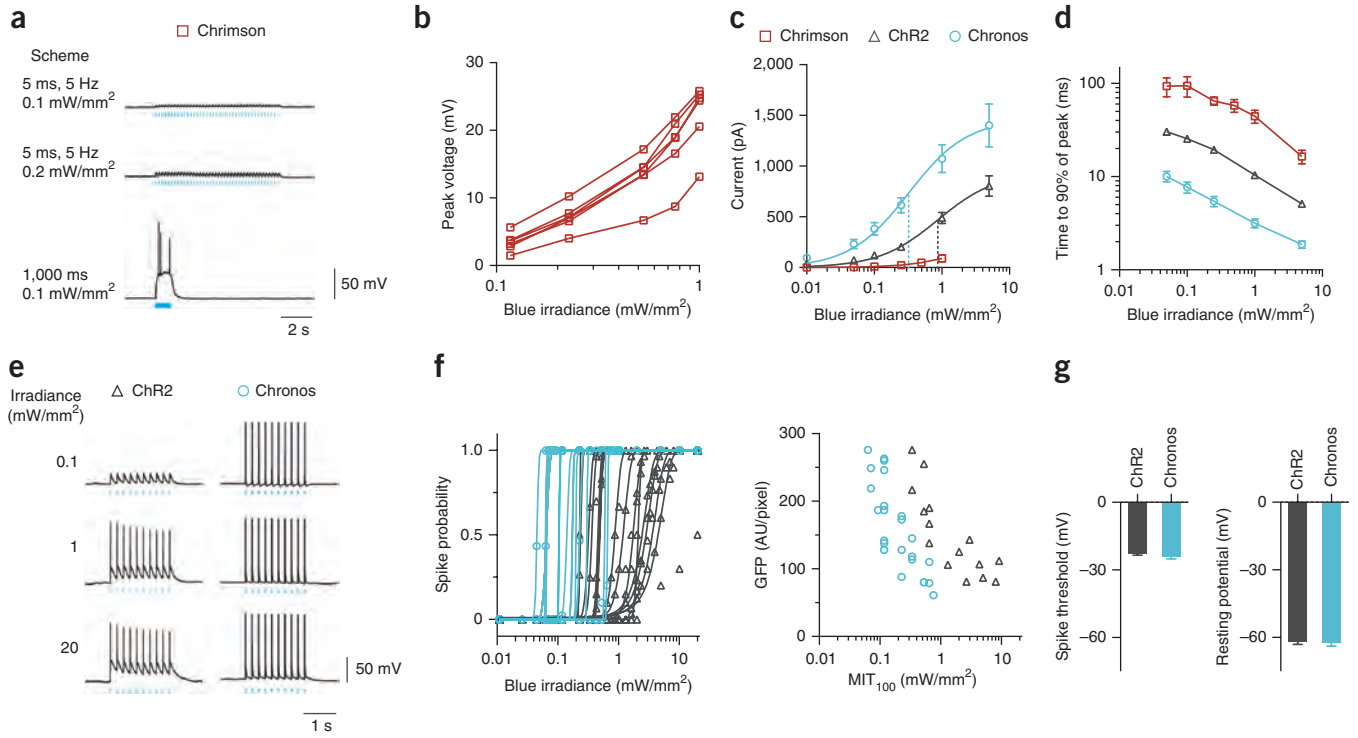

Figure 4 | Characterization of channelrhodopsin blue light (470-nm) sensitivities for two-color excitation in cultured neurons. (**a**) Current-clamp traces of representative Chrimson-expressing neuron under pulsed vs. continuous illumination. (**b**) Chrimson blue light–induced cross-talk voltages vs. irradiances for individual cells under pulsed illumination (5 ms, 5 Hz, $n = 5$ cells). (**c**) Photocurrent vs. blue irradiances (5-ms pulses; $n = 4$ cells for Chrimson, $n = 8$–10 cells for others). Vertical dashed lines indicate half-maximal points up the curves for ChR2 and Chronos as fitted. (**d**) Turn-on kinetics (1-s pulse; $n = 4$–7 cells; see **Supplementary Fig. 17b,c** for raw traces). (**e**–**g**) Comparison between ChR2 and Chronos spike probability over three logs of blue irradiance. All pulsed illuminations used 10 pulses, 5 Hz, 5 ms pulse width. (**e**) Representative spiking traces at the indicated irradiances. (**f**) Spike probability vs. blue light irradiance, plotted for individual Chronos- or ChR2-expressing neurons and minimum irradiance threshold for 100% spiking (MIT_{100}) as a function of GFP fluorescence. AU, arbitrary units. (**g**) Neuron spike threshold and resting potentials ($n = 16$–23 cells). Error bars, s.e.m.

conditions at which spike-level cross-talk occurred (**Fig. 5a–e**). We expressed Chrimson or Chronos in mouse cortical (layer 2/3) neurons via *in utero* electroporation and measured spike probabilities in opsin-expressing neurons in acute brain slices. As expected, we found that red light elicited spikes in only Chrimson-expressing cells (**Fig. 5c**) and blue light elicited spikes in Chronos-expressing cells using light powers as low as 0.05 mW/mm^2 (**Fig. 5d**). Chrimson-expressing neurons began to spike in response to blue light only when light powers were above 0.5 mW/mm^2 (**Fig. 5d**). This suggests that Chronos-expressing neurons can be driven with high fidelity without inducing spikes in Chrimson-expressing cells when using blue light irradiances between 0.2 and 0.5 mW/mm^2. Throughout this operational blue range, Chrimson-expressing cells showed subthreshold membrane depolarization events in response to blue light (**Fig. 5e**) comparable to the culture data (**Fig. 4b**).

We expressed Chrimson and Chronos in independent sets of neurons within the same cortical microcircuit in layer 2/3 neurons by electroporating Cre-on and Cre-off vectors[38]. To measure the synaptic output signal from the two targeted populations, we patch-clamped postsynaptic non-opsin-expressing neurons and measured optically evoked postsynaptic currents (PSCs) (**Fig. 5f–h**). For these experiments we chose a blue irradiance of 0.3 mW/mm^2 to elicit 100% Chronos spiking without Chrimson activation, and we used red irradiances of 1–4 mW/mm^2 to reliably activate Chrimson. We observed distinct PSC amplitudes when the cells were activated at the different wavelengths and light intensities (**Fig. 5i** and **Supplementary Figs. 18e** and **19a–c**). To examine whether these postsynaptic responses were cross-talk free at the synaptic transmission level, just as spiking events were at the action potential level, we singly expressed each opsin in distinct mouse brains, and we patch-clamped cells postsynaptic to opsin-expressing cells (**Fig. 5j–m** and **Supplementary Figs. 19d–g** and **20**). As expected, Chronos reliably drove synaptic events in response to blue light and never under red light (**Fig. 5k**; $P = 0.1$, paired t-test of peak current 30 ms before vs. 30 ms after red light delivery). Chrimson-expressing neurons reliably drove synaptic events upon red illumination and never upon blue illumination (**Fig. 5l**; $P = 0.43$, paired t-test of current before vs. after blue light delivery). Blue light–induced PSCs by Chrimson-expressing neurons began only outside this range, at 0.65 mW/mm^2 (**Fig. 5m**). We thus conclude it is possible to independently drive Chronos and Chrimson at the neural synaptic transmission level by using light powers determined by the operational blue irradiance range. As a final demonstration of Chronos's experimental utility, we found that pure axonal Chronos stimulation of retinal ganglion cell axons in the superior colliculus reliably elicited PSCs in downstream neurons (**Supplementary Fig. 21**).

DISCUSSION

We here present the results from a broad systematic screen of 61 algal opsins, sequenced *de novo* as part of a massive plant

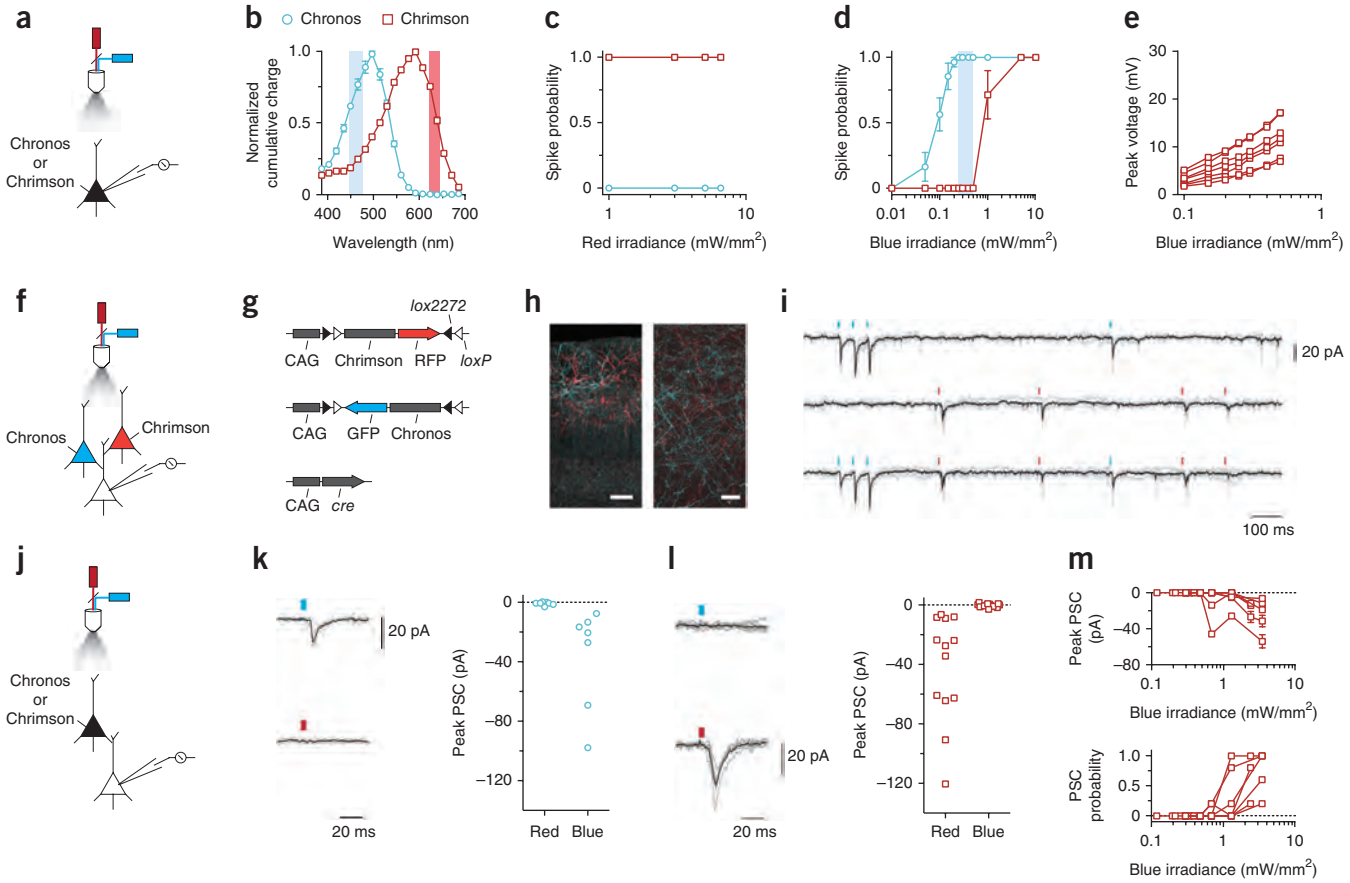

Figure 5 | Independent optical excitation of neural populations in mouse cortical slice using Chrimson and Chronos. (**a**–**e**) Spike and cross-talk characterization in opsin-expressing cells. Experimental optical configurations are depicted in **a**,**f**,**j**. (**b**) Chrimson and Chronos action spectra emphasizing (vertical shaded bars) the blue (470-nm) and red (625-nm) wavelengths used in this figure. (**c**–**e**) Current-clamp characterizations of Chrimson or Chronos expressing neurons in slice to determine optimal irradiance range for two-color excitation. Chrimson-GFP and Chronos-GFP were independently expressed in cortical layer 2/3 neurons in separate mice. 5-ms, 5-Hz light pulses were used; $n = 7$ cells from 3 animals for Chrimson; $n = 11$ cells from 4 animals for Chronos. (**c**,**d**) Spike probability vs. irradiance for red (**c**) and blue light (**d**). The blue vertical shaded bar represents the blue irradiance range where Chronos drove spikes at 100% probability and no cross-talk spike was ever observed for any Chrimson neurons. (**e**) Chrimson subthreshold cross-talk voltage in individual neurons vs. blue irradiances; compare to **Figure 4b**. (**f**–**i**) Postsynaptic currents (PSCs) in non-opsin-expressing neurons downstream of Chrimson and Chronos expressing neurons in brain slice with both opsins introduced into separate neural populations. Stimulation parameters: 0.3 mW/mm^2 for blue, 4 mW/mm^2 for red, 5-ms pulses; 6 neurons from 3 animals. All synaptic transmission slice experiments were done using wide-field illumination (**Supplementary Fig. 18**). (**g**) Triple-plasmid electroporation scheme for mutually exclusive Chrimson and Chronos expression in different sets of layer 2/3 cortical pyramidal cells. (**h**) Histology of intermingled Chrimson- (red) and Chronos-expressing (blue) neurons in layer 2/3 (left, taken at 10× magnification) and their axons (right, taken at 60× magnification). Scale bars: 100 µm (left), 20 µm (right). (**i**) PSCs in response to optical Poisson stimulation with blue and red light; shown are raw voltage traces (gray) with average trace (black) from a single neuron experiencing blue (top), red (center) or both (bottom) light pulses. (PSC traces from neurons downstream of mutually exclusive Chrimson- and Chronos-expressing neurons in response to blue or red light are in **Supplementary Fig. 18e**.) (**j**–**m**) PSCs in non-opsin-expressing neurons downstream of Chronos- or Chrimson-expressing neurons. Conditions are as in **f**–**i**, except pulses were delivered at 0.2 Hz. $n = 7$ cells from 2 animals for Chronos; $n = 12$ cells from 4 animals for Chrimson. The black trace is the averaged response; gray traces are individual trials. (**k**) Chronos-driven PSCs under blue or red light, obtained from a representative neuron (left), with population data (right). (**l**) Chrimson-driven PSCs under blue or red light traces, obtained from a representative neuron (left), with population data (right). (**m**) Chrimson-driven PSC amplitudes (top) and the probability of observing a PSC at all (bottom) vs. blue irradiances.

transcriptome endeavor[20] (http://www.onekp.com/). We discovered Chronos, an ultra-light-sensitive blue channelrhodopsin with faster kinetics than previously described opsins and which might represent an excellent general-use channelrhodopsin. We also discovered Chrimson, a red light–drivable channelrhodopsin 45 nm more red shifted than any previous channelrhodopsin and which might be useful in scenarios in which red light stimulation is essential. Previous channelrhodopsins that can be driven off-peak by red light (630 nm) have on-off kinetics exceeding 100 ms (refs. 9,14): perhaps a limitation of their original VChR1 scaffold. The spectral and kinetic properties of Chrimson and Chronos will enable fundamentally new types of experiments.

We explored the utility of CsChrimson with red light in *D. melanogaster*. CsChrimson was able to mediate responses in larval and adult flies with extremely low light powers across all wavelengths tested, most likely owing to the high expression achieved with the expression cassette used (see Online Methods). Further, light-induced startle responses of adult flies were significantly reduced at longer wavelengths (720 nm) when visual distractors of shorter wavelength were provided. Thus, CsChrimson may be

useful for temporally precise neuronal stimulation in *Drosophila* behavioral experiments. Curiously, our results suggest that the photosensitivity of the fly eye extends well beyond the wavelength of typical room light for fly experiments (~650 nm), highlighting the utility of the 720-nm stimulation protocol we introduce for a wider range of behavioral experiments. Wavelengths lower than 720 nm will be useful in situations in which startle responses do not affect measurements of the parameters under study, such as stimulating neurons in the brain through intact cuticle to induce nonvisually driven behaviors as here shown with 617-nm light and CO_2-responding neurons, something that has not yet been reliably demonstrated using optogenetic techniques. The ability to perform optogenetic behavioral experiments in intact flies with CsChrimson at redder wavelengths than ReaChR[14,29], due to the ~45-nm spectral shift, may permit lower light levels to be used and reduce visual system–mediated artifacts.

Using both Chronos and Chrimson, we found an ample blue light irradiance range that evoked reliable Chronos-induced spikes without any Chrimson-induced spikes in mouse cortical slice and that also allowed Chronos-induced synaptic transmission without any Chrimson-induced synaptic transmission. As most two-color experimental setups will not be identical to our slice demonstration, several constraints exist upon the use of effective blue light sensitivity to achieve two-color separation. Whenever possible, Chronos should be expressed under the stronger promoter and the more excitable neuron type to minimize Chrimson-induced depolarization. The experiments in this paper characterized two-color excitation with symmetric promoters and cell types to stringently test whether Chronos and Chrimson can, without exploiting differences in cellular excitability, present a clear separation due to biophysical properties. Neuroscientists seeking to manipulate two different cell populations may find that expressing Chronos at high levels in the more excitable cell type may further increase the reliable blue dynamic range.

Although Chronos has the fastest kinetic properties among reported channelrhodopsins, blue light pulses delivered at very high frequencies as part of a two-color experiment could in principle lead to charge integration and, thus, to Chrimson blue spiking cross-talk. The temporal precision of Chronos- versus Chrimson-mediated synaptic events may also depend on light power, potentially limiting usage in scenarios requiring submillisecond timing of synaptic release, although ~1-ms jitter is achievable. We have additionally observed in postsynaptic experiments that the stimulation frequency for both red and blue pulses is fundamentally limited by the wild-type Chrimson, the slowest of the opsin pair. This is why we engineered ChrimsonR, a faster Chrimson kinetic mutant, which has similar blue light sensitivity to the wild type but allows modulation at above the 20-Hz range. It may be desirable to further improve Chrimson's kinetics and decrease its light sensitivity to enable high-frequency modulation in both the red and blue channels and to increase the usable blue irradiance range.

For applications *in vivo*, it would be important to illuminate the circuit region of interest with powers that fall within the windows here defined; for mammals, one might use alternative illumination methods such as three-dimensional optical waveguides[39] or wireless LED implants[40]. Although these constraints add complexity to experiments, they may also enable *in vivo* two-color experiments not previously possible.

METHODS

Methods and any associated references are available in the online version of the paper.

Accession codes. GenBank/EMBL/DDBJ: new channelrhodopsins identified here are listed under accession codes KF992030–KF992090; see also **Supplementary Table 1**.

Note: Any Supplementary Information and Source Data files are available in the online version of the paper.

ACKNOWLEDGMENTS

We thank A. Karpova (Janelia Farm) for technical advice, reagents and generous assistance with construct preparation for *Drosophila*; K. Hibbard and members of the Janelia Fly Core for fly husbandry and assistance with fly crosses; and J. Pulver for technical advice and assistance with data analysis software. We thank Y. Aso, W. Ming and G. Rubin (Janelia Farm) for kindly allowing us to use their circular light arena and for useful discussion. We thank I. Negrashov, S. Sawtelle and J. Liu for arena-related development and support. We thank J.R. Carlson (Yale University) for Gr64f-Gal4 flies, W.D. Tracey Jr. (Duke University) for UAS-Chr2 flies, G.M. Rubin (Janelia Farm) for pBDP-Gal4 flies and B.J. Dickson (IMP, Vienna and Janelia Farm) for VT031497-Gal4 flies.

S.S.K., S.R.P. and V.J. were supported by the Howard Hughes Medical Institute. The 1000 Plants (1KP) initiative, led by G.K.-S.W., is funded by the Alberta Ministry of Enterprise and Advanced Education, Alberta Innovates Technology Futures (AITF) Innovates Centre of Research Excellence (iCORE), Musea Ventures, and BGI-Shenzhen. B.Y.C. and E.S.B. were funded by Defense Advanced Research Projects Agency (DARPA) Living Foundries HR0011-12-C-0068. B.Y.C. was funded by the US National Science Foundation (NSF) Biophotonics Program. M.C.-P. was funded by US National Institutes of Health (NIH) grant 5R01EY014074-18. E.S.B. was funded by the MIT Media Lab, Office of the Assistant Secretary of Defense for Research and Engineering, Harvard/MIT Joint grants in Basic Neuroscience, NSF (especially CBET 1053233 and EFRI 0835878), NIH (especially 1DP2OD002002, 1R01NS067199, 1R01DA029639, 1R01GM104948, 1RC1MH088182 and 1R01NS075421), Wallace H. Coulter Foundation, Alfred P. Sloan Foundation, Human Frontiers Science Program, New York Stem Cell Foundation Robertson Neuroscience Investigator Award, Institution of Engineering and Technology A.F. Harvey Prize, and Skolkovo Institute of Science and Technology.

AUTHOR CONTRIBUTIONS

N.C.K., E.S.B., M.C.-P. and V.J. contributed to the study design and data analysis. G.K.-S.W. and B.Y.C. oversaw transcriptomic sequencing. E.S.B. and M.C.-P. supervised mammalian opto/electrophysiological parts of the project. N.C.K. coordinated all experiments and data analysis. N.C.K., Y.K.C., A.S.C. and T.K.M. conducted and analyzed all *in vitro* electrophysiology. M.M., B.S., N.C.K., T.K.M., E.J.C., Z.T., J.W., Y.X., Z.Y. and Y.Z. conducted algal RNA experiments or transcriptome sequencing and analysis. N.C.K., Y.M. and A.B.-B. performed and analyzed all slice electrophysiology. V.J. prepared CsChrimson for injection into *Drosophila*. S.S.K. and V.J. designed adult fly behavior experiments. S.S.K. performed all fly behavior experiments and data analysis. S.R.P. designed, performed and analyzed all larval *Drosophila* experiments. Correspondence should be addressed to V.J. (vivek@janelia.hhmi.org) for CsChrimson flies. All authors contributed to the discussions and writing of the manuscript.

COMPETING FINANCIAL INTERESTS

The authors declare competing financial interests: details are available in the online version of the paper.

1. Boyden, E.S., Zhang, F., Bamberg, E., Nagel, G. & Deisseroth, K. Millisecond-timescale, genetically targeted optical control of neural activity. *Nat. Neurosci.* **8**, 1263–1268 (2005).
2. Han, X. & Boyden, E.S. Multiple-color optical activation, silencing, and desynchronization of neural activity, with single-spike temporal resolution. *PLoS ONE* **2**, e299 (2007).
3. Chow, B.Y. *et al.* High-performance genetically targetable optical neural silencing by light-driven proton pumps. *Nature* **463**, 98–102 (2010).
4. Zhang, F. *et al.* Multimodal fast optical interrogation of neural circuitry. *Nature* **446**, 633–639 (2007).

5. Gradinaru, V. *et al.* Molecular and cellular approaches for diversifying and extending optogenetics. *Cell* **141**, 154–165 (2010).
6. Boyden, E.S. A history of optogenetics: the development of tools for controlling brain circuits with light. *F1000 Biol. Rep.* **3**, 11 (2011).
7. Zhang, F. *et al.* Red-shifted optogenetic excitation: a tool for fast neural control derived from Volvox carteri. *Nat. Neurosci.* **11**, 631–633 (2008).
8. Erbguth, K., Prigge, M., Schneider, F., Hegemann, P. & Gottschalk, A. Bimodal activation of different neuron classes with the spectrally red-shifted channelrhodopsin chimera C1V1 in *Caenorhabditis elegans*. *PLoS ONE* **7**, e46827 (2012).
9. Yizhar, O. *et al.* Neocortical excitation/inhibition balance in information processing and social dysfunction. *Nature* **477**, 171–178 (2011).
10. Prigge, M. *et al.* Color-tuned channelrhodopsins for multiwavelength optogenetics. *J. Biol. Chem.* **287**, 31804–31812 (2012).
11. Wang, W. *et al.* Tuning the electronic absorption of protein-embedded all-trans-retinal. *Science* **338**, 1340–1343 (2012).
12. Waddell, W.H., Schaffer, A.M. & Becker, R.S. Visual pigments. 3. Determination and interpretation of the fluorescence quantum yields of retinals, Schiff bases, and protonated Schiff bases. *J. Am. Chem. Soc.* **95**, 8223–8227 (1973).
13. Govorunova, E.G., Spudich, E.N., Lane, C.E., Sineshchekov, O.A. & Spudich, J.L. New channelrhodopsin with a red-shifted spectrum and rapid kinetics from *Mesostigma viride*. *mBio* **2**, e00115–e00111 (2011).
14. Lin, J.Y., Knutsen, P.M., Muller, A., Kleinfeld, D. & Tsien, R.Y. ReaChR: a red-shifted variant of channelrhodopsin enables deep transcranial optogenetic excitation. *Nat. Neurosci.* **16**, 1499–1508 (2013).
15. Kleinlogel, S. *et al.* Ultra light-sensitive and fast neuronal activation with the Ca^{2+}-permeable channelrhodopsin CatCh. *Nat. Neurosci.* **14**, 513–518 (2011).
16. Berndt, A., Yizhar, O., Gunaydin, L.A., Hegemann, P. & Deisseroth, K. Bi-stable neural state switches. *Nat. Neurosci.* **12**, 229–234 (2009).
17. Bamann, C., Gueta, R., Kleinlogel, S., Nagel, G. & Bamberg, E. Structural guidance of the photocycle of channelrhodopsin-2 by an interhelical hydrogen bond. *Biochemistry* **49**, 267–278 (2010).
18. Mattis, J. *et al.* Principles for applying optogenetic tools derived from direct comparative analysis of microbial opsins. *Nat. Methods* **9**, 159–172 (2012).
19. Govorunova, E.G., Sineshchekov, O.A., Li, H., Janz, R. & Spudich, J.L. Characterization of a highly efficient blue-shifted channelrhodopsin from the marine alga *Platymonas subcordiformis*. *J. Biol. Chem.* **288**, 29911–29922 (2013).
20. Johnson, M.T. *et al.* Evaluating methods for isolating total RNA and predicting the success of sequencing phylogenetically diverse plant transcriptomes. *PLoS ONE* **7**, e50226 (2012).
21. Lin, J.Y. A user's guide to channelrhodopsin variants: features, limitations and future developments. *Exp. Physiol.* **96**, 19–25 (2011).
22. Nagel, G. *et al.* Light activation of channelrhodopsin-2 in excitable cells of *Caenorhabditis elegans* triggers rapid behavioral responses. *Curr. Biol.* **15**, 2279–2284 (2005).
23. de Vries, S.E. & Clandinin, T.R. Loom-sensitive neurons link computation to action in the *Drosophila* visual system. *Curr. Biol.* **22**, 353–362 (2012).
24. Schroll, C. *et al.* Light-induced activation of distinct modulatory neurons triggers appetitive or aversive learning in *Drosophila* larvae. *Curr. Biol.* **16**, 1741–1747 (2006).
25. Gaudry, Q., Hong, E.J., Kain, J., de Bivort, B.L. & Wilson, R.I. Asymmetric neurotransmitter release enables rapid odour lateralization in *Drosophila*. *Nature* **493**, 424–428 (2013).
26. Honjo, K., Hwang, R.Y. & Tracey, W.D. Jr. Optogenetic manipulation of neural circuits and behavior in *Drosophila* larvae. *Nat. Protoc.* **7**, 1470–1478 (2012).
27. Zhang, W., Ge, W. & Wang, Z. A toolbox for light control of *Drosophila* behaviors through Channelrhodopsin 2-mediated photoactivation of targeted neurons. *Eur. J. Neurosci.* **26**, 2405–2416 (2007).
28. Xiang, Y. *et al.* Light-avoidance-mediating photoreceptors tile the *Drosophila* larval body wall. *Nature* **468**, 921–926 (2010).
29. Inagaki, H.K. *et al.* Optogenetic control of *Drosophila* using a red-shifted channelrhodopsin reveals experience-dependent influences on courtship. *Nat. Methods* doi:10.1038/nmeth.2765 (22 December 2013).
30. Claridge-Chang, A. *et al.* Writing memories with light-addressable reinforcement circuitry. *Cell* **139**, 405–415 (2009).
31. Pulver, S.R., Pashkovski, S.L., Hornstein, N.J., Garrity, P.A. & Griffith, L.C. Temporal dynamics of neuronal activation by Channelrhodopsin-2 and TRPA1 determine behavioral output in *Drosophila* larvae. *J. Neurophysiol.* **101**, 3075–3088 (2009).
32. Bernstein, J.G., Garrity, P.A. & Boyden, E.S. Optogenetics and thermogenetics: technologies for controlling the activity of targeted cells within intact neural circuits. *Curr. Opin. Neurobiol.* **22**, 61–71 (2012).
33. Hwang, R.Y. *et al.* Nociceptive neurons protect *Drosophila* larvae from parasitoid wasps. *Curr. Biol.* **17**, 2105–2116 (2007).
34. Dahanukar, A., Lei, Y.T., Kwon, J.Y. & Carlson, J.R. Two *Gr* genes underlie sugar reception in *Drosophila*. *Neuron* **56**, 503–516 (2007).
35. Minke, B. & Kirschfeld, K. The contribution of a sensitizing pigment to the photosensitivity spectra of fly rhodopsin and metarhodopsin. *J. Gen. Physiol.* **73**, 517–540 (1979).
36. Salcedo, E. *et al.* Blue- and green-absorbing visual pigments of *Drosophila*: ectopic expression and physiological characterization of the R8 photoreceptor cell-specific Rh5 and Rh6 rhodopsins. *J. Neurosci.* **19**, 10716–10726 (1999).
37. Lin, H.H., Chu, L.A., Fu, T.F., Dickson, B.J. & Chiang, A.S. Parallel neural pathways mediate CO_2 avoidance responses in *Drosophila*. *Science* **340**, 1338–1341 (2013).
38. Atasoy, D., Aponte, Y., Su, H.H. & Sternson, S.M. A FLEX switch targets Channelrhodopsin-2 to multiple cell types for imaging and long-range circuit mapping. *J. Neurosci.* **28**, 7025–7030 (2008).
39. Zorzos, A.N., Scholvin, J., Boyden, E.S. & Fonstad, C.G. Three-dimensional multiwaveguide probe array for light delivery to distributed brain circuits. *Opt. Lett.* **37**, 4841–4843 (2012).
40. Kim, T.I. *et al.* Injectable, cellular-scale optoelectronics with applications for wireless optogenetics. *Science* **340**, 211–216 (2013).

ONLINE METHODS

Opsins and species. Key opsins are abbreviated throughout the paper and figures as follows, with species or derivation listed in parentheses: VChR1 (*Volvox carteri*), $C1V1_{TT}$ (VChR1/ChR1 chimera), ChR1 (*Chlamydomonas reinhardtii*), CsChR (*Chloromonas subdivisa*), AgChR (*Asteromonas gracillis-B*), ChR2 (*Chlamydomonas reinhardtii*), CoChR (*Chloromonas oogama*), NsChR (*Neochlorosarcina* sp.), ShChR (*Stigeoclonium helveticum*; also called Chronos), MvChR1 (*Mesostigma viride*), SdChR (*Scherffelia dubia*), TsChR (*Tetraselmis striata*), TcChR (*Tetraselmis cordiformis*), BsChR (*Brachiomonas submarina*), CnChR (*Chlamydomonas noctigama*; also called Chrimson), HdChR (*Haematococcus droebakensis*), CbChR (*Chlamydomonas bilatus-A*), PsChR (*Proteomonas sulcata*). For a detailed list of all opsins found, their species of origin, and their GenBank accession numbers, see **Supplementary Table 1**.

Molecular cloning. All opsin genes were synthesized (Genscript) with mammalian codon optimization and subcloned as previously described[3]. $C1V1_{TT}$ and ReaChR were synthesized with the same codon usage as previously described[9,14]. For cultured neuron studies, all genes were subcloned into a lentiviral backbone under a CaMKII promoter and with a C-terminal GFP fusion. No trafficking sequences were added to any opsin-encoding genes. The tdTomato plasmid used for cotransfection in cultured neuron was also subcloned into a lentiviral backbone, but with a ubiquitin promoter instead. For *in utero* electroporation experiments, all genes were subcloned into pCAGIG vector (Addgene 11159) with C-terminal GFP, tdTomato, or mOrange2 fusion. The Cre-dependent vectors were generated using the same pCAGIG vector but with *lox* sites flanking the protein-coding region as done previously[38].

We performed RACE on some of the sequences (**Supplementary Fig. 1**) by using 5′ RNA ligation to enrich for full-length transcripts (**Supplementary Table 3**). This protocol is the same as in the Ambion RLM-RACE kit, and PCR primers were designed on the basis of partial transcriptome sequencing results. RACE products were blunt cloned (Invitrogen Zero Blunt kit) into a vector for Sanger sequencing.

Characterization of channel kinetics and ion selectivity in HEK293FT cells. Whole-cell patch-clamp recordings were performed in isolated HEK293FT cells to avoid space clamp issues. All recordings were performed using an Axopatch 200B amplifier and Digidata 1440 digitizer (Molecular Devices) at room temperature. To allow isolated cell recording, we plated cells at a density of 15,000 cells per well in 24-well plates that contained round glass coverslips (0.15 mm thick, 25 mm in diameter, coated with 2% growth factor–reduced Matrigel in DMEM for 1 h at 37 °C). To ensure accurate measurements, we used cells with access resistance <25 MΩ and holding current within ±50 pA. Typical membrane resistance was between 500 MΩ and 2 GΩ, and pipette resistance was between 3 and 6 MΩ. Photostimulation of patch-clamped cells was conducted with a 470-nm LED (Thorlabs) at irradiance of 10 mW/mm for ChR2, ChR2 E123A, and Chronos, and by a 590-nm LED (Thorlabs) at irradiance of 4.6 mW/mm for Chrimson.

For characterizing channel kinetics, the extracellular solution (Tyrode's solution) consisted of (in mM) 125 NaCl, 2 KCl, 3 $CaCl_2$, 1 $MgCl_2$, 10 HEPES, 30 glucose, pH 7.3 (NaOH adjusted), 305 mOsm; and the intracellular solution consisted of (in mM) 125 K-gluconate, 8 NaCl, 0.1 $CaCl_2$, 0.6 $MgCl_2$, 1 EGTA, 10 HEPES, 4 Mg-ATP, 0.4 Na-GTP, pH 7.3 (KOH adjusted), with 295–300 mOsm (sucrose adjusted). Channel closing rates (τ_{off}; for example, as in **Fig. 3a**) were measured by fitting the decay of photocurrent after 2-ms light pulses to monoexponential curves, and time to peak (time to reach 90% of peak photocurrent after the beginning of illumination, as in **Fig. 3b**) values were measured from 1-s pulses.

Ion selectivity characterization (**Supplementary Fig. 4**) was done using solutions listed in **Supplementary Table 4**. The liquid junction potentials were 5.8 mV and 4.9 mV for 90 mM $CaCl_2$ and 5 mM NaCl solutions, respectively, and were corrected during recording; the others were <1 mV in liquid junction potential. The peak component of the photocurrent during a 1-s illumination was used to calculate photocurrent density ratios.

HEK 293FT cell culture and transfection. HEK 293FT cells (Invitrogen) were maintained between 10% and 70% confluence in D10 medium (Cellgro) supplemented with 10% FBS (Invitrogen), 1% penicillin/streptomycin (Cellgro), and 1% sodium pyruvate (BioWhittaker). For recording, cells were plated at 5–20% confluence on glass coverslips coated with Matrigel (BD Biosciences). Adherent cells were transfected approximately 24 h post plating either with TransLT 293 Lipofectamine transfection kits (Mirus) or with calcium phosphate transfection kits (Invitrogen) and recorded via whole-cell patch clamp between 36 and 72 h post transfection. 1.25 µg of DNA was delivered. 1 µM of all-*trans*-retinal was supplemented to the culture medium for 1 h before patch-clamp experiments.

Primary neuron culture and transfection. All procedures involving animals were in accordance with the US National Institutes of Health Guide for the Care and Use of Laboratory Animals and approved by the Massachusetts Institute of Technology Committee on Animal Care. Hippocampal neuron culture was prepared from postnatal day 0 or day 1 Swiss Webster (Taconic or Charles River) mice as previously described[3] but with the following modifications: dissected hippocampal tissues were digested with 50 units of papain (Worthington Biochem) for 5 min, and the digestion was stopped with ovomucoid trypsin inhibitor (Worthington Biochem). Cells were plated at a density of 16,000–20,000 per glass coverslip coated with Matrigel (BD Biosciences).

Cultured neurons were transfected at 4 days *in vitro* (DIV) with a commercial calcium phosphate kit (Invitrogen). We added an additional washing with acidic MEM buffer (pH 6.8–6.9) after calcium phosphate precipitate incubation to completely resuspend residual precipitates[41]. tdTomato was used as a cotransfectant DNA reagent to assist with unbiased selection of opsin-expressing neurons (see main text); in this condition, we delivered 2 µg of opsin DNA and 0.2 µg tdTomato. When no tdTomato was used, we used 2 µg of opsin DNA alone.

Whole-cell electrophysiology *in vitro* and in slice. Whole-cell patch-clamp recordings were made using the Axopatch 200B or Multiclamp 700B amplifier, a Digidata 1440 digitizer, and a PC running pClamp (Molecular Devices). For *in vitro* current-clamp recordings, neurons were patched 14–18 DIV (10–14 d post

transfection) to allow for sodium channel maturation. Neurons were bathed in room-temperature Tyrode solution containing 125 mM NaCl, 2 mM KCl, 3 mM $CaCl_2$, 1 mM $MgCl_2$, 10 mM HEPES, 30 mM glucose, 0.01 mM NBQX and 0.01 mM GABAzine. The Tyrode pH was adjusted to 7.3 with NaOH, and the osmolarity was adjusted to 300 mOsm with sucrose. For *in vitro* voltage-clamp recordings, neurons were patched 11–14 DIV (7–10 d post transfection); the recording conditions here were similar to those for current-clamp recordings, except the Tyrode solution also contained 1 µM tetrodotoxin (TTX, Tocris Bioscience). No all-*trans*-retinal was supplemented for any cultured neuron recordings.

For slice recordings, room-temperature artificial cerebrospinal fluid (ACSF) was continuously perfused over slices, and no blockers were used. ACSF contained 127 mM NaCl, 2.5 mM KCl, 25 mM $NaHCO_3$, 1.25 mM NaH_2PO_4, 12 mM D-glucose, 0.4 mM sodium ascorbate, 2 mM $CaCl_2$, and 1 mM $MgCl_2$ and was bubbled continuously with 95% oxygen/5% CO_2.

For both *in vitro* and slice recordings, borosilicate glass pipettes (Warner Instruments) with an outer diameter of 1.2 mm and a wall thickness of 0.255 mm were pulled to a resistance of 3–7 MΩ with a P-97 Flaming/Brown micropipette puller (Sutter Instruments) and filled with a solution containing 125 mM K-gluconate, 8 mM NaCl, 0.1 mM $CaCl_2$, 0.6 mM $MgCl_2$, 1 mM EGTA, 10 mM HEPES, 4 mM Mg-ATP, and 0.4 mM Na-GTP. The pipette solution pH was adjusted to 7.3 with KOH, and the osmolarity was adjusted to 298 mOsm with sucrose. For voltage-clamp experiments, cells were clamped at −65 mV for *in vitro* (HEK293, cultured neuron) recordings and between −65 and −80 mV for slice recordings. For current-clamp experiments, <50-pA constant current injection was used for *in vitro* recordings, and no current injection was used for slice recordings. To ensure accurate measurements, we used cells with access resistance between 5 and 35 MΩ and holding current within ±100 pA (at −65 mV, in voltage clamp). Access resistance was monitored throughout recording. Data were analyzed using Clampfit (Molecular Devices) and custom Matlab scripts (MathWorks).

Light delivery and imaging. All neuron culture and slice experiments were done with the LEDs mounted on microscope for wide-field illumination, with nominal wavelength at 470 nm, 530 nm, 625 nm, 660 nm and 735 nm (Thorlabs, M470L2, M530L2, M625L3, M660L3 and M735L3 respectively). We additionally filtered LEDs spectrum with the following bandpass filters (Semrock): 530-nm LED with 543 ± 11 nm filter, 625-nm LED with 632 ± 11 nm, and 660-nm LED with 661 ± 10 nm. The 735-nm LED was not additionally filtered. Light power was controlled through the LED driver using analog voltage modulation (LEDD1B or DC4100, Thorlabs), and voltage pulse width was adjusted to obtain the desired illumination duration as measured with a photometer (S120VC, Thorlabs). Illumination spot size with different objectives was measured by focusing on a microscope slide coated with appropriate-wavelength Alexa dye and photobleaching it for 10 min under full-intensity illumination. The photobleached slide was then imaged with a micrometer calibration slide to determine the photobleached radius.

Action spectrum data were taken with a monochromator (Till-Photonics Polychrome IV, bandwidth 15 nm centered around each value), and a separate (Uniblitz) shutter was used to gate the light pulses to 10 ms. Equal photon fluxes of ~2.5×10^{21} photons/s/m^2 (~1.1 mW/mm^2 at 450 nm) were used across wavelengths by using the monochromator's built-in intensity adjustment. We additionally corrected for any photon dosage difference (12% at the most) between wavelengths by dividing the recorded opsin response by the measured photon dose. A (QuickMacros) script was used to automate the wavelength and intensity selections and to synchronize with electrophysiology recording. For each cell, wavelengths were swept from blue to red and from red to blue, and the responses were averaged.

Photocurrent measurements were single trial, and input resistance was monitored throughout. For color-ratio comparisons, the order of illumination wavelength was shuffled between different cells. For photocurrent recovery kinetics measurements, an additional 2-min wait in the dark preceded the protocol to allow for recovery before the measurement was begun. In protocols where irradiances (or stimulation frequencies) were varied, the irradiances (or stimulation frequencies) were either shuffled or measured both from low to high and high to low. In the acute slice postsynaptic experiments, at least five sweeps were taken for each condition.

Unless otherwise specified, all experiments included a 20- to 30-s wait in the dark between sweeps to allow for opsin recovery.

Quantitative fluorescence comparison of opsin-GFP and cytosolic tdTomato expressed in cultured neurons was imaged with Leica HCX APO L 20× objective (air, numerical aperture (NA) = 0.5) using Hamamatsu Orca Flash 2.8 under identical illumination conditions throughout: 445-nm LED (Thorlabs) at 4.28 mW/mm^2 using EN GFP filter cube (Leica) for GFP fluorescence; 530-nm LED (Thorlabs) with 543 nm ± 11 nm filter (Semrock) at 2.14 mW/mm^2 using Custom R filter cube (Leica) for tdTomato fluorescence.

***In utero* electroporation and virus delivery for acute slice experiments.** All procedures were in accordance with the National Institutes of Health Guide for the Care and Use of Laboratory Animals and approved by the Massachusetts Institute of Technology Committee on Animal Care. C57BL/6J E16-timed pregnant mice were used for electroporation. Surgery was done under ketamine-xylazine anesthesia and buprenorphine analgesia. For cortical experiments, DNA solution containing plasmids of interest was injected into the lateral ventricle of each embryo using a pulled capillary tube. Five square pulses (50-ms width, 1 Hz, 35 V) were applied using a tweezer electrode for electroporation (Harvard Apparatus, ECM 830). Brains of mice for experiments in which opsin-expressing cells were to be experimentally characterized were electroporated with pCAG-opsin-GFP plasmid. Brains of mice in which downstream, non-opsin-expressing neurons were to be experimentally characterized were electroporated with pCAG-FLEX-rc[Chronos-GFP] and/or pCAG-FLEX-Chrimson-mOrange2, and pCAG-Cre plasmids. pCAG-Chrimson-tdTomato was additionally used in half of the single postsynaptic experiments.

For the retinal ganglion cell–superior colliculus experiment, intravitreal virus injection was performed on P0 C57BL/6 mice with Nanoject II (Drummond) under cold anesthesia. 100 nL of rAAV2/8-Synapsin-Chronos-GFP (titer: 1.4×10^{13} particles/mL)

doi:10.1038/nmeth.2836

was injected into the eye. AAV particles were produced by the University of North Carolina Chapel Hill Vector Core.

Data analysis. Phylogenetic trees were generated using the neighbor-joining method with *p*-distance model (MEGA5).

Opsin-GFP and tdTomato fluorescence was measured with custom Matlab script using masks around neuron soma region. Masks were generated (on the basis of either GFP or tdTomato images) using CellProfiler (http://www.cellprofiler.org/) and manually edited in ImageJ to remove neuronal processes. The same mask was used to quantify both GFP and tdTomato fluorescence.

Action spectra were computed by integrating charge from light onset to the half-max time. Half-max time refers to the time that the highest amplitude response wavelength has half of its peak current. This is to ensure the measured response is the transition from ground state as opposed to secondary photoproducts. Given that the integration window is the same across wavelengths for a given cell (typically 1–3 ms), this is effectively measuring the initial slope as was done previously by other labs[13].

The points halfway up the curve (e.g., analogous to the pharmacology concept of EC_{50}) in **Figure 4c** were calculated by fitting 5-ms blue irradiance photocurrents to the one-site specific binding model ($y = B_{max} \times x/(K_d + x)$ using Prism (GraphPad Software), where the K_d corresponds to EC_{50} and B_{max} corresponds to the extrapolated maximum photocurrent at saturating irradiance. This is the same convention as previously published paper[18].

Spikes were defined as depolarizing above 0 mV and then repolarizing below −30 mV within each stimulation interval. Spike threshold was measured with a 500-ms current ramp (400–800 pA) current injection protocol and determined with custom Matlab script. Threshold was defined as the voltage at which the slope (dV/dt) has exceeded 0.3 mV/s.

Slice preparation. P20–P40 mice were used for slice preparation unless otherwise specified. Mice were anesthetized with isofluorane and transcardially perfused with ice-cold cutting solution containing 110 mM choline chloride, 25 mM $NaHCO_3$, 25 mM D-glucose, 11.6 mM sodium ascorbate, 7 mM $MgCl_2$, 3.1 mM sodium pyruvate, 2.5 mM KCl, 1.25 mM NaH_2PO_4, and 0.5 mM $CaCl_2$. The brain was then carefully removed and mounted in a vibrating-blade microtome (Leica VT1000S). 300-mm-thick coronal slices of the cortex (varying regions of brain were sectioned, depending on where the electroporation resulted in expressing neurons; they were as a rule found in layer 2/3 of the cortical area obtained) were cut with a vibrating metal blade at 90 Hz and 0.1 mm/s cutting speed. Sectioned slices were incubated in 37 °C cutting solution for 30–45 min before being transferred to room-temperature oxygenated artificial cerebrospinal fluid (ACSF) for recording. ACSF contained 127 mM NaCl, 2.5 mM KCl, 25 mM $NaHCO_3$, 1.25 mM NaH_2PO_4, 12 mM D-glucose, 0.4 mM sodium ascorbate, 2 mM $CaCl_2$, and 1 mM $MgCl_2$. For spiking characterization (**Fig. 5c–e**), we used a Nikon CFI Apo 60× NIR objective (water immersion, NA = 1); for synaptic characterizations (**Fig. 5f–m**), we used a Nikon CFI Super Plan Fluor ELWD 20xC objective (air, NA = 0.45) in order to recruit as many synapses as possible to insure stringency of the zero–cross-talk synaptic control. For slice experiments, electrical artifacts were apparent in the recorded traces as a result of LED on-off coupling to fluids flowing by the slice, as LED was in the Faraday cage; we include raw traces with artifacts interpolated in **Figure 5** and those without artifact interpolation in **Supplementary Figure 22**.

Fly stocks. CsChrimson constructs were prepared with additional Golgi and ER export motifs[42–45] in the pJFRC7-20XUAS-IVS vector[46] and inserted in attP18/+;+/+;+/+. To express CsChrimson in larval motor neurons, we crossed UAS-CsChrimson-mVenus flies to flies containing a Gal4 driver (OK371-Gal4) that drives expression in all glutamatergic neurons[47]. We used the same Gal4 line to express ChR2 (ref. 33) in larval motor neurons. Gr64f-Gal4 flies were obtained from J.R. Carlson[34]; UAS-ChR2 flies, from W.D. Tracey Jr.[33]; and pBDP-Gal4, from G.M. Rubin[48]. Control flies for adult fly experiments were obtained by crossing CsChrimson virgin female flies to wild-type Berlin (WTB) flies. VT031497-Gal4 flies were from B. Dickson[37].

Larval NMJ experiments. *Fly handling and preparation.* Flies were raised on standard cornmeal-based medium with 0.2 mM all-*trans*-retinal at 25 °C. Wandering 3rd instar larvae were dissected in HL3.1 physiological saline containing (in mM) 70 NaCl, 5 KCl, 0.4 $CaCl_2$, 4 $MgCl_2$, 10 $NaHCO_3$, 5 trehalose, 115 sucrose, 5 HEPES, pH 7.15. Animals were filleted as described previously[31], and the central nervous system was removed. Larval fillets were then mounted on a standard intracellular electrophysiology rig. Temperature was maintained at ~22 °C.

Intracellular recording and stimulation parameters. We used 10- to 15-MΩ sharp intracellular electrodes filled with 3M KCl to record light evoked excitatory junctional potentials in larval muscle 6 (m6). The electrode was maneuvered using an MP-285 micromanipulator (Sutter Instruments). Recordings were amplified with an Axopatch 200B (Molecular Devices) and collected using a Powerlab 16/30 and Chart 7.1 software (both from AD Instruments). We delivered light pulses of either 1, 2, 4, 8, and 16 ms at 470 nm (0.14 mW/mm^2) and 617 nm (0.06 mW/mm^2) or 10, 20, 40, 80, and 160 ms at 720 nm (1 mW/mm^2). Light pulses were generated with LED light sources (470 nm, 617 nm: OptoLED, Cairn Instruments; 720 nm: Thorlabs LED controller), triggered by the Powerlab 16/30 data acquisition system. For each genotype tested, we recorded from two muscles in each of three separate animals. Electrophysiological data were analyzed with custom scripts in Spike2 (Cambridge Electronic Designs).

Adult fly experiments. *Fly handling.* Flies were raised from the egg stage[49] on standard cornmeal and soybean–based medium with 0.2 mM all-*trans*-retinal. Vials were wrapped in aluminum foil to protect retinal from light and kept in a 23 °C, 60% humidity incubator. Flies were transferred to fresh retinal food vials on the first day of eclosion. We used 2- to 3-d-old female flies in PER characterization experiments for 470 nm and 617 nm, and we used 4- to 5-d-old female flies for 720 nm. All flies used to measure behavioral artifacts and the corresponding PER were crossed on the same day, raised side by side in two vials of the same batch of medium and collected on the same day.

Setup for behavioral experiments. The fly preparation and LED display have been published elsewhere[50]. Briefly, female flies were cold anesthetized and placed in a sarcophagus under

a dissection microscope. Then they were tethered with a wire placed between the head and the thorax with UV-activated glue. They were centered in a modular display system[50] (IO Rodeo), which consists of five rows and seven columns of 8 × 8 LED panels (Bright LED Electronics Corp., BM-10B88MD) covering the upper visual field from −105° to +105°. The LED emission surface was covered with a layer of conductive film to minimize electrical noise (Clear Shield, Transparent Conductive Film), two layers of bandpass filter gel (ROSCO, Roscolux #59 indigo), another layer of conductive film, and a layer of stencil paper to prevent reflection. Behavior was recorded using a camera (camera: PointGrey, FFMV-03M2M, lens: Computar, MLM3x-MP, software: Matlab Image Acquisition Toolbox, MathWorks) with an IR illumination source (Oslon, SFH4715S), longpassed at 850 nm (Thorlabs, FGL850) to prevent CsChrimson activation. The same filter was used in front of the imaging camera to prevent image corruption from LEDs used for CsChrimson activation. We used three high-power LEDs for CsChrimson activation (Thorlabs, M470L2, M617L2, and M735L3, respectively) after collimation (Thorlabs, ACL2520-DG6-A for 470 nm and 617 nm, ACL2520-DG6-B for 735 nm, and additional bandpass filtering for 735 nm: Semrock, FF01-720/12-25). Light intensity was measured at the position of the fly (Thorlabs, S130C). The intensity of the random dot pattern was 40 nW/mm^2, and that of IR illumination was 240 μW/mm^2. The overall configuration is shown in **Supplementary Video 1**. PERs to 470-nm and 617-nm light sources by control flies are shown in **Supplementary Figure 15**.

Design and analysis of PER experiments. Pulse width (ms) and LED light intensity (mW/mm^2) were varied in PER experiments. The number of pulses (25) and the frequency (40 Hz) were fixed. For each fly, a total of ten parameter sets (five per parameter) were tested in each lighting condition with five repetitions. The interstimulus interval (ISI) was 30 s. To minimize desensitization, we ordered trials from low to higher light intensity and low to higher pulse widths. The LED was controlled using a data acquisition device (Measurement Computing, USB-1208FS) and the Data Acquisition Toolbox (MathWorks). Fly behavior was recorded using a camera from 1 s before to 2 s after the initiation of each trial. The positions of the neck connectives and the root of the antennae were manually determined. The position of the tip of the proboscis was determined by finding the maximum horizontal coordinate of nonzero pixels after the image was thresholded. The PER score was scaled by the size of the head capsule (**Supplementary Fig. 15a**). All trials were manually proofread to correct image corruption by leg movement. Five flies were used for each combination of wavelength and fly group.

Measurement of light-induced behavioral artifacts. The setup used to measure light-induced behavioral artifacts was similar to that used for PER characterization with the following exceptions: nine CsChrimson flies (Gr64f × CsChrimson) and nine control flies (WTB × CsChrimson) were tested for all conditions in a single day. Flies were given 3 h to settle after tethering. For each wavelength, we used the minimum LED intensity that reliably evoked a PER (**Fig. 3f**). We manually triggered each trial only when flies stopped moving (minimum ISI: 6.5 s). Flow speed for the blue random dot pattern presented on the LED display was 20 pixels/s. For the dark condition, the LED arena was removed from the setup. The startle score was manually assessed by counting the number of legs moving within 2 s of initiation of each trial (scores thus ranged from 0 to 6 with flight assigned a score of 7). Trials were discarded if flies moved before stimulation. No pair of dark and lit arena conditions showed significant difference (paired *t*-test or Wilcoxon signed rank test after Jarque-Bera normality test; *P* level 0.05) except the 720-nm condition for WTB × CsChrimson (Wilcoxon signed rank test; $P = 0.004$). For testing differences between the random dot condition at 720 nm and all other conditions (WTB × CsChrimson), data in all six conditions were randomly reassigned into each condition to obtain a null distribution of differences between the conditions (10,000 repetitions). No sample showed greater difference than the original one (thus $P < 1/10{,}000$). Matlab and the Statistics Toolbox (MathWorks) were used for all analyses.

Optogenetics of freely behaving intact flies. An LED array (array of Luxeon Rebel, 700 mA, 617 nm, Philips LXM2-PH01-0070) and its driver circuit were custom designed to independently illuminate each quadrant of a circular light arena from the bottom and were controlled by a microcontroller (Arduino) using custom software (see **Supplementary Fig. 16a** for schematic of setup). A diffuser (Optically Colored Cast Acrylic Sheet, 1/8-inch thick, 12 inch × 12 inch, white, McMaster 8505K11) was placed on top of an LED array to produce a homogeneous light field under a white opaque plastic panel with a circular hole, which served as the behavior arena (3D printed, Vero White, Objet Connex 350; hole dimensions: 100-mm diameter, 3-mm depth). The arena was covered by a transparent plastic panel (optically clear cast acrylic sheet, 1/8-inch thick, 12 inch × 12 inch, McMaster 8560K239) to allow video recording. For fly movement imaging, the whole arena was illuminated from above by an IR light source (850 nm), and a thin IR absorption film (Laser-gard PVC film, YAG, Edmund Optics 53-738) was placed between the arena and the diffuser to prevent IR reflection. In a single session (see **Supplementary Video 6**), we illuminated two opposing quadrants of the arena with the LED array for 30 s (0.015mW/mm^2) and switched to the other two quadrants for the next 30 s. The switching protocol was repeated three times for a total video recording of 120 s. For each session (a total of nine sessions were performed for each genotype), we put ~10–20 flies (~2- to 5-d-old males and females) in the arena. The behavior was recorded using a USB3 camera (Flea3, PointGrey, with longpass filter of 800 nm) and custom software. Image analysis was done in Matlab. The background image (an average image over all frames) was subtracted from each frame. Next, any pixels with less than 20% of the maximum pixel value of the frame were set to 0 and others to 1. This generates a white IR-reflected body image of flies with black background. This image was divided into four quadrants. The percentage of flies in quadrants 1 (northeast) and 3 (southwest) was approximated by the percentage of white pixels in those quadrants relative to the total number of white pixels. Finally, we picked a snapshot of each light condition just before switching (at 60 s and 90 s) and performed a paired *t*-test after Jarque-Bera normality test (VT031497-Gal4 × UAS-CsChrimson attP18: degrees of freedom (df) = 8, $P = 0.007$; WTB × UAS-CsChrimson attP18: df = 8, $P = 0.502$).

41. Jiang, M. & Chen, G. High Ca^{2+}-phosphate transfection efficiency in low-density neuronal cultures. *Nat. Protoc.* **1**, 695–700 (2006).

doi:10.1038/nmeth.2836

42. Stockklausner, C. & Klocker, N. Surface expression of inward rectifier potassium channels is controlled by selective Golgi export. *J. Biol. Chem.* **278**, 17000–17005 (2003).
43. Stockklausner, C., Ludwig, J., Ruppersberg, J.P. & Klocker, N. A sequence motif responsible for ER export and surface expression of Kir2.0 inward rectifier K^+ channels. *FEBS Lett.* **493**, 129–133 (2001).
44. Gradinaru, V., Thompson, K.R. & Deisseroth, K. eNpHR: a Natronomonas halorhodopsin enhanced for optogenetic applications. *Brain Cell Biol.* **36**, 129–139 (2008).
45. Ma, D. *et al.* Role of ER export signals in controlling surface potassium channel numbers. *Science* **291**, 316–319 (2001).
46. Pfeiffer, B.D. *et al.* Refinement of tools for targeted gene expression in *Drosophila*. *Genetics* **186**, 735–755 (2010).
47. Mahr, A. & Aberle, H. The expression pattern of the *Drosophila* vesicular glutamate transporter: a marker protein for motoneurons and glutamatergic centers in the brain. *Gene Expr. Patterns* **6**, 299–309 (2006).
48. Pfeiffer, B.D. *et al.* Tools for neuroanatomy and neurogenetics in *Drosophila*. *Proc. Natl. Acad. Sci. USA* **105**, 9715–9720 (2008).
49. Guo, A. *et al.* Conditioned visual flight orientation in *Drosophila*: dependence on age, practice, and diet. *Learn. Mem.* **3**, 49–59 (1996).
50. Reiser, M.B. & Dickinson, M.H. A modular display system for insect behavioral neuroscience. *J. Neurosci. Methods* **167**, 127–139 (2008).

Corrigendum: Independent optical excitation of distinct neural populations

Nathan C Klapoetke, Yasunobu Murata, Sung Soo Kim, Stefan R Pulver, Amanda Birdsey-Benson, Yong Ku Cho, Tania K Morimoto, Amy S Chuong, Eric J Carpenter, Zhijian Tian, Jun Wang, Yinlong Xie, Zhixiang Yan, Yong Zhang, Brian Y Chow, Barbara Surek, Michael Melkonian, Vivek Jayaraman, Martha Constantine-Paton, Gane Ka-Shu Wong & Edward S Boyden
***Nat. Methods* 11, 338–346 (2014); published online 9 February 2014; corrected after print 28 August 2014**

In the version of this article initially published, the *Drosophila* transgenic strains were incorrectly reported as generated using Chrimson (Fig. 3, Supplementary Figs. 14–16 and Supplementary Videos 2–6). Owing to a miscommunication, the *Drosophila* strains were actually generated with CsChrimson, a CsChR-Chrimson chimera replacing the Chrimson N terminus with the CsChR N terminus. CsChrimson has the same spectral and kinetic properties as Chrimson; these data have been added to the paper in the form of an addendum, and incorrectly listed strains have been fixed in the main text and supplementary materials. The error has been corrected in the HTML and PDF versions of the article.

Addendum: Independent optical excitation of distinct neural populations

Nathan C Klapoetke, Yasunobu Murata, Sung Soo Kim, Stefan R Pulver, Amanda Birdsey-Benson, Yong Ku Cho, Tania K Morimoto, Amy S Chuong, Eric J Carpenter, Zhijian Tian, Jun Wang, Yinlong Xie, Zhixiang Yan, Yong Zhang, Brian Y Chow, Barbara Surek, Michael Melkonian, Vivek Jayaraman, Martha Constantine-Paton, Gane Ka-Shu Wong & Edward S Boyden

Nat. Methods **11**, 338–346 (2014); published online 9 February 2014; addendum published after print 28 August 2014

A trafficking variant of the Chrimson molecule (**Fig. 1c**) was used for the *Drosophila* experiments in the original version of the paper (i.e., Fig. 3, Supplementary Figs. 14–16 and Supplementary Videos 2–6). This trafficking variant, called CsChrimson-KGC-GFP-ER2, is a CsChR-Chrimson chimera in which the Chrimson N terminus is replaced with the CsChR N terminus (**Fig. 1a** and **Supplementary Fig. 1**), with appended KGC and ER2 trafficking sequences (**Fig. 1c**).

In the original paper, we found CsChR to have high membrane expression levels (original Supplementary Figs. 5 and 6). We therefore attempted to boost Chrimson expression by swapping the Chrimson N terminus with the CsChR N terminus. As no transmembrane regions were modified, we unsurprisingly found that CsChrimson has the same spectral and kinetic properties as Chrimson in murine cultured neurons (**Fig. 1b**,**d**,**f**,**g**). We additionally compared CsChrimson with and without KGC and/or ER2 trafficking sequences and found all variants to have similar photocurrents in cultured neurons (**Fig. 1d**,**e**). However, we observed more cytosolic aggregates with the KGC version and a reduction of aggregates with the ER2 version (**Supplementary Fig. 2**). It is therefore likely that CsChrimson will be of use with the ER2 trafficking sequence in some biological contexts.

METHODS

Methods and any associated references are available in the online version of the paper.

Accession codes. GenBank/EMBL/DDBJ: CsChrimson is listed under accession code KJ995863.

Note: Any Supplementary Information and Source Data files are available in the online version of the paper.

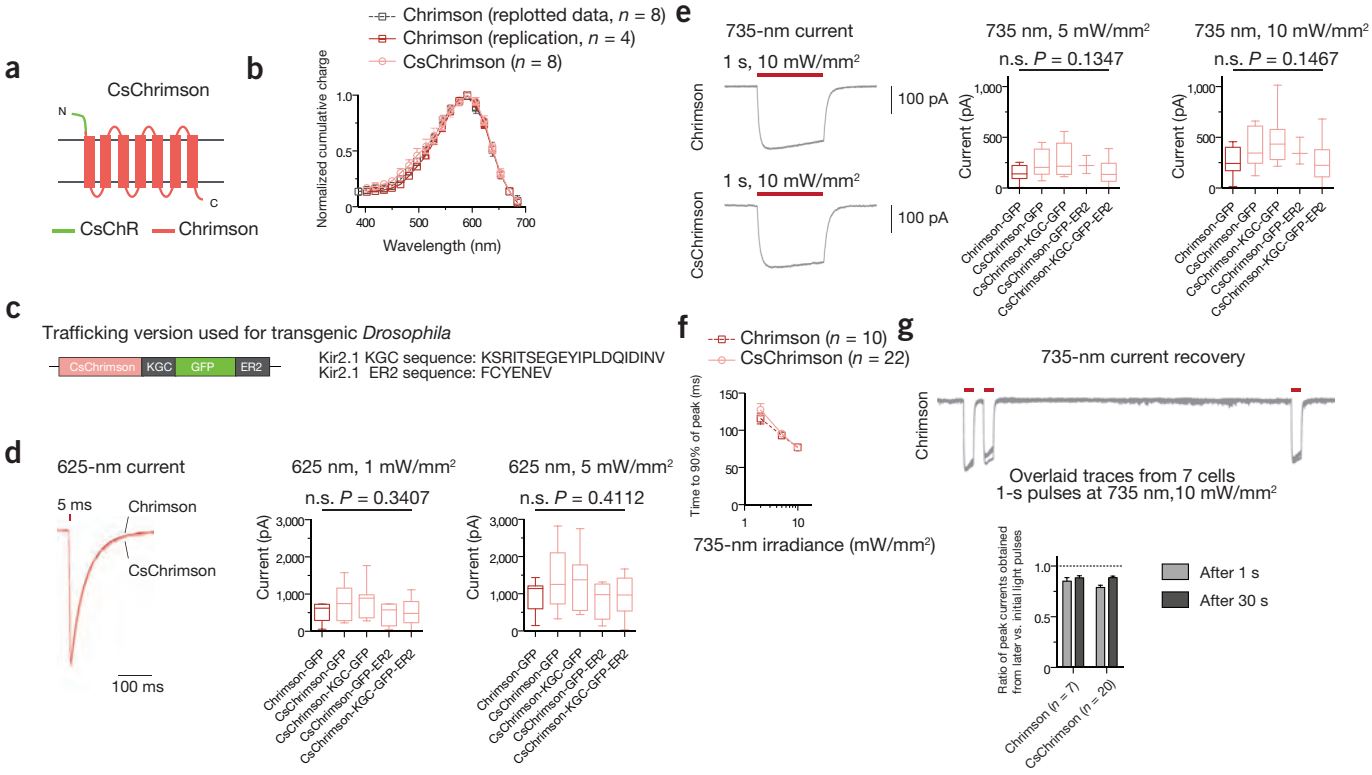

Figure 1 | CsChrimson characterization in cultured cells. (**a**) Schematic of the CsChrimson chimera. (**b**) Action spectra for Chrimson and CsChrimson as well as the Chrimson spectrum data from the original manuscript plotted in Figure 1e (HEK293 cells; measured using equal photon fluxes of ~2.5 × 10^{21} photons/s/m^2). (**c**) Schematic of trafficking sequences used to generate the CsChrimson *Drosophila* transgenics. (**d**,**e**) Maximum photocurrents in response to red (625-nm) and far-red (735-nm) light as measured in cultured neurons. (**f**,**g**) Turn-on (**f**) and recovery kinetics (**g**) in response to 735-nm light. CsChrimson kinetic data were pooled from all trafficking versions. All constructs in this panel were expressed under CaMKII promoter and selected solely on the basis of the presence of cotransfected cytosolic tdTomato expression. Illumination conditions are as labeled in each panel. Box-plot whiskers represent minimum and maximum data points. Box limits represent 25th percentile, median and 75th percentile. Chrimson-GFP: $n = 9$ cells in **d**, $n = 12$ cells in **e**; CsChrimson-GFP: $n = 7$ cells in **d**, $n = 8$ cells in **e**; CsChrimson-KGC-GFP: $n = 7$ cells in **d**,**e**; CsChrimson-GFP-ER2: $n = 4$ cells in **d**, $n = 3$ cells in **e**; CsChrimson-KGC-GFP-ER2: $n = 10$ cells in **d**, $n = 11$ cells in **e**. Plotted data are mean ± s.e.m. in **b**,**f**,**g**. ANOVA with Dunnett's *post hoc* test with Chrimson-GFP as reference in **d**,**e**. n.s., not significant.

ONLINE METHODS

Whole-cell patch-clamp recordings were made using a Multiclamp 700B amplifier and a Digidata 1550 digitizer (Molecular Devices). All other experimental conditions are the same as previously described.

NOTE: This is the Supplementary Material for the Addendum, not the Supplementary Material for the Original Paper.

Supplementary Figure 1. CsChrimson sequence

Transmembrane regions are based on an alignment against C1C2 crystal structure. Putative transmembrane helices are flagged. Orange and blue sequences highlight the differences between Chrimson and CsChrimson.

Chrimson-GFP

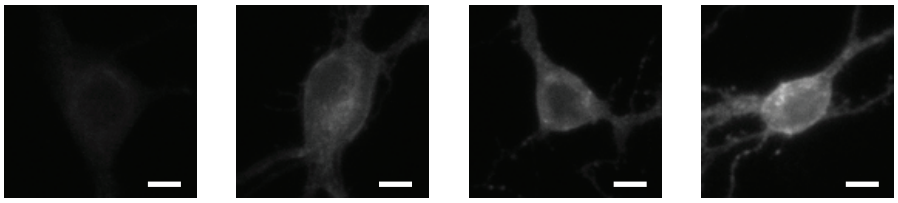

CsChrimson-GFP

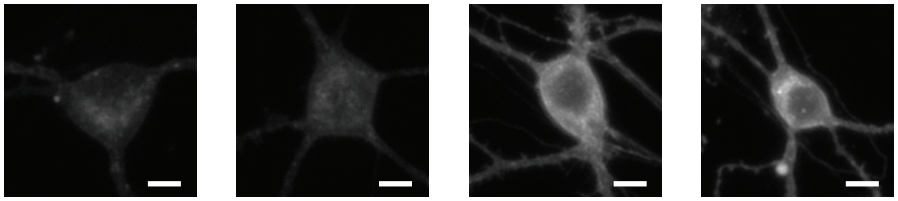

CsChrimson-KGC-GFP

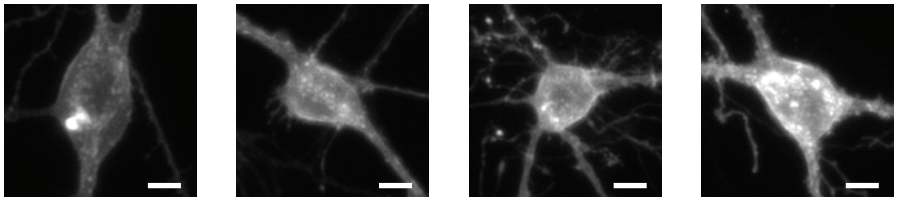

CsChrimson-GFP-ER2

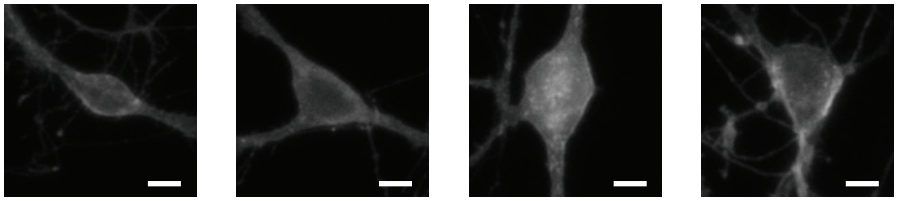

CsChrimson-KGC-GFP-ER2

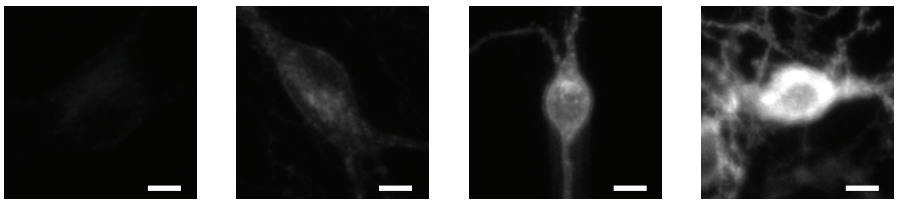

Supplementary Figure 2. Trafficking in cultured neurons

Representative GFP epi-fluorescence images for Chrimson and CsChrimson trafficking variants taken on 20x objective and imaged under identical conditions. All images have identical brightness and contrast settings. Scale bar, 10 µm.

NOTE: This is the Supplementary Material for the Original Paper, not the Supplementary Material for the Addendum.

Independent Optical Excitation of Distinct Neural Populations

Nathan C Klapoetke[1-5], Yasunobu Murata[4-5], Sung Soo Kim[6], Stefan R. Pulver[6], Amanda Birdsey-Benson[4-5], Yong Ku Cho[1-5], Tania K Morimoto[1-5], Amy S Chuong[1-5], Eric J Carpenter[7], Zhijian Tian[8], Jun Wang[8], Yinlong Xie[8], Zhixiang Yan[8], Yong Zhang[8], Brian Y Chow[9], Barbara Surek[10], Michael Melkonian[10], Vivek Jayaraman[6], Martha Constantine-Paton[4-5], Gane Ka-Shu Wong[7,8,11], Edward S Boyden[1-5]

[1] The MIT Media Laboratory, Synthetic Neurobiology Group, Massachusetts Institute of Technology, Cambridge, Massachusetts, USA

[2] Department of Biological Engineering, Massachusetts Institute of Technology, Cambridge, Massachusetts, USA

[3] MIT Center for Neurobiological Engineering, Massachusetts Institute of Technology, Cambridge, Massachusetts, USA

[4] Department of Brain and Cognitive Sciences, Massachusetts Institute of Technology, Cambridge, Massachusetts, USA

[5] MIT McGovern Institute for Brain Research, Massachusetts Institute of Technology, Cambridge, Massachusetts, USA

[6] Janelia Farm Research Campus, Howard Hughes Medical Institute, Ashburn, Virginia, USA

[7] Department of Biological Sciences, University of Alberta, Edmonton, Alberta, Canada

[8] Beijing Genomics Institute-Shenzhen, Shenzhen, China

[9] Department of Bioengineering, University of Pennsylvania, Philadelphia, Pennsylvania, USA

[10] Institute of Botany, Cologne Biocenter, University of Cologne, Cologne, Germany

[11] Department of Medicine, University of Alberta, Edmonton, Alberta, Canada

Co-corresponding authors, Edward S Boyden (esb@media.mit.edu), Gane KS Wong (gane@ualberta.ca)

Supplementary Figure 1	Phylogenetic relation of algal opsins.
Supplementary Figure 2	Sequence alignment.
Supplementary Figure 3	Characterization of channel kinetics of Chronos and Chrimson in HEK293FT cells.
Supplementary Figure 4	Comparison of ion selectivity of Chronos, Chrimson, and ChR2.
Supplementary Figure 5	Opsin screening in cultured neurons.
Supplementary Figure 6	Opsin trafficking in cultured neurons.
Supplementary Figure 7	Inactivation and recovery kinetics.
Supplementary Figure 8	Chronos full inactivation and recovery kinetics.
Supplementary Figure 9	ReaChR and Chrimson comparison in cultured neurons.
Supplementary Figure 10	Green light driven spiking frequency responses in cultured neurons.
Supplementary Figure 11	Electrical versus green light driven spiking fidelity in cultured neurons.
Supplementary Figure 12	Red light driven spiking in cultured neurons.
Supplementary Figure 13	Red and far-red spiking with ChrimsonR in acute cortical slice.
Supplementary Figure 14	Larval motor axons expressing ChR2 fire in response to blue but not red light pulses.
Supplementary Figure 15	Proboscis extension reflex (PER).
Supplementary Figure 16	Optogenetics of freely behaving intact flies.
Supplementary Figure 17	Two-color excitation controls in cultured neurons.
Supplementary Figure 18	Optically evoked post-synaptic currents (PSCs) in acute slice.
Supplementary Figure 19	Optically evoked paired-pulse responses in acute slice.
Supplementary Figure 20	Comparisons of spiking and post-synaptic response timing in acute slice.
Supplementary Figure 21	Retina to superior colliculus projection stimulation with Chronos.
Supplementary Figure 22	Post-synaptic current raw traces.
Supplementary Table 1	Naming convention
Supplementary Table 2	Statistical analysis for opsin comparisons
Supplementary Table 3	Primer sequences
Supplementary Table 4	Solutions used to characterize ion selectivity
Supplementary Video 1	Experimental setup with a visual arena.
Supplementary Video 2	PER of a Gr64f x CsChrimson fly to 720 nm light in darkness.
Supplementary Video 3	Startle response to 720 nm light in darkness
Supplementary Video 4	PER of a Gr64f x CsChrimson fly to 720 nm light in a blue random dot arena.
Supplementary Video 5	Inhibited startle response to 720 nm light in a blue random dot arena.
Supplementary Video 6	Optogenetics in freely behaving intact flies.

Supplementary Figure 1 – Phylogenetic relation of algal opsins.

Phylogenetic tree of novel opsins discovered from *de novo* transcriptomic sequencing of over 100 algal species. Only full length opsin sequences (i.e. has seven transmembrane helices) were analyzed. In some cases the transcriptome sequencing resulted in truncated opsin sequences, and rapid amplification of cDNA ends (RACE) was additionally performed on the original algal species to obtain the full length opsin sequence. See **Supplementary Table 1** for algal genus/species names, as well as the nicknames or aliases used in the main text of the paper (not all of the channelrhodopsins we obtained, were assigned nicknames or aliases, but instead are referred to just by number). Scale bar is the number of amino acid substitutions per site.

Nature Methods: doi:10.1038/nmeth.2836

Supplementary Figure 1

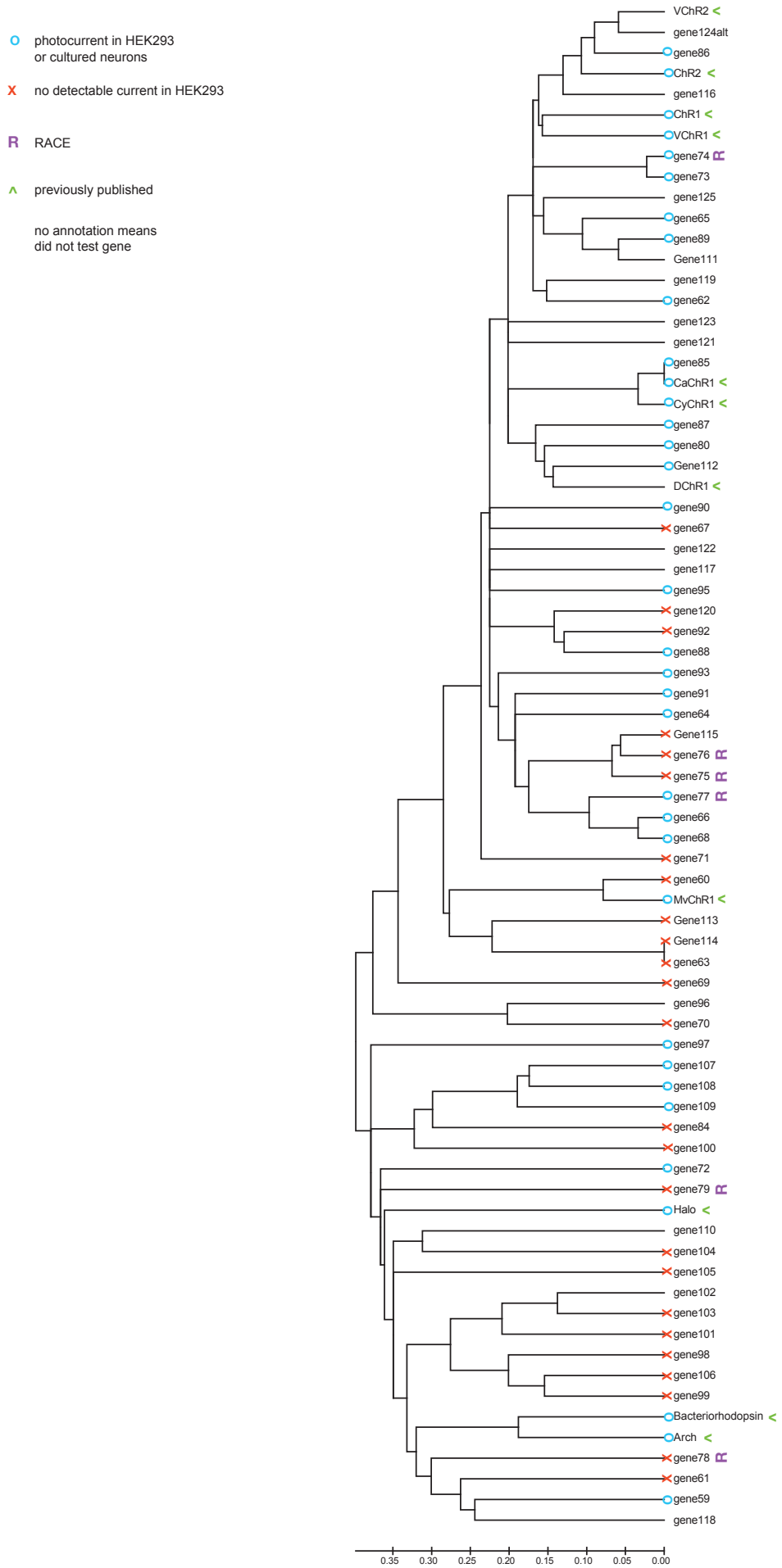

Supplementary Figure 2 – Sequence alignment.

Protein sequence alignment of algal opsins screened in cultured neurons (Fig. 1). Acidic residues are shown in red, basic residues are shown in blue. Transmembrane regions are denoted by black bar above alignment based on C1C2 crystal structure annotation. Schiff base lysine is annotated as *.

Nature Methods: doi:10.1038/nmeth.2836

Supplementary Figure 2

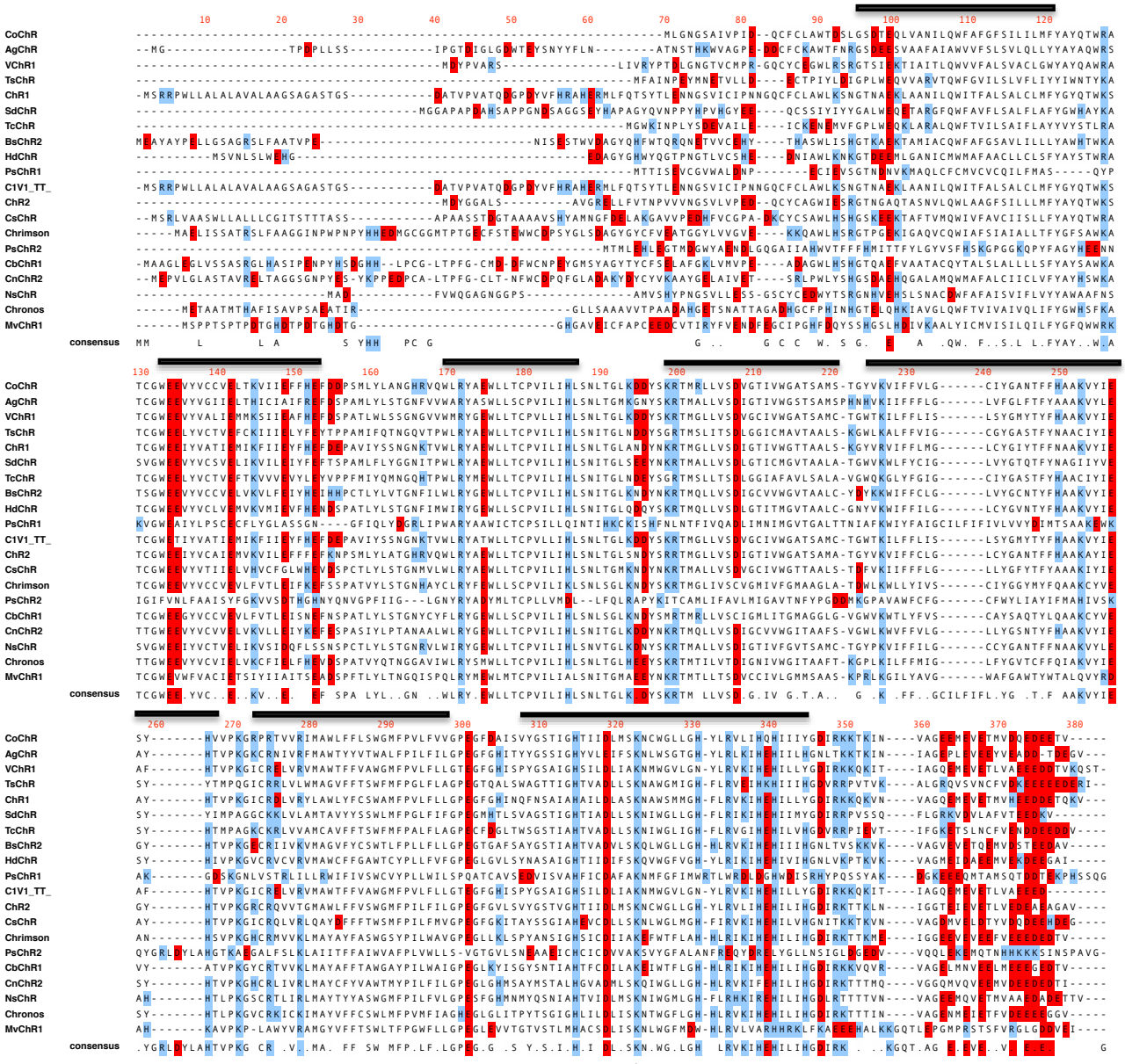

Nature Methods: doi:10.1038/nmeth.2836

Supplementary Figure 3 – Characterization of channel kinetics of Chronos and Chrimson in HEK293FT cells.

(a-b) Population data for channel closing rate (tau off) **(a)** and time to peak (time to reach 90% of peak photocurrent after the beginning of illumination) **(b)**, measured with 470 nm illumination and irradiance of 10 mW/mm^2, for ChR2, ChR2 E123A (aka ChETA$_A$), and Chronos, and 590 nm illumination and irradiance 4.6 mW/mm^2 for Chrimson (n = 5 – 8 HEK293FT cells each).
(c) Comparison of channel closing rate (tau off) at various holding potentials for ChR2 E123A and Chronos, measured with 470 nm illumination, irradiance of 10 mW/mm^2. Pulse durations were 2 ms for panels **a, c**, and 1 s for panel **b**. Statistics for panels **a** and **b**: ***, $P < 0.001$, t-test comparing ChR2 E123A (ChETA$_A$) vs. Chronos. All data are plotted as mean ± s.e.m. throughout.

Nature Methods: doi:10.1038/nmeth.2836

Supplementary Figure 3

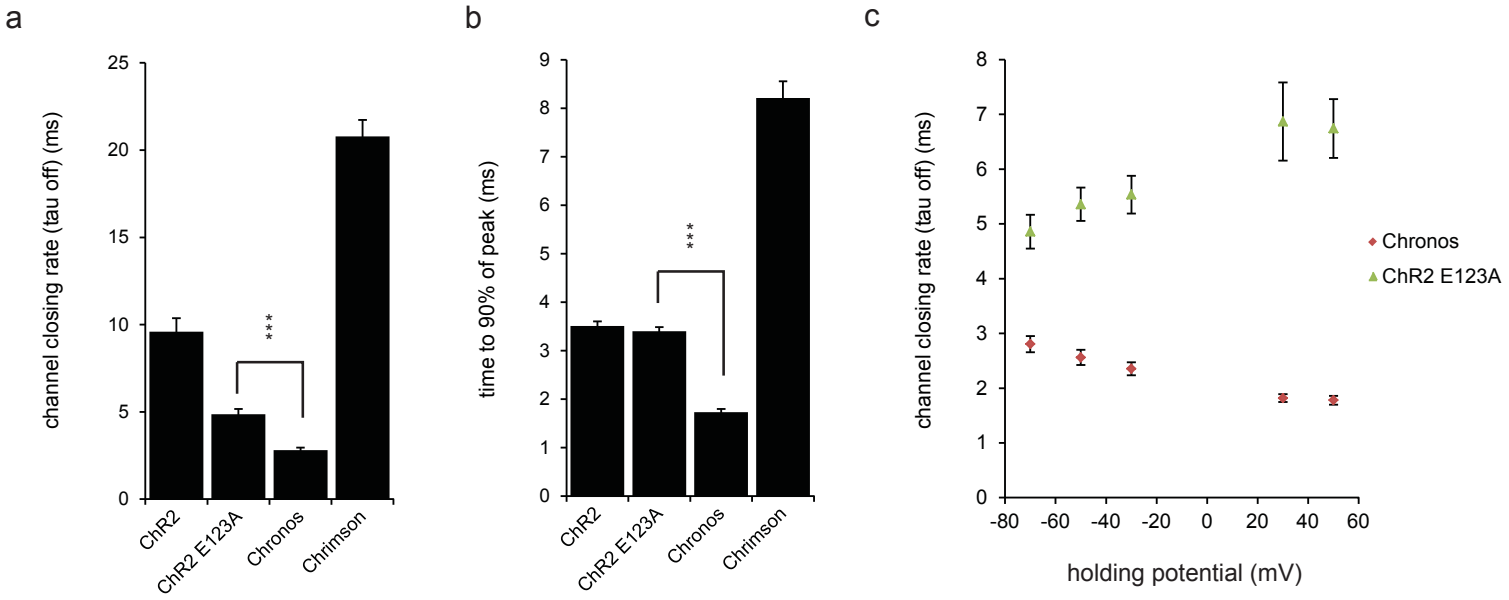

Nature Methods: doi:10.1038/nmeth.2836

Supplementary Figure 4 – Comparison of ion selectivity of Chronos, Chrimson, and ChR2.

(a-c) Population data for photocurrent density ratios, measured using whole-cell patch clamp in HEK cells in ion-specific extracellular solutions (see **Methods**); using 1 s illumination of 470 nm, irradiance of 10 mW/mm^2 for ChR2 and Chronos, 1s illumination of 590 nm, irradiance of 4.6 mW/mm^2 for Chrimson. Shown is data for ChR2, Chronos, and Chrimson (*n* = 6 – 10 HEK293FT cells each). **(a)** Calcium photocurrent (I_calcium) measured in 90 mM $CaCl_2$, pH 7.4, vs. sodium photocurrent (I_sodium) measured in 145 mM NaCl, pH 7.4. **(b)** Proton photocurrent (I_proton) measured in 135 mM NMDG, pH 6.4 vs. sodium photocurrent (I_sodium). **(c)** Potassium photocurrent (I_potassium) measured in 145 mM KCl, pH 7.4 vs. sodium photocurrent (I_sodium).

Supplementary Figure 4

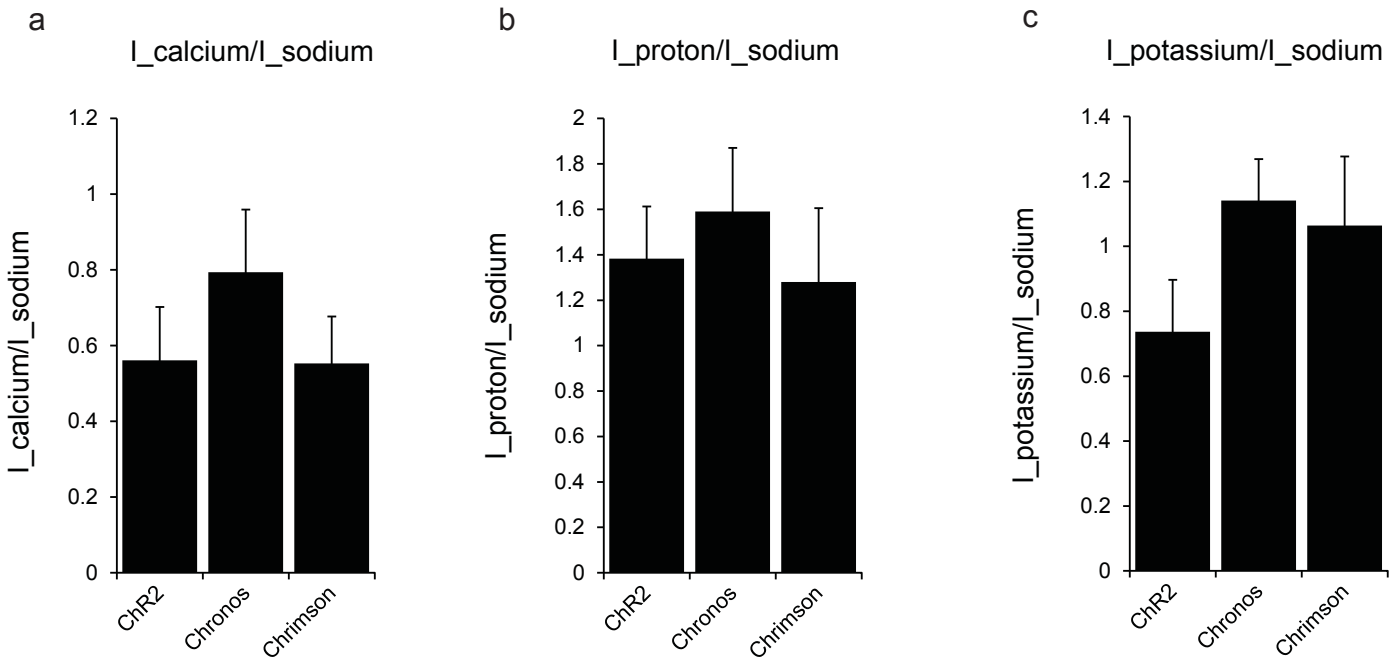

Supplementary Figure 5 – Opsin screening in cultured neurons.

(a) Representative GFP (left), tdTomato (center) and phase-contrast images (right) of a tdTomato and opsin-GFP fusion–transfected neuron in culture. The yellow border indicates the mask boundary used to quantify soma fluorescence. Scale bars, 10 μm. **(b)** Comparison of fluorescence and current density across all opsins screened. Each dot represents the data from a cell expressing one of the opsins in Fig. 1, pooled over all opsins. Photocurrent was measured for each opsin with the wavelength nearest its peak using 5 ms pulses (equal photon fluxes across wavelength; 470 nm, 4.23 mW/mm^2; 530 nm, 3.66 mW/mm^2; 625 nm, 3.14 mW/mm^2). **(c)** Opsin-GFP and tdTomato fluorescence for each construct patched and the membrane parameters indicated on the y-axes (n = 3 – 12 cells each). **(d)** Photocurrent measured at equal photon fluxes using 5 ms pulses (same irradiances as part **a**: n = 6 CsChR cells, n = 2 C1V1$_{TT}$ cells, n = 8 Chrimson cells). **(e)** Action spectra in HEK293FT cells done under the same conditions as Fig. 1e. Statistics for panels **b**: $^{*}P < 0.05$, $^{**}P < 0.01$ and $^{***}P < 0.001$, ANOVA with Dunnett's post hoc test, with ChR2 as the reference.

Supplementary Figure 5

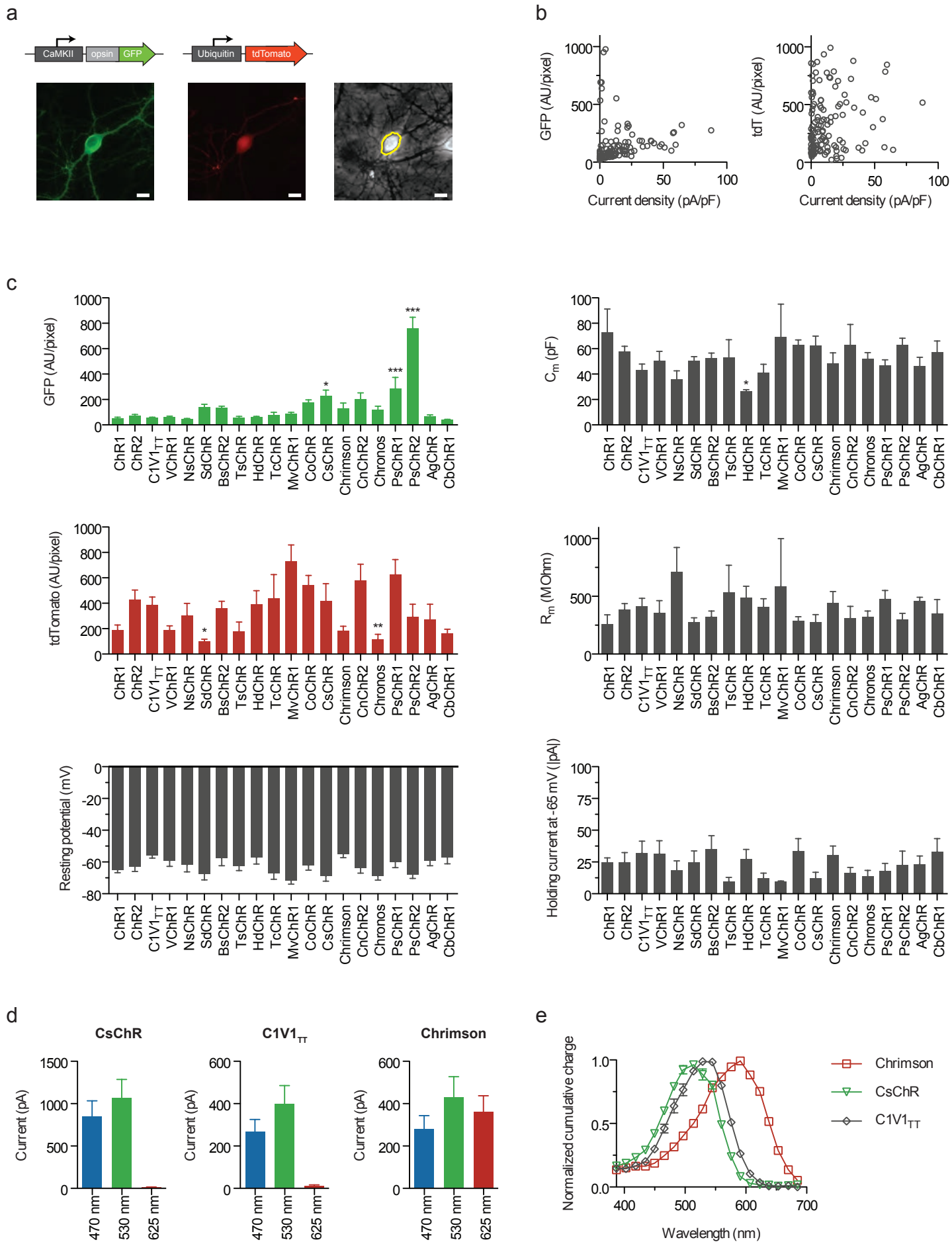

Supplementary Figure 6 – Opsin trafficking in cultured neurons.

Channelrhodopsin trafficking and photocurrent comparison from cultured neuron screening. Quantitative soma GFP fluorescence versus current measured at the light power of peak sensitivity (same conditions as Supplementary Fig. 5a) for each neuron experimented on (indicated by a circle) (left), GFP images for the median current (middle) and maximum current (right) cells are shown for each opsin. Scale bar, 10 μm. Note that in the GFP versus current plot, the GFP intensity values are absolute, and thus can be compared across opsins. However due to two-log-unit variance in absolute GFP intensity, the brightness and contrast settings used for the median images are varied across the different opsins, so the GFP images should not be used to compare brightness across constructs. That said, the brightness and contrast settings for each opsin's median and maximum current cells are matched, to illustrate whether higher expression correlates with increased photocurrent. See Methods for imaging conditions and **Supplementary Table 1** for full genus/species names.

Supplementary Figure 6

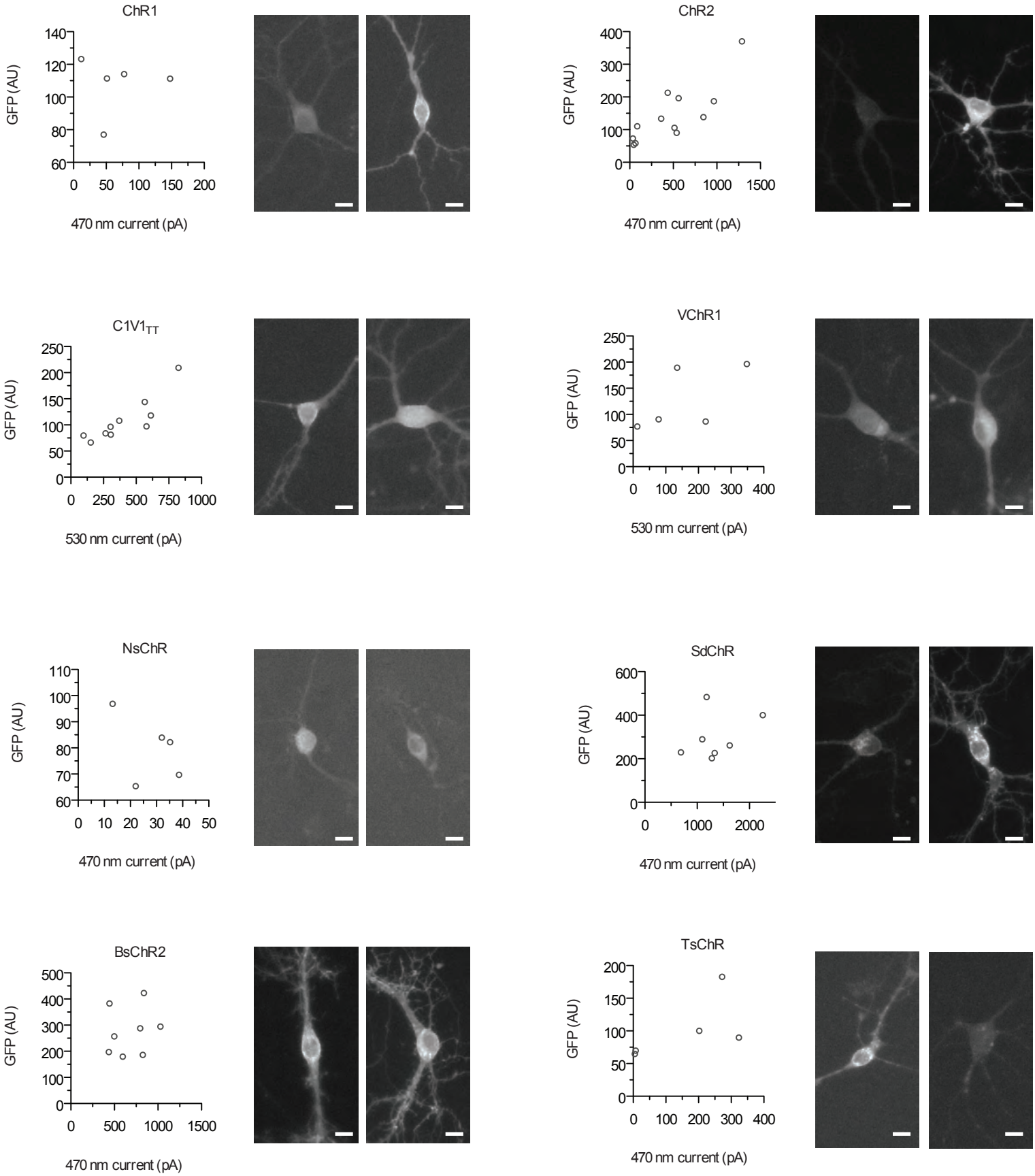

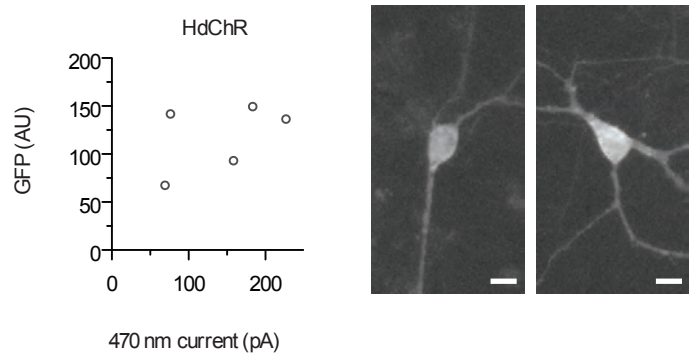

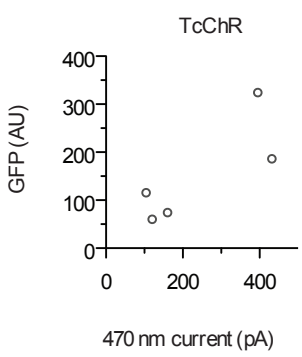

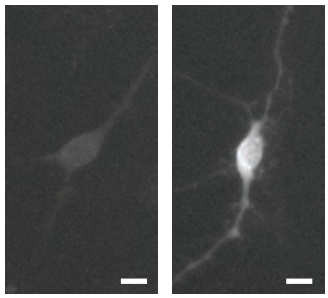

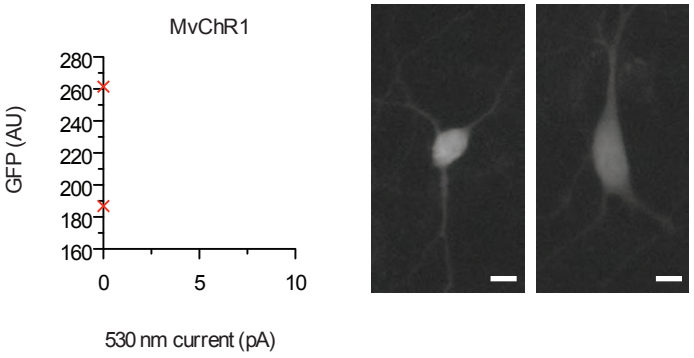

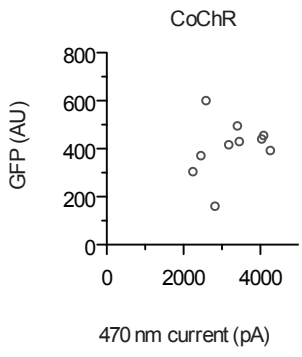

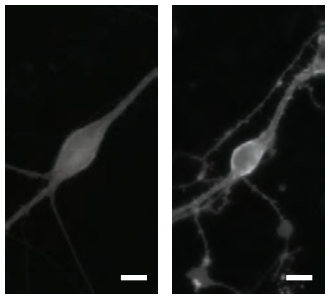

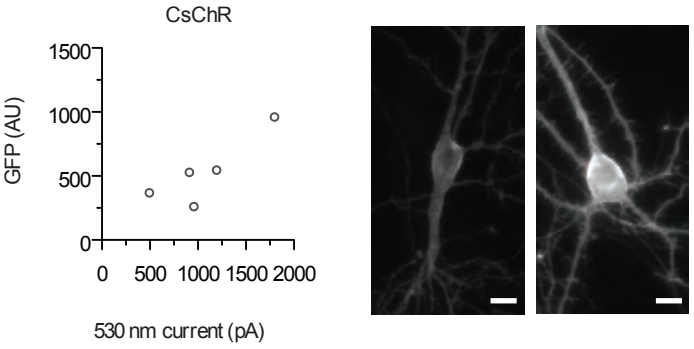

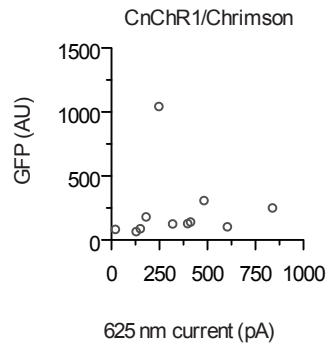

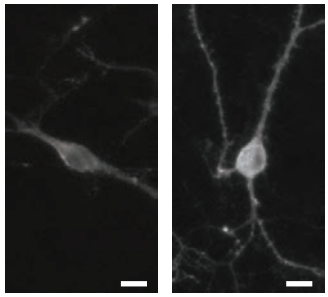

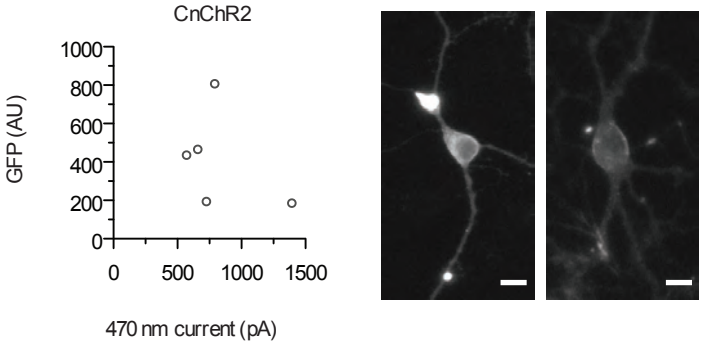

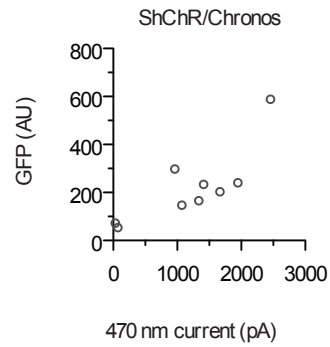

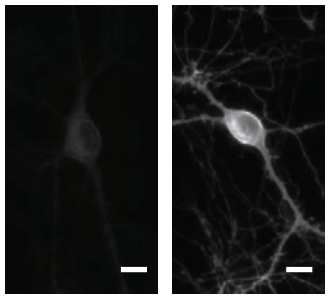

Nature Methods: doi:10.1038/nmeth.2836

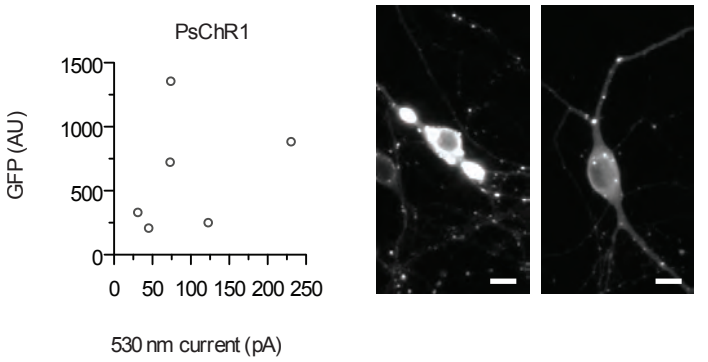
PsChR1
GFP (AU)
1500
1000
500
0
0 50 100 150 200 250
530 nm current (pA)

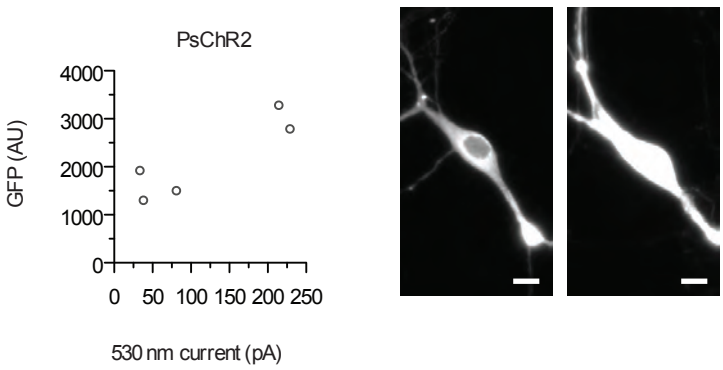
PsChR2
GFP (AU)
4000
3000
2000
1000
0
0 50 100 150 200 250
530 nm current (pA)

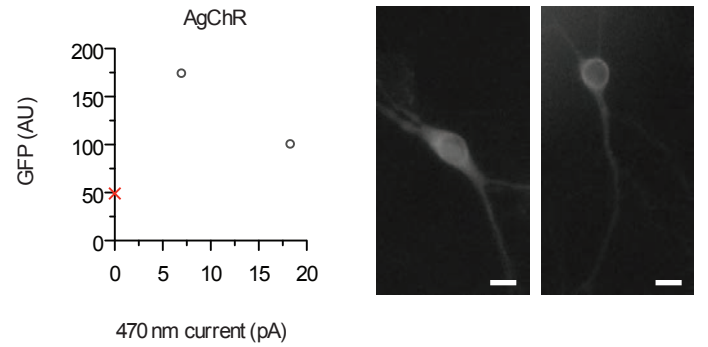
AgChR
GFP (AU)
200
150
100
50
0
0 5 10 15 20
470 nm current (pA)

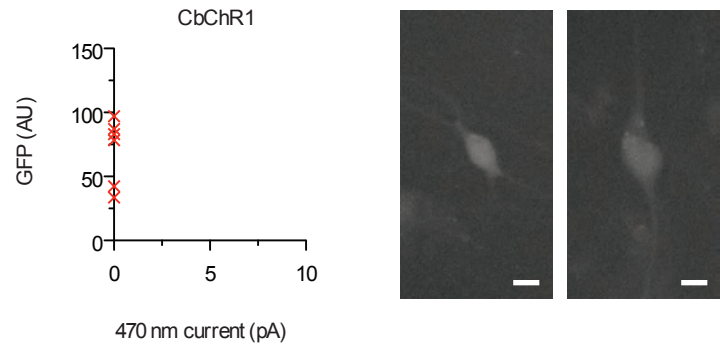
CbChR1
GFP (AU)
150
100
50
0
0 5 10
470 nm current (pA)

Supplementary Figure 7 – Inactivation and recovery kinetics.

Normalized traces of photocurrent recovery kinetics, with traces from each patched cell overlaid, with experiments as performed in **Fig. 1h**.

Nature Methods: doi:10.1038/nmeth.2836

Supplementary Figure 7

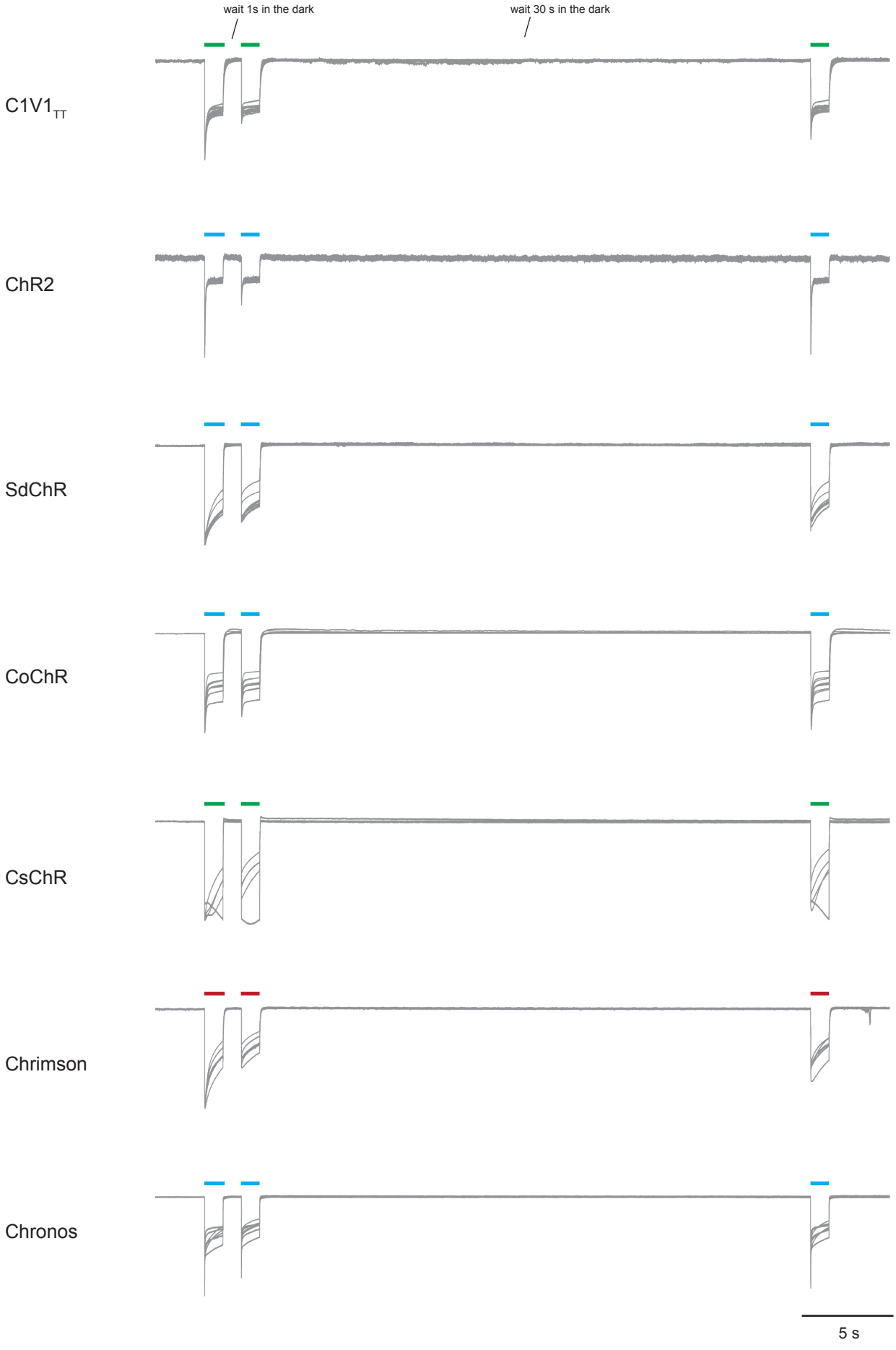

Nature Methods: doi:10.1038/nmeth.2836

Supplementary Figure 8 – Chronos full inactivation and recovery kinetics.

(a) Peak current recovery ratio vs. waiting time in darkness after 20 s of illumination (*n* = 3 cells), followed by a variable period of darkness, and assessed with a 50 ms pulse. **(b)** Representative trace showing Chronos inactivation has a fast and a slow component under continuous illumination.

Nature Methods: doi:10.1038/nmeth.2836

Supplementary Figure 8

a

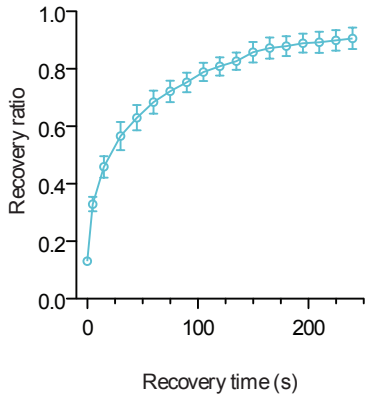

b

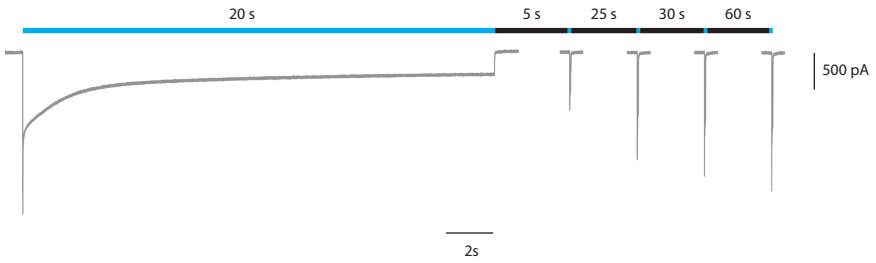

Supplementary Figure 9 – ReaChR and Chrimson comparison in cultured neurons.

Side-by-side comparisons of Chrimson and ReaChR's spectral sensitivity. tdTomato was co-expressed with opsin-GFP for unbiased selection of neurons. **(a-d)** Raw traces and photocurrent measurements at equal photon fluxes across wavelengths. All measurements were done first with red, then green, then blue (*n* = 5 cells; 5 ms pulse; 470 nm, 4.23 mW/mm^2; 530 nm, 3.66 mW/mm^2; 625 nm, 3.14 mW/mm^2). **(e)** Short vs. long pulse activation of ReaChR at 625 nm. Raw traces from a representative cell showing current in response to a 5 ms (left) vs. 1 s (middle) pulse of red light. Additional dashed lines on the 1 s pulse trace correspond to the current amplitude at the indicated time post-light-onset. Individual cell data is plotted on the right (*n* = 4 cells; 5 ms, 3.14 mW/mm^2; 1 s, 5 mW/mm^2). **(f)** Turn-on kinetics comparison in response to a 1 s pulse. (*n* = 4 – 6 cells; 625 nm, 5 mW/mm^2).

Supplementary Figure 9

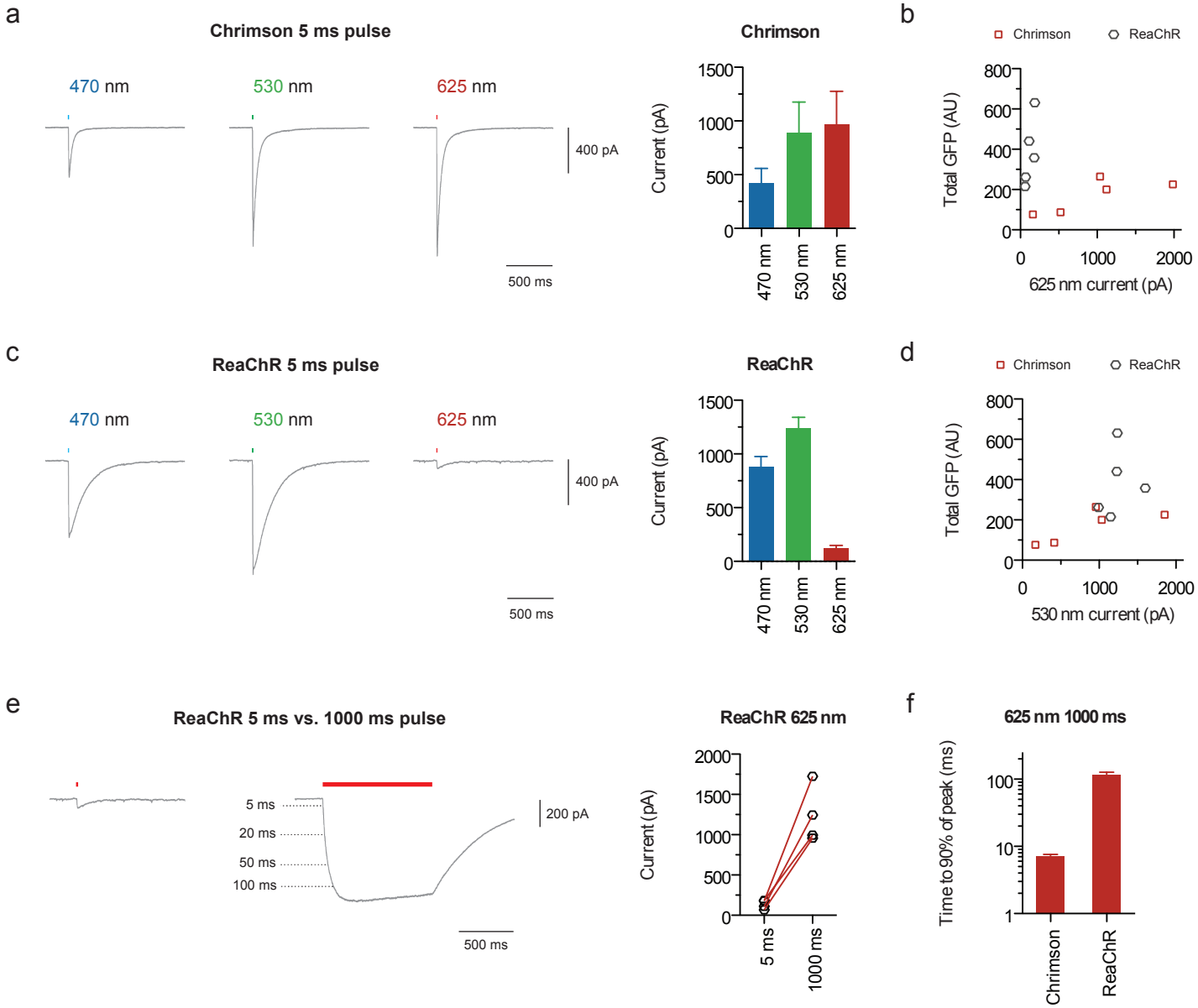

Nature Methods: doi:10.1038/nmeth.2836

Supplementary Figure 10 – Green light driven spiking frequency responses in cultured neurons.

(a-b) tdTomato was co-expressed with opsin-GFP for unbiased selection of neurons to patch. Any neuron that could not drive a train of 1 Hz, 10 pulses, of green (530nm) light at 5 mW/mm^2 with 100% spike probability was excluded from further spike frequency analysis, since the focus here was on high spike frequency fidelity. Generally neurons that could not drive spikes at 1Hz (indicated by red X's, as depicted in **a**) had lower GFP intensity than the neurons that could (indicated by black squares), in **b**. Each symbol is one cell. **(c)** Comparison of current measured at the end of 1 s green light (5 mW/mm^2), defined as I_{min} in the trace (left). Asterisk indicates escaped spike-like sodium current since TTX was not used. J_{min} is I_{min} divided by membrane capacitance. Symbols are defined in the same manner as in **a-b**. **(d-h)** Characterization of green light driven spike frequency responses for cells that passed the 1 Hz spiking test in **a-b**. Stimulation train consisted of 40 pulses of green light in all cases (n = 5 – 8 cells for each opsin). **(d)** Individual cell spike probability vs. frequencies over irradiances. Population summary is shown on the right. **(e)** Population data for spike fidelity within the 40 pulse stimulation train. **(f)** Individual cells' spike latency, defined as time from light onset to spike peak. **(g)** Membrane parameter controls to show that the observed spiking differences were not due to changes in neural excitability. **(h)** Comparison of measured and projected current density to estimate the effective driving force during optical spiking for cells that passed

the 1 Hz spiking test in **a-c**. Measured current density J_{min} is the same data set as panel **c**. Projected current densities (J_{max}, J_{max} for 2 ms pulse) are calculated by multiplying the measured J_{min} (from **h**) by the ratios (J_{max}/J_{min} or J_{max} for 2 ms/J_{min}) derived under the same illumination conditions but with TTX blockade (see **Supplementary Fig. 7**, for TTX data). "J_{max} for 2 ms pulse" refers to the maximum current density within the 2 ms post-light-onset interval. Statistics for panels **h**: $^{*}P < 0.05$, $^{**}P < 0.01$ and $^{***}P < 0.001$, ANOVA with Dunnett's post hoc test, with $C1V1_{TT}$ as the reference.

Nature Methods: doi:10.1038/nmeth.2836

Supplementary Figure 10

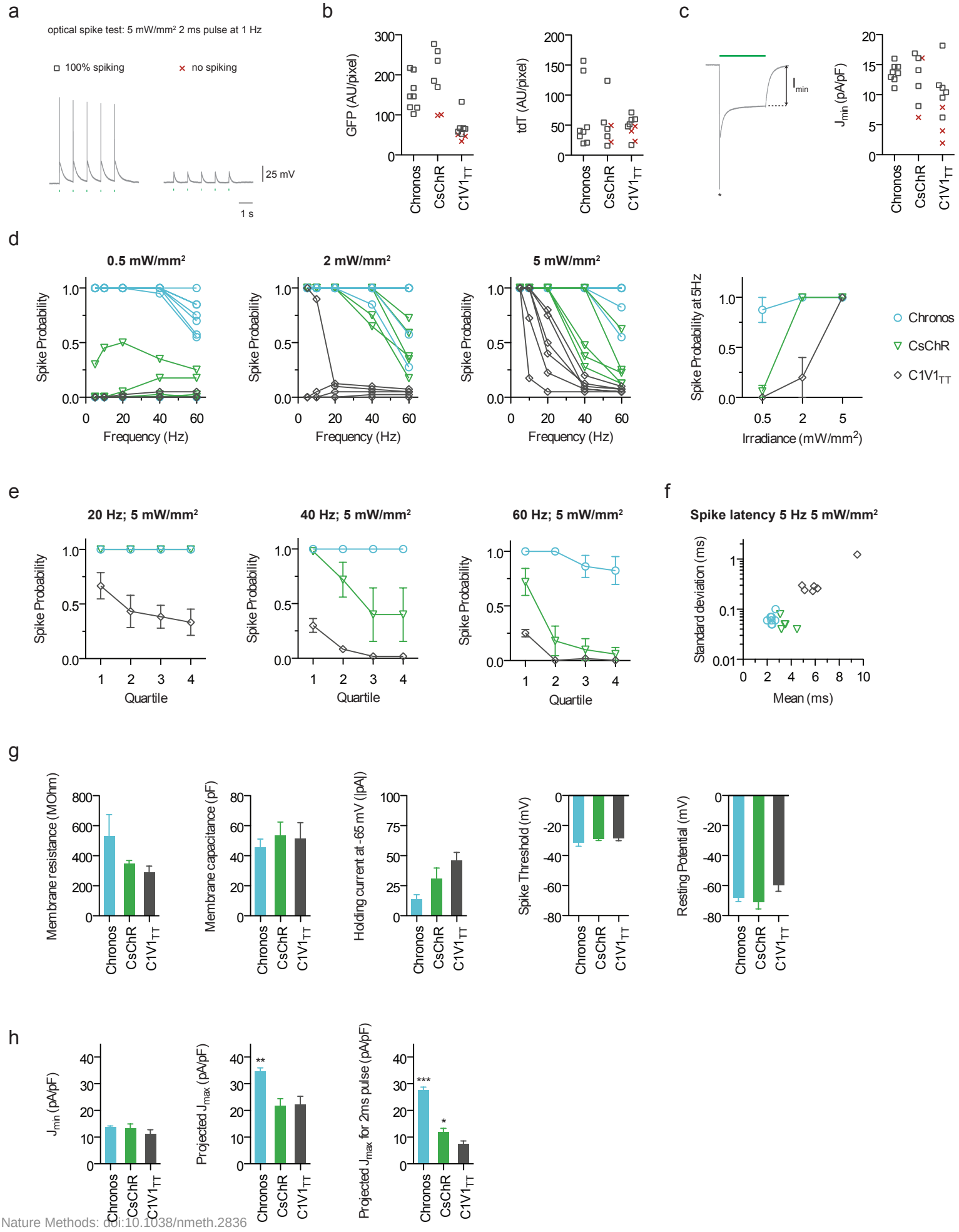

Nature Methods: doi:10.1038/nmeth.2836

Supplementary Figure 11 – Electrical versus green light driven spiking fidelity in cultured neurons.

Additional analysis of optical versus electrical spike probability over various frequencies at 5 mW/mm^2; same dataset as **Supplementary Fig. 10d-h**. Electrical stimulation protocol was the same as optical, except the pulse duration was 5 ms and the input current was varied between 200-800 pA to maximize spike probability. Plateau potential was measured as the voltage difference between two horizontal dotted lines as shown in each trace. A single dash to the left of electrical traces indicates –65 mV. Statistics for **b, e,** and **h**: Paired t-test between electrical and optical spiking were computed at each frequency: $^{*}P < 0.05$, $^{**}P < 0.01$ and $^{***}P < 0.001$.

Supplementary Figure 11

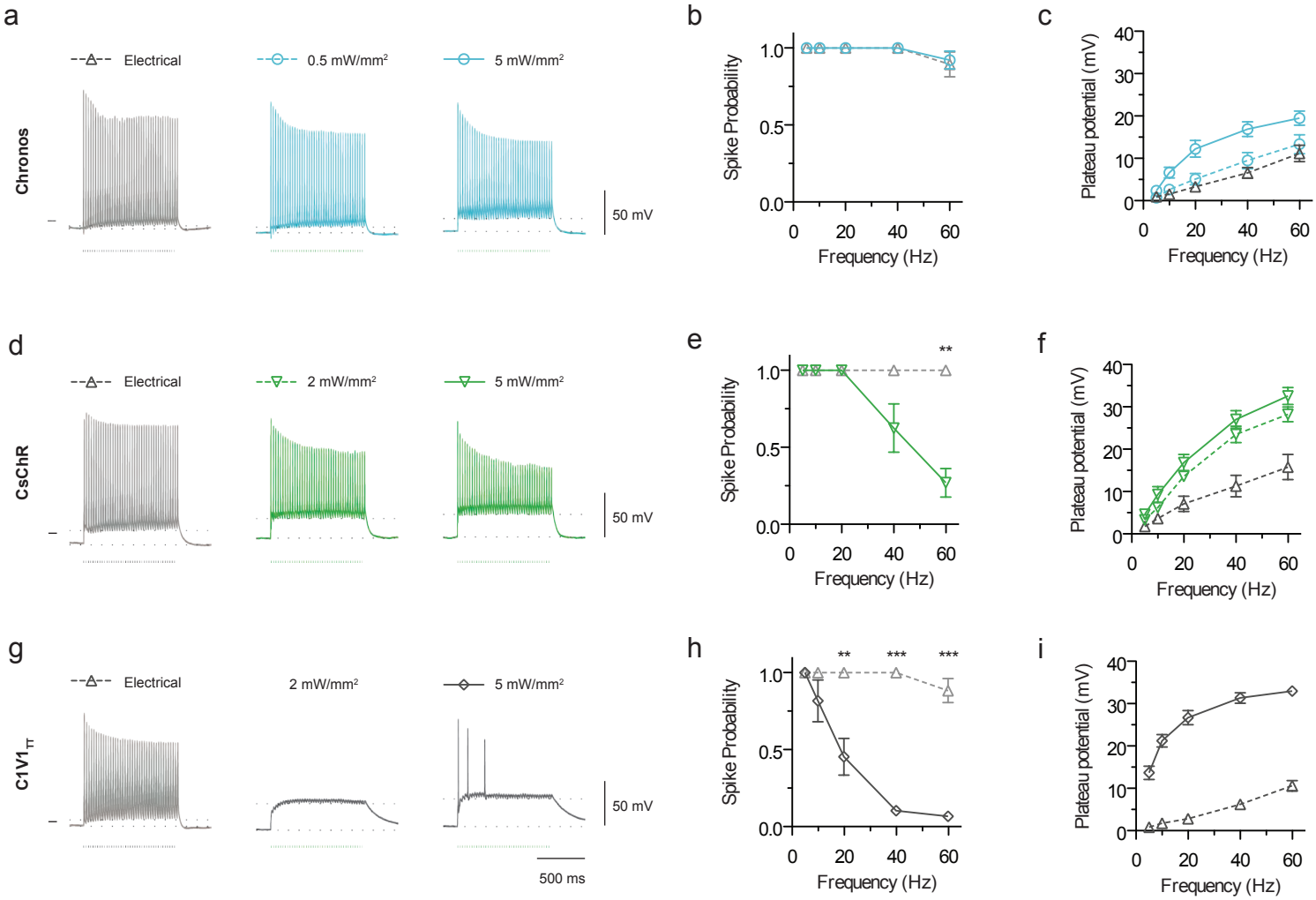

Nature Methods: doi:10.1038/nmeth.2836

Supplementary Figure 12 – Red light driven spiking in cultured neurons.

(a-d) Red (625 nm) light spike frequency data for Chrimson-expressing neurons selected based on the presence of tdTomato co-expression (*n* = 6 cells). Stimulations were as performed in Fig. 2e (train of 40 pulses, 2 ms pulse duration). **(a)** Optical vs. electrical spiking showing Chrimson can reliably drive spikes only at <20 Hz. **(b)** Chrimson's spike fidelity can decrease at higher red irradiance due to channel inactivation and/or depolarization block. **(c-d)** Spike latency, defined as light onset to spike peak, is both a function of irradiance **(c)** and Chrimson expression level **(d)**. **(e)** Action spectrum of a ChrimsonR expressing HEK293 cell (*n* = 1 cell). **(f)** Current measured at the end of 1 s light pulse (I_{min}) for Chrimson- or ChrimsonR-expressing cultured neurons. Population mean and s.e.m. are plotted as black line. **(g)** Chronos red (625 nm) light crosstalk characterization (*n* = 4 cells). Peak voltage crosstalk for 5 ms pulses at 5 Hz and for continuous 500 ms pulse, representative cell (left) and population average (right). Statistics for **a**: Paired t-test between electrical and optical spiking were computed at each frequency: $^{*}P < 0.05$, $^{**}P < 0.01$ and $^{***}P < 0.001$.

Supplementary Figure 12

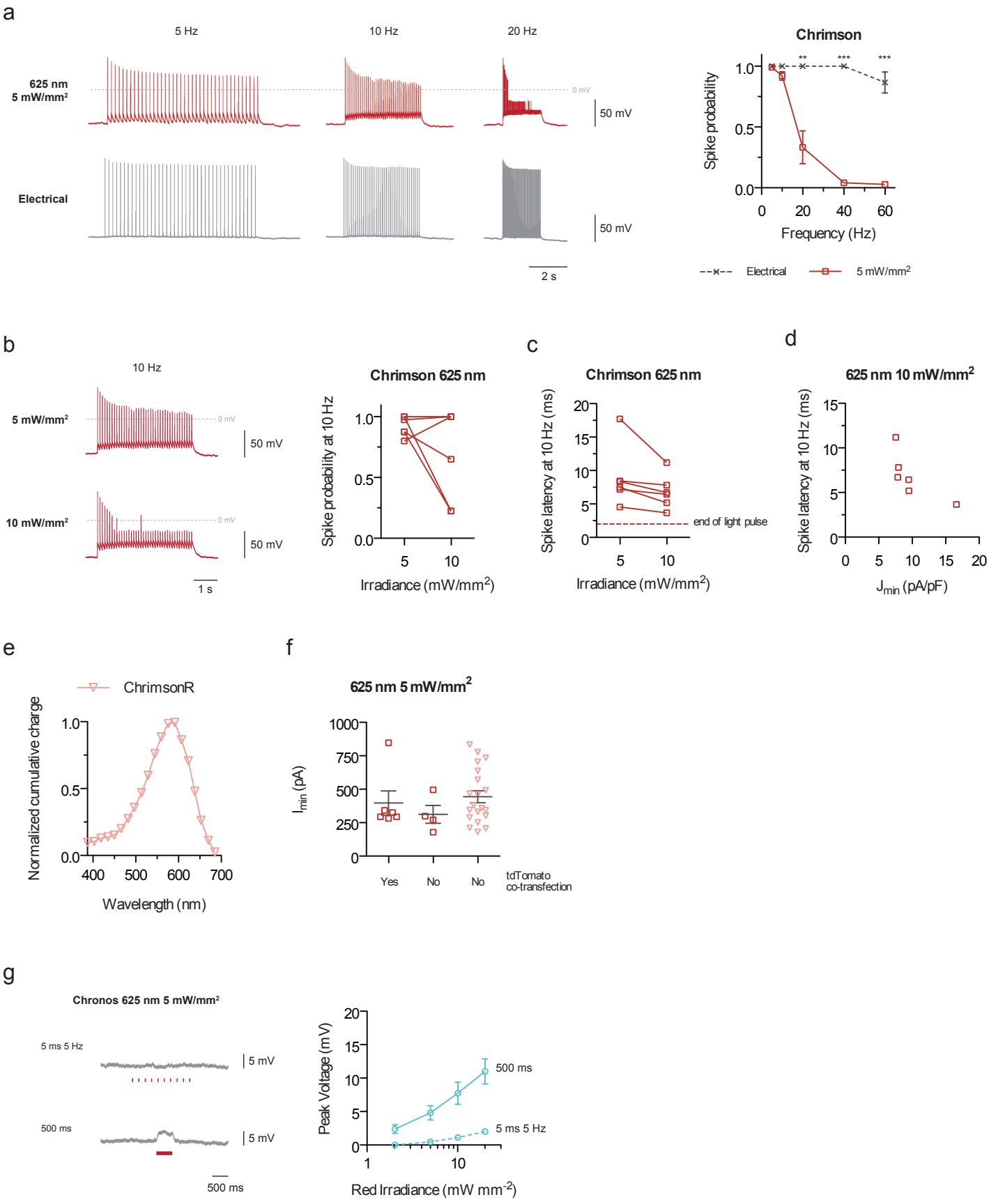

Supplementary Figure 13 – Red and far-red spiking with ChrimsonR in acute cortical slice.

Spectral and kinetic characterization of ChrimsonR in slice (*n* = 4 neurons from one P60 mouse throughout figure; pCAG-ChrimsonR-tdTomato was electroporated as specified in Methods). **(a)** ChrimsonR histology showing layer 2/3 expression (left, scale bar = 50 μm) and individual neuron expression (right, scale bar = 10 μm). **(b)** 625 nm spiking fidelity at 20 Hz (5 ms, 40 pulses, 3 sweeps overlaid). **(c)** Far-red 735 nm spiking with ChrimsonR (5 sweeps overlaid per condition). Traces from a representative trace from a single neuron (left), population average (middle), and membrane properties (right).

Nature Methods: doi:10.1038/nmeth.2836

Supplementary Figure 13

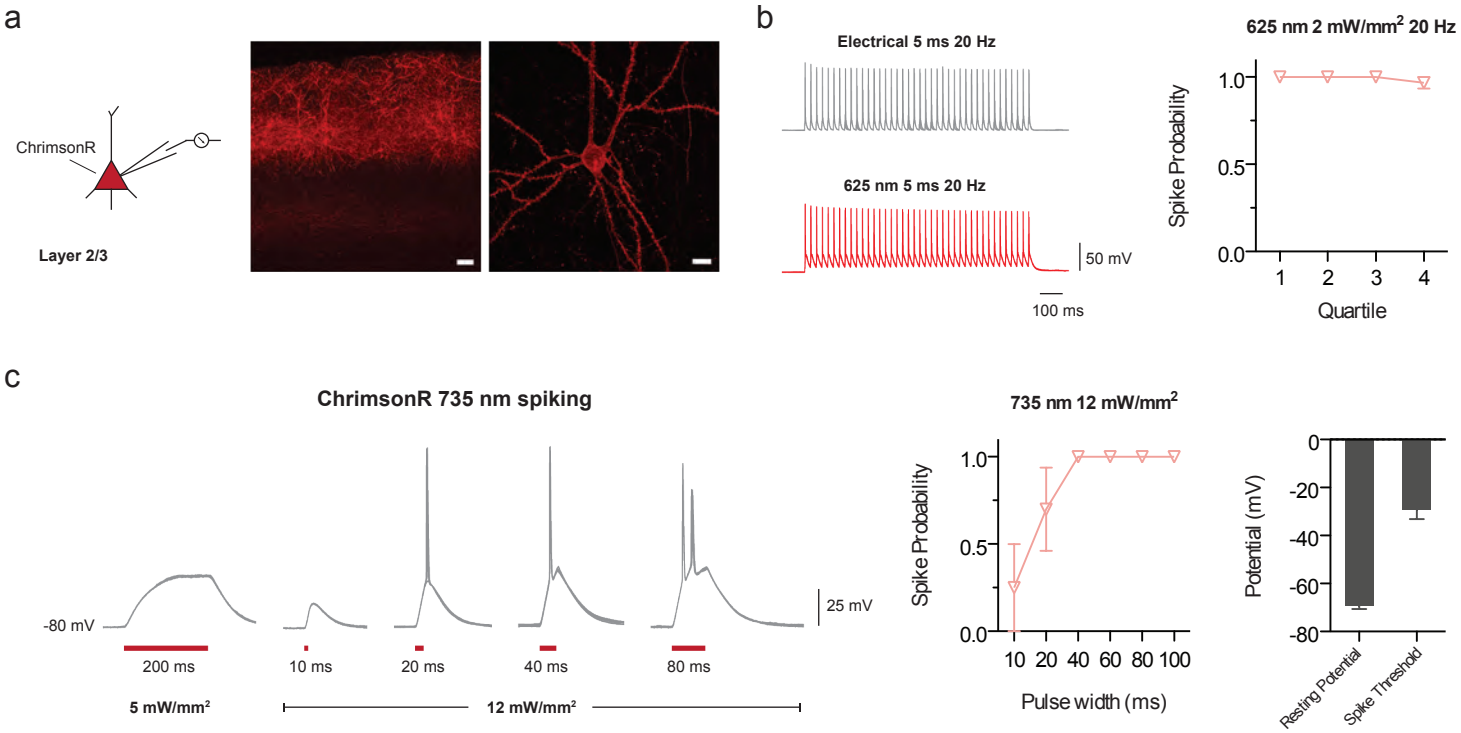

Nature Methods: doi:10.1038/nmeth.2836

Supplementary Figure 14 – Larval motor axons expressing ChR2 fire in response to blue but not red light pulses.

(a,b) Intracellular recordings from m6 muscles in 3rd instar larvae expressing ChR2 in motor neurons. Responses to 470 nm and 617 nm light pulses of increasing duration are shown. EJPs were only triggered by 16 ms pulses. Dashes in each panel indicate –50 mV. **(c)** Probability of light-evoked EJPs after 1, 2, 4, 8, and 16 ms pulses in response to 470nm and 617nm light. As in **Fig. 3d**. **(d)** Mean ± s.e.m. number of EJPs evoked in response to light pulses. As in **Fig. 3e**. Sample size in each case: *n* = 6 muscles from 3 animals.

Supplementary Figure 14

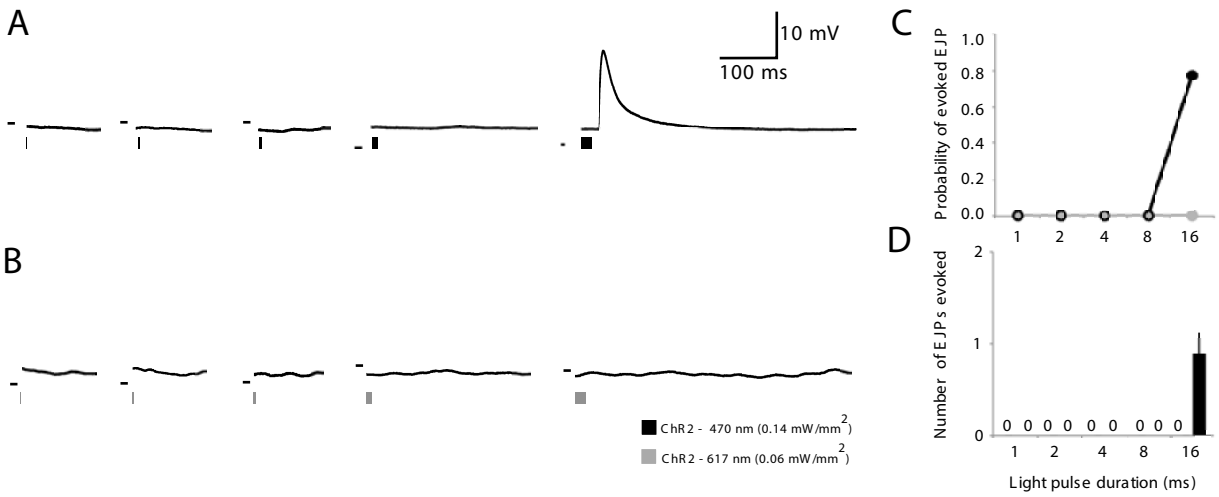

Supplementary Figure 15 – Proboscis extension reflex (PER).

(a) PER score was computed as (P-H)/H, where H is the pixel distance between the root of antennae and the neck connective (i.e., the head capsule) and P is the maximum horizontal pixel distance from the center of the head to the tip of proboscis during 0–2 seconds after initiation of each trial. **(b, c)** PER of three different fly groups to 25 light pulses at 470nm **(b)** and 617nm **(c)**. *n* = 5 for each population. (**d**) PER to light stimulation without CsChrimson expression in sugar receptors. Data is from the same video recording analyzed for startle response in **Fig. 3g**.

Nature Methods: doi:10.1038/nmeth.2836

Supplementary Figure 15

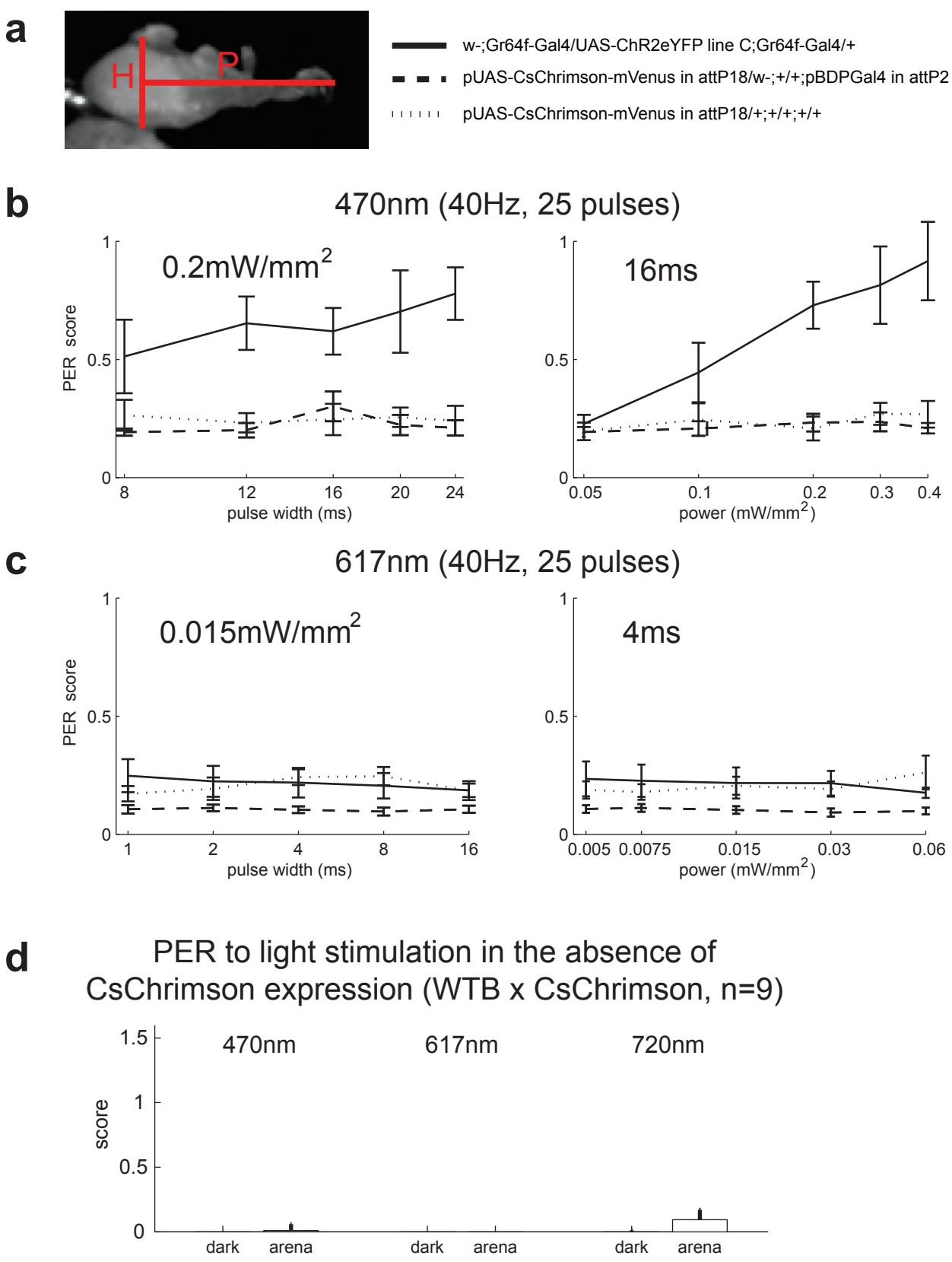

Nature Methods: doi:10.1038/nmeth.2836

Supplementary Figure 16 – Optogenetics of freely behaving intact flies.

(a) Hardware configuration of a circular light arena for deep brain stimulation of freely behaving flies with intact cuticle. Note that the LED array is divided into 4 quadrants (Q1~Q4). (**b**) Fraction of flies in quadrants 1 and 3 for the experimental group. If more than 50% of flies are in the illuminated quadrants, the error bar enters into to the red-shaded zones of the plot. Flies with CsChrimson expression in PNv-1 neurons avoid illuminated area. See also **Supplementary Video 6**. (**c**) Flies of control group do not avoid illuminated area.

Nature Methods: doi:10.1038/nmeth.2836

Supplementary Figure 16

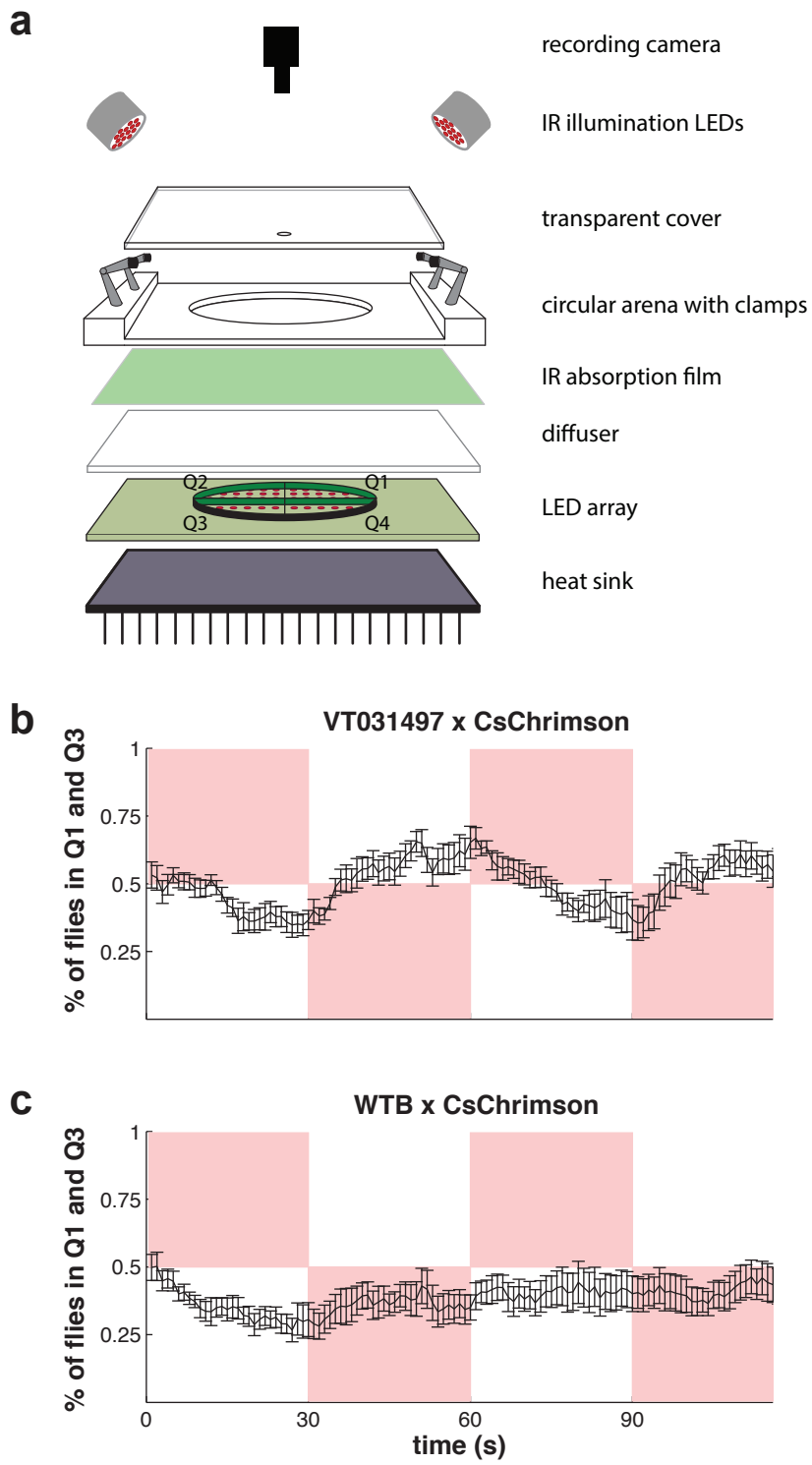

Supplementary Figure 17 – Two-color excitation controls in cultured neurons.

(a) Current density at end of 1 s light pulse (5 mW/mm^2, 470 nm light) J_{min} is defined in the same manner as **Supplementary Fig. 10c**. This is from the same dataset as **Fig. 4f**. **(b)** Averaged traces of ChR2-, Chronos-, and Chrimson-expressing neurons at the indicated irradiances of 470 nm light (*n* = 4 – 7 cells for each opsin; 1 second pulse; traces are truncated to the first half of illumination). **(c)** Chrimson blue current in response to 5 ms or 1 s pulses. Traces from a representative cell (left) and population average (right) (*n* = 4 cells). **(d)** ChrimsonR blue light voltage crosstalk for individual cells (*n* = 7 cells). Same condition as **Fig. 4b**.

Nature Methods: doi:10.1038/nmeth.2836

Supplementary Figure 17

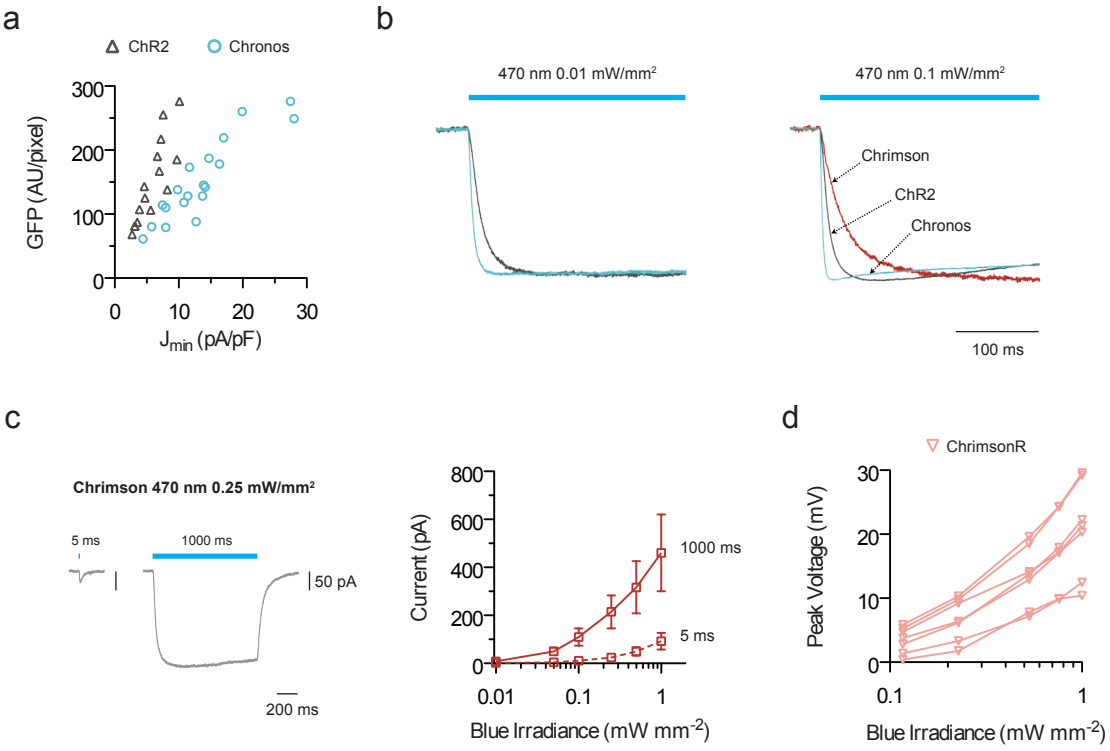

Supplementary Figure 18 – Optically evoked post-synaptic currents (PSCs) in acute slice.

(a) Widefield illumination with 20x objective (1.6 mm diameter spot size at the focal plane) was used to optically drive spikes in the opsin expressing pre-synaptic neurons. Both pre- and post-synaptic neurons are in layer 2/3. **(b-d**) Either Chronos or Chrimson is expressed in the cortical brain slice; not both. All stimulations were done at 0.2 Hz. Color and irradiance are as used in **Fig. 5g-j** unless otherwise indicated. **(b)** Chronos PSC from the same neuron shows faster onset and greater amplitude (potentially with multiple PSC peaks) at higher blue irradiance. Trials are overlaid for each irradiance. Vertical dashed lines denote the start and end of 5 ms light pulse for all traces (and also providing a time scale reference). **(c)** Multiple traces, not overlaid, showing trial-to-trial variability for Chrimson PSC at 4 mW/mm^2 of red light. **(d)** Chronos PSC at various holding voltages shows immediate excitatory PSC followed by strong inhibitory PSC in response to 1 mW/mm^2 of blue light. **(e)** Red and blue light driven post-synaptic responses from five different non-expressing neurons downstream of opsin-expressing neurons, in brain slice now expressing both Chronos and Chrimson. Here, the dashed lines indicate timing, and the color of the shaded bar within, the color of light delivered. Black trace is the averaged response, grey traces are individual trials, throughout this figure.

Supplementary Figure 18

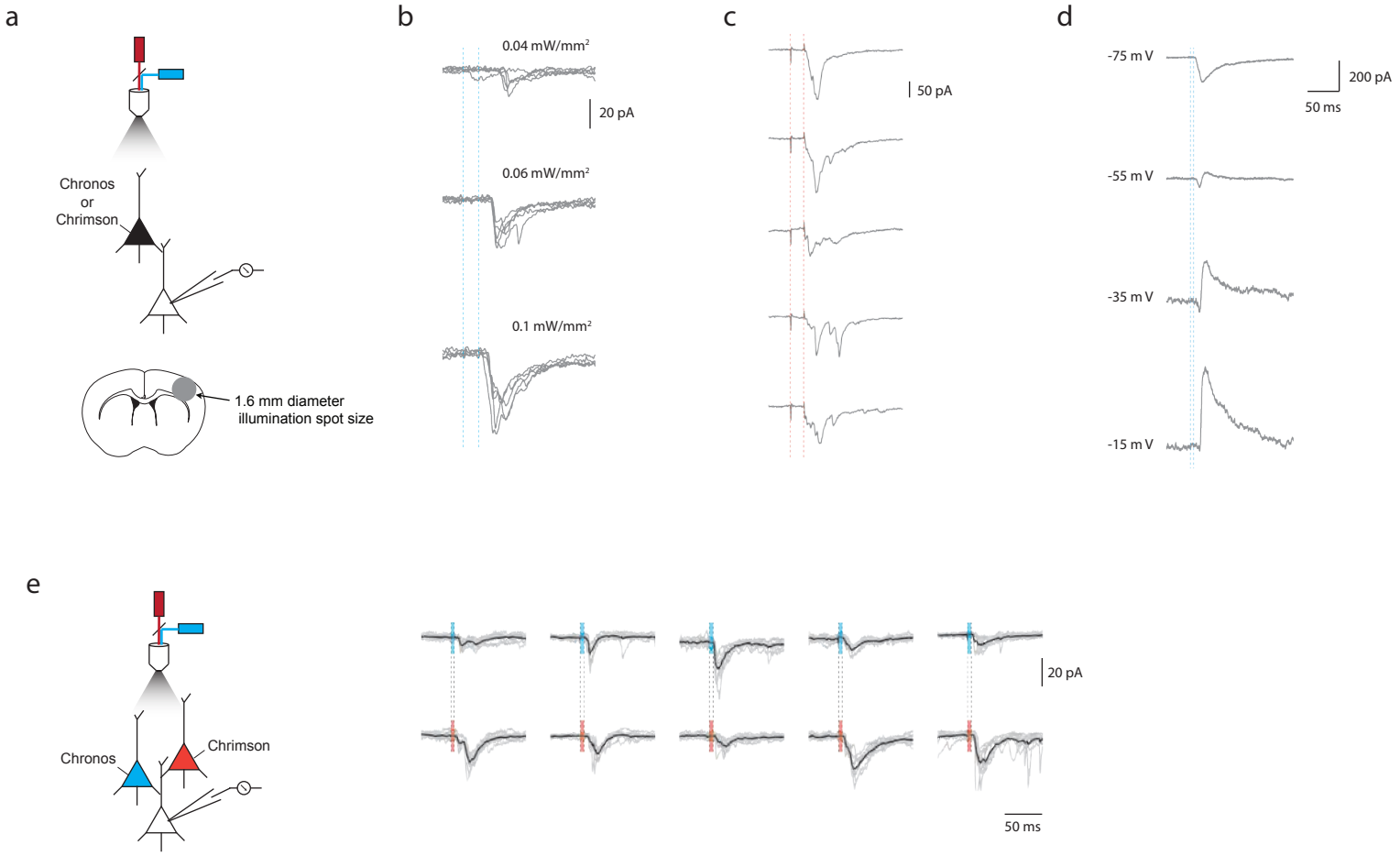

Supplementary Figure 19 – Optically evoked paired-pulse responses in acute slice.

(a-c) Chrimson and Chronos expressed in separate neurons in the same slice using triple plasmid in utero electroporation. Patched neurons are post-synaptic to both Chrimson and Choronos based on optical response to blue and red light. **(a)** Paired-pulse responses (PPR) for an exemplar neuron. Blue-blue stimulation exhibited facilitation, while other paired pulses were linear summation of individual pulse response. 470 nm, 0.2 mW/mm^2; 625 nm, 1 mW/mm^2. 5 ms pulse width and inter-pulse interval 50 ms throughout this figure. Black trace is the averaged response, grey traces are individual trials, throughout this figure. **(b-c)** Blue-blue and red-red responses from the same neuron showed no differences in the blue paired PSC, while the second red pulse response often failed at 50 ms.470 nm, 0.37 mW/mm^2; 625 nm, 1mW/mm^2. **(d-g)** Chrimson and Chronos expressed in separate slices. 470nm, 0.3 mW/mm^2, 625 nm, 4 mW/mm^2 used throughout. **(d-e)** PPR recorded downstream of Chronos-expressing neurons. Representative trace **(d)** and averaged PPR in four different neurons **(e),** showing reliable Chronos drive . **(f-g)** PPR recorded downstream of Chrimson-expressing neurons. Representative trace **(f)** and averaged PPR in four different neurons **(g)**, showing second pulse fails due to kinetic limitation of Chrimson. An inhibitory PSC (voltage clamped at –55 mV) was recorded from one neuron, most likely due to mistargeting during *in utero* electroporation.

Nature Methods: doi:10.1038/nmeth.2836

Supplementary Figure 19

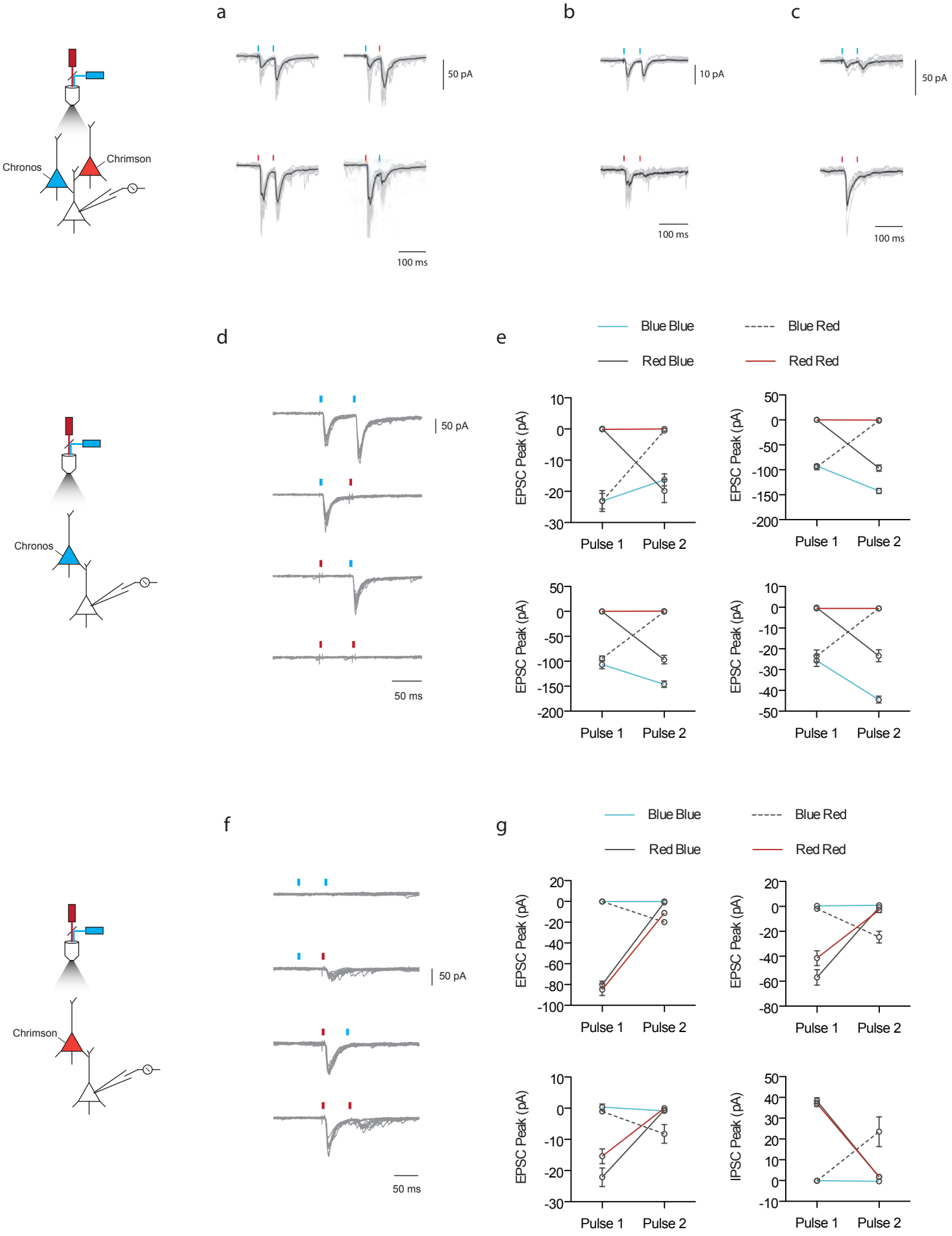

Nature Methods: doi:10.1038/nmeth.2836

Supplementary Figure 20 – Comparisons of spiking and post-synaptic response timing in acute slice.

(a) Time-to-spike-peak as a function of irradiance when optically driving Chrimson neurons in the red and Chronos neurons in the blue; color and pulse duration as in **Fig. 5b-d.** Values shown are population average ± standard deviation. In all subpanels, red squares denote Chrimson, blue circles denote Chronos (*n* = 9 cells, 3 mice, Chrimson; *n* = 11 cells, 4 mice, Chronos). **(b)** Time-to-spike-peak for individual Chronos- (0.3 mW/mm^2 blue light) and Chrimson-expressing (5 mW/mm^2 red light) neurons. Values are trial mean and standard deviation (cells patched from 3-4 mice for each opsin). **(c)** Post-synaptic current latency (time from beginning of light pulse, to 10% of synaptic current peak) for individual neurons post-synaptic to Chronos (0.3 mW/mm^2 blue) or post-synaptic to Chrimson (4 mW/mm^2 red). Values shown are trial averages and standard deviation (cells patched from 2-4 mice for each opsin).

Nature Methods: doi:10.1038/nmeth.2836

Supplementary Figure 20

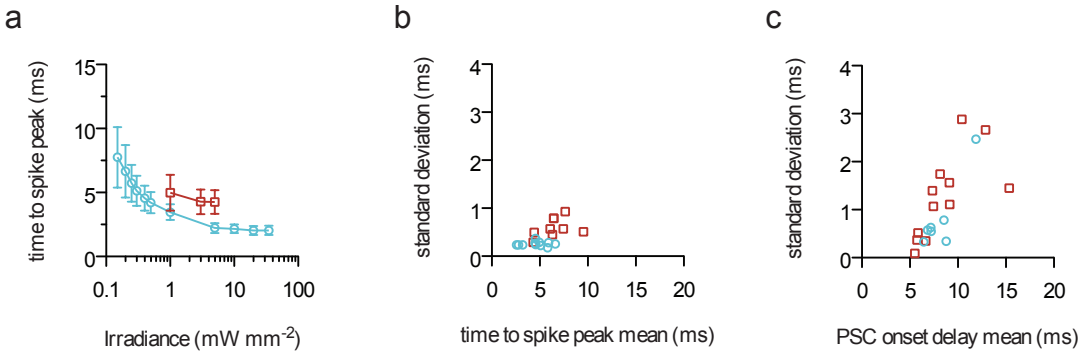

Supplementary Figure 21 – Retina to superior colliculus projection stimulation with Chronos.

Post-synaptic responses recorded in a superior colliculus neuron, downstream of Chronos expressed in retinal ganglion cells. See methods for retinal virus delivery details. **(a)** Diagram of retina projection to superior colliculus (adapted from Paxinos, G. & Franklin, K.B.J. *The Mouse Brain in Stereotaxic Coordinates* 2nd edn. Academic Press, 2001). **(b)** Histology of Chronos-GFP axons from sagittal section of superior colliculus. Scale bar is 100 μm. **(c-d)** Post-synaptic current and potential in response to blue light at multiple irradiances (5 pulses, 1 Hz, 5 ms pulse duration in all cases. Traces from a neuron recorded from a P18 mouse).

Nature Methods: doi:10.1038/nmeth.2836

Supplementary Figure 21

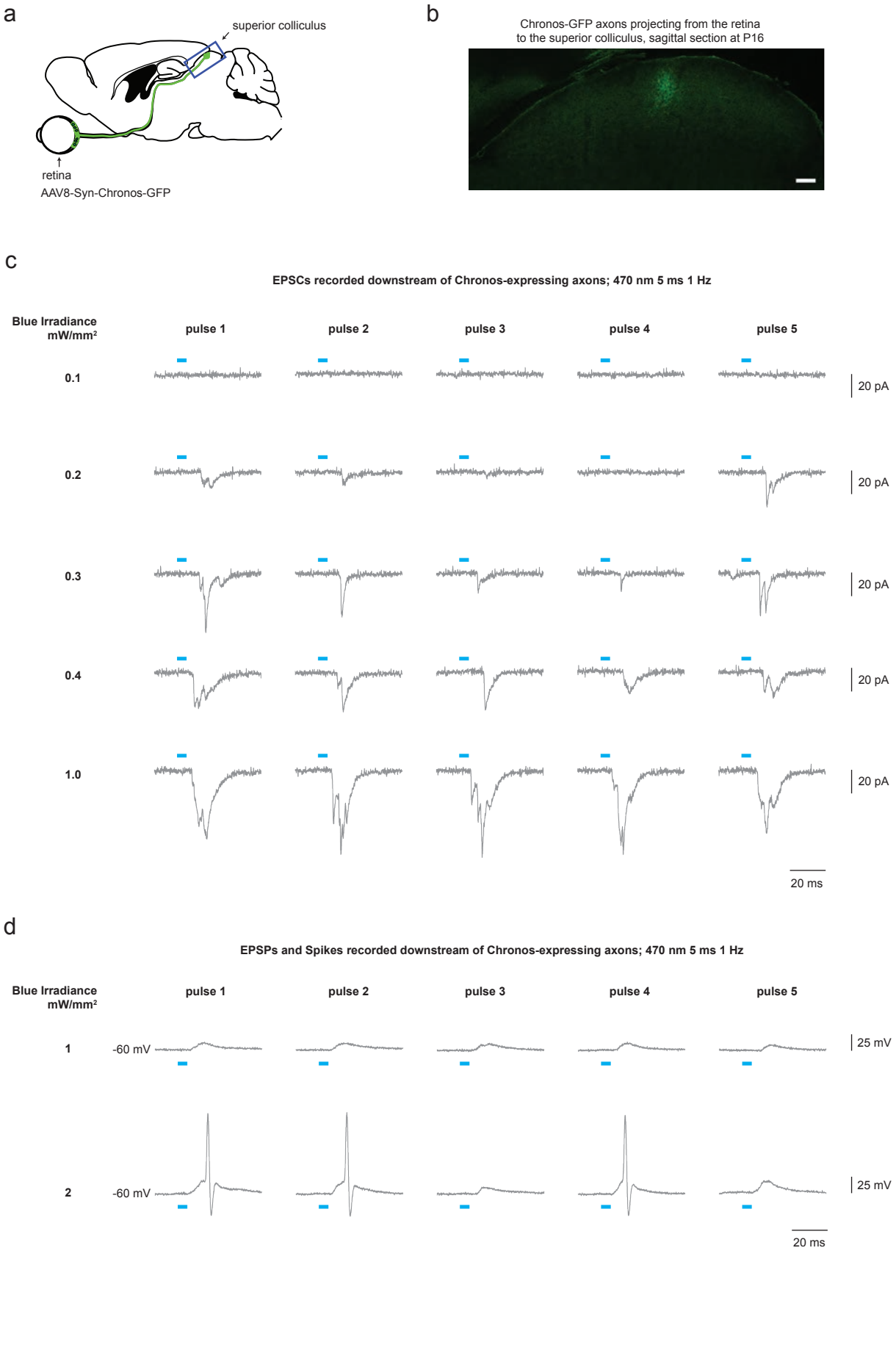

Supplementary Figure 22 – Post-synaptic current raw traces.

Unfiltered traces with LED stimulation artifact. Panel **(a)**, **(b)**, and **(c)** corresponds to the filtered traces in **Fig. 5g**, **h**, and **i** respectively.

Nature Methods: doi:10.1038/nmeth.2836

Supplementary Figure 22

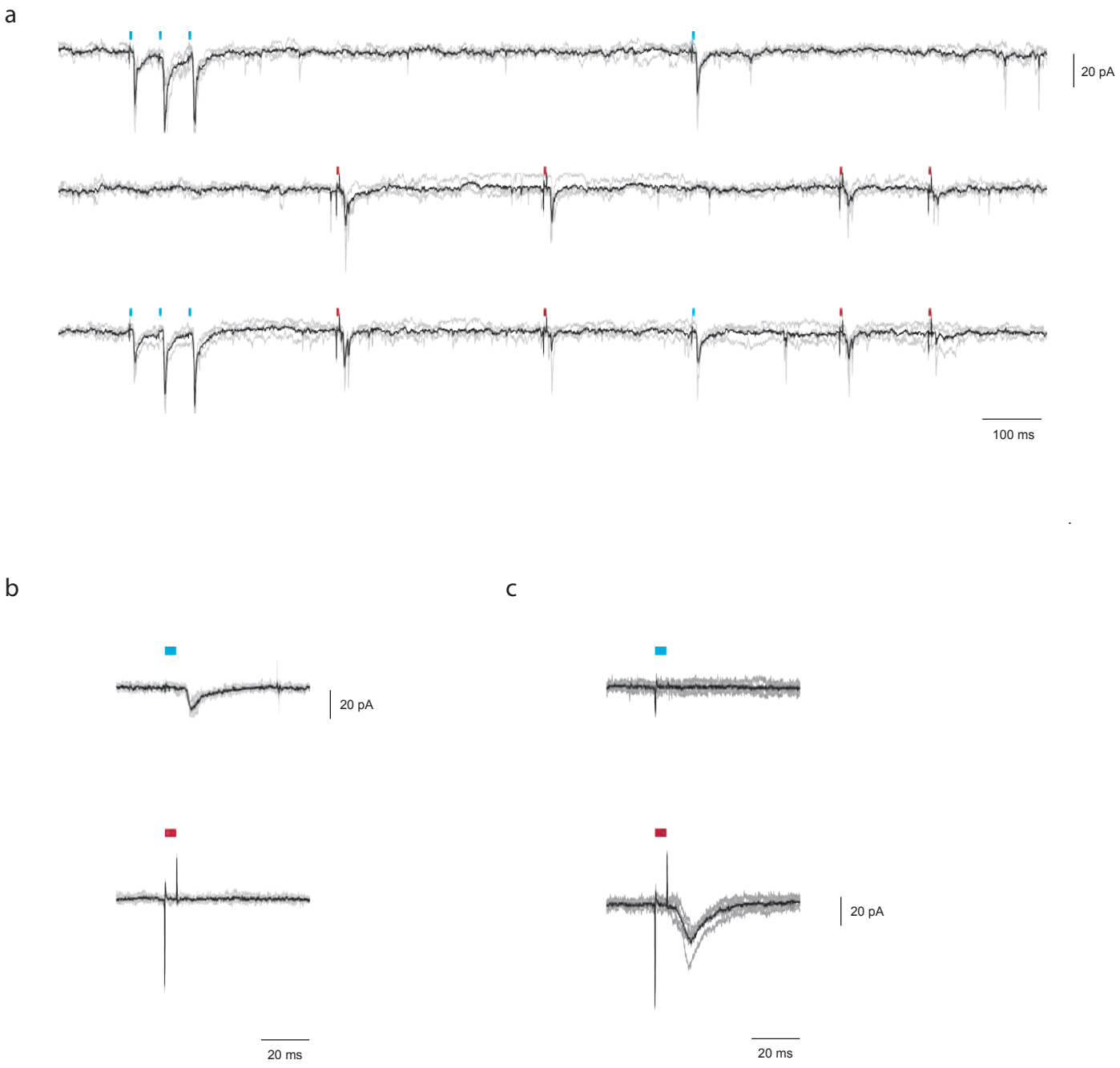

Nature Methods: doi:10.1038/nmeth.2836

Supplementary Table 1 – Naming convention

Gene #	NCBI #	Alias	Genus	species
		ChR1	Chlamydomonas	reinhardtii
		ChR2	Chlamydomonas	reinhardtii
		VChR1	Volvox	carteri
		MvChR1	Mesostigma	viride
60	KF992067		Mesostigma	viride
62	KF992054	NsChR	Neochlorosarcina	sp.
63	KF992043		Monomastix	opisthostigma
64	KF992072	SdChR	Scherffelia	dubia
65	KF992034	BsChR2	Brachiomonas	submarina
66	KF992089	TsChR	Tetraselmis	striata
67	KF992071		Tetraselmis	chui
68	KF992081		Tetraselmis	chui
69	KF992087		Tetraselmis	chui
70	KF992084		Spermatozopsis	exsultans
71	KF992066		Pedinomonas	minor
72	KF992045		Cyanophora	paradoxa
73	KF992053		Stephanosphaera	pluvialis
74	KF992059	HdChR	Haematococcus	droebakensis
75	KF992058		Tetraselmis	striata
76	KF992070		Tetraselmis	chui
77	KF992057	TcChR	Tetraselmis	cordiformis
78	KF992042		Pavlova	lutheri
79	KF992077		Scherffelia	dubia
80	KF992086	BsChR1	Brachiomonas	submarina
84	KF992047		Rhodomonas	sp.
85	KF992030		Chloromonas	reticulata-A
86	KF992041	CoChR	Chloromonas	oogama
87	KF992078	CsChR	Chloromonas	subdivisa
88	KF992060	CnChR1/Chrimson	Chlamydomonas	noctigama
89	KF992073	CnChR2	Chlamydomonas	noctigama
90	KF992040	ShChR/Chronos	Stigeoclonium	helveticum
91	KF992032		Microthamnion	kuetzigianum-A
92	KF992049		Chlamydomonas	bilatus-A
93	KF992052		Heterochlamydomonas	inaequalis
95	KF992076		Chloromonas	reticulata-A
96	KF992036		Chlamydomonas	noctigama
97	KF992074	PsChR1	Proteomonas	sulcata
98	KF992083		Cryptomonas	curvata

99	KF992085		Chroomonas	sp.
100	KF992088		Chroomonas	sp.
101	KF992051		Chroomonas	sp.
102	KF992090		Chroomonas	sp.
103	KF992033		Proteomonas	sulcata
104	KF992065		Chroomonas	sp.
105	KF992064		Gloeochaete	wittrockiana
106	KF992061		Hemiselmis	virescens
107	KF992055		Proteomonas	sulcata
108	KF992056	PsChR2	Proteomonas	sulcata
109	KF992063		Proteomonas	sulcata
110	KF992037		Rhodomonas	sp.
111	KF992044		Chlamydomonas	bilatus-A
112	KF992038	AgChR	Asteromonas	gracilis-B
113	KF992046		Pyramimonas	parkeae
114	KF992035		Monomastix	opisthostigma
115	KF992079		Tetraselmis	striata
116	KF992075		Lobomonas	rostrata
117	KF992031		Lobomonas	rostrata
118	KF992050		Stichococcus	bacillaris
119	KF992080		Hafniomonas	reticulata
120	KF992062	CbChR1	Chlamydomonas	bilatus-A
121	KF992039		Hafniomonas	reticulata
122	KF992069		Carteria	crucifera
123	KF992048		Carteria	crucifera
124	KF992068		Volvox	aureus
125	KF992082		Phacotus	lenticularis

Supplementary Table 2 – Statistical Analysis for Figure 1

Figure 1b – 660 nm current

C1V1$_{TT}$ used as control group for Dunnett's post hoc test

Molecule	Abs(Dif)-LSD	p-Value	# of cells	mean	s.e.m.
AgChR	-221	1	3	0	0
BsChR2	-169	1	6	0	0
C1V1$_{TT}$	-166	1	10	22.646	4.12
CbChR1	-169	1	6	0	0
ChR1	-180	1	5	0	0
ChR2	-139	1	11	0	0
Chrimson	489.4	<.0001	11	673.841	119.57
Chronos	-149	1	9	1.08	0.61
CnChR2	-180	1	5	0	0
CoChR	-143	1	10	0	0
CsChR	-184	1	5	3.836	1.46
HdChR	-180	1	5	0	0
MvChR1	-264	1	2	0	0
NsChR	-180	1	5	0	0
PsChR1	-171	1	6	1.985	1.2
PsChR2	-182	1	5	2.192	1.44
SdChR	-160	1	7	0	0
TcChR	-180	1	5	0	0
TsChR	-196	1	4	0	0
VChR1	-207	1	4	35.13	11.75

Figure 1c – 530 nm current

C1V1$_{TT}$ used as control group for Dunnett's post hoc test

Molecule	Abs(Dif)-LSD	p-Value	# of cells	mean	s.e.m.
AgChR	-138	0.3059	3	0.32	0.16
BsChR2	-154	0.4857	5	108.41	18.68
C1V1$_{TT}$	-371	1	10	408.07	72.59
CbChR1	-82.1	0.1787	4	0	0
ChR1	-188	0.4964	3	50.47	29.79
ChR2	7.531	0.0419	11	38.5	9.73
Chrimson	-347	1	10	431.7	96.15
Chronos	204.1	0.0002	8	1005.24	253.54
CnChR2	-213	0.7878	5	167.35	51.07
CoChR	417.3	<.0001	10	1195.9	107.95
CsChR	210.4	0.0005	5	1072.3	213.64
HdChR	-152	0.356	3	14.88	3.85

MvChR1	-234	0.5428	2	0	0
NsChR	-141	0.316	3	3.38	1.69
PsChR1	-116	0.3403	6	96.16	29.81
PsChR2	-165	0.5412	5	119.2	42.73
SdChR	-188	0.7707	7	188.22	40.1
TcChR	-51.8	0.1227	5	6.07	2.83
TsChR	-49.2	0.1174	5	3.38	1.46
VChR1	-205	0.7498	5	159.38	58.38

Figure 1d – 470 nm current

ChR2 used as control group for Dunnett's post hoc test

Molecule	Abs(Dif)-LSD	p-Value	# of cells	mean	s.e.m.
AgChR	-281	0.5733	3	4.76	3.62
BsChR2	-330	0.9825	8	683.24	77.56
$C1V1_{TT}$	-296	0.9554	9	259.56	51.76
CbChR	-196	0.3878	4	0	0
ChR1	-211	0.4931	5	66.92	22.74
ChR2	-478	1	12	478.96	115.55
Chrimson	-304	0.9773	10	281.87	61.26
CnChR2	-274	0.734	5	828	145.97
CoChR	2274	<.0001	10	3253.58	227.96
CsChR	-254	0.6609	5	847.42	186.25
HdChR	-287	0.78	5	142.9	30.65
MvChR1	-414	0.7877	2	0	0
NsChR	-172	0.3578	5	28.22	4.67
PsChR1	-151	0.322	6	44.74	17.51
PsChR2	-236	0.5912	5	92.53	32.98
SdChR	316.4	0.0001	7	1351.67	184.47
Chronos	222.8	0.0006	9	1217.6	266.72
TcChR	-386	0.9837	5	242.45	70.72
TsChR	-306	0.8417	9	162.12	66.48
VChR1	-516	0.9577	2	101.41	95.66

Figure 1h – channel turn off kinetics

ChR2 used as control group for Dunnett's post hoc test

Molecule	Abs(Dif)-LSD	p-Value	# of cells	mean	s.e.m.	λ (nm)
BsChR2	-351	0.9996	6	126.4	21.47	470
$C1V1_{TT}$	-374	1	10	37	2.89	530
ChR1	-526	1	4	5.61	1.08	470
ChR2	-378	1	12	14.59	1.39	470
Chrimson	-379	1	11	22.4	1.43	625

Chronos	-429	1	7	3.59	0.21	470
CnChR2	1101	<.0001	5	1608.54	634.85	470
CoChR	-369	1	7	86.03	11.63	470
CsChR	-487	1	5	8.45	0.71	530
HdChR	-485	1	5	21.98	2.03	470
PsChR1	-500	1	4	48.86	4.97	530
PsChR2	-516	1	4	33.22	1.51	530
SdChR	-430	1	7	24.99	1.81	470
TcChR	-485	1	5	6.96	0.76	470
TsChR	-587	1	3	3.83	0.38	470
VChR1	-452	1	4	97.43	15.03	530

Figure 1i – time to 90% of peak

ChR2 used as control group for Dunnett's post hoc test

Molecule	Abs(Dif)-LSD	p-Value	# of cells	mean	s.e.m.	λ (nm)
BsChR2	-0.08	0.0756	4	7.075	0.42696	470
$C1V1_{TT}$	-0.11	0.1051	9	6.76667	0.17341	530
ChR2	-0.93	1	10	5.92	0.25768	470
Chrimson	0.188	0.0143	6	7.18333	0.39951	625
Chronos	2.644	<.0001	8	2.2875	0.28185	470
CoChR	0.351	0.0038	7	4.54286	0.31912	470
CsChR	0.559	0.0011	5	4.22	0.33675	530
SdChR	2.065	<.0001	7	2.82857	0.18988	470

Supplementary Table 3 – Primer sequences

Primers for generating cDNA library

Name	Sequence	Comment
RNA adapter 2	AAUCAUACGACGACCACCGAGAUCAGG	5' mRNA ligation adaptor
DNA adapter 1	AAGCAGTGGTATCAACGCAGACTAC$(T)_{30}$VN	Reverse transcription

Primers for algae PCR

Name	Sequence
DNA adapter 2	AATCATACGACGACCACCGAGATCAGG
55 GSP5	GAAACACCTCAATCATCACCTTGACC
55 GSP6	CAGCCTGTCCCGCATCACCAGGAACG
55 GSP8	CGGGCTTACAAGACCAGTACAGCAAG
2565 GSP12	ATCTTGACCTGGAGGTAATGGGCG
232 GSP6	GTGATAATCTTGATTAAGCCGTGGCG
51 GSP2	CGTTCAGCCCCGTTATATTCGATAG
1293 GSP2	AAAAGCAGCCGATGTAGAAGAGGAGC
CCAC19 GSP1	TACGCTACCTCCTTTGTGGTGGAG
CCAC19 GSP2	GTAGTCCACACCACTATCGTCAGCAG

Primer pairs for algae PCR

Gene #	Algae source	Template	Primer 1	Primer 2
74	UTEX 55	cDNA	DNA adapter 2	55 GSP5
		cDNA	55 GSP8	55 GSP6
75	UTEX 2565	cDNA	DNA adapter 2	2565 GSP12
76	UTEX 232	cDNA	DNA adapter 2	232 GSP6
77	CCAC 51	cDNA	DNA adapter 2	51 GSP2
78	UTEX 1293	cDNA	DNA adapter 2	1293 GSP2
79	CCAC 19	genomic DNA	CCAC19 GSP1	CCAC19 GSP2

UTEX: http://web.biosci.utexas.edu/utex/
CCAC: http://www.ccac.uni-koeln.de

Primers for cloning

Name	Sequence
Cloning P12	GGAGGTGGAAGTGGAAGAGTTCGTGGAGG
Cloning P13	actaggtacctaggcttaCTTATACAGCTCATCCATGCCGTACAG
Cre P1	caaaGAATTCtgagccgccaccATGcccaagaagaagaggaaggtgtccAATTTACTGACCG TACACCAAAATTTGCC
Cre P2	ggacccgccaccactcccgccaccagaATCGCCATCTTCCAGCAGGC
Cre P3	GGCTTCTGGCGTGTGACC
GB1 (dsDNA)	CTGTCTCATCATTTTGGCAAAGAATTCCCATAACTTCGTATAAAGTATCCTAT ACGAAGTTATATCAAAATAGGAAGACCAATGCTTCACCATCGACCCGAATTG CCAAGCATCACCATCGACCCATAACTTCGTATAATGTATGCTATACGAAGTT ATACTAGCTAGCGCCGCCACCATGGAAACAGC
GB2 (dsDNA)	GAGCTGTACAAGTAATGAGCGGCCTAGGTACCTAGTATAACTTCGTATAGG ATACTTTATACGAAGTTATCATTGGGATTCTTCCTATTTTGATCCAAGCATCA CCATCGACCCTCTAGTCCAGATCTCACCATCGACCCATAACTTCGTATAGCA TACATTATACGAAGTTATGTCCCTCGAAGAGGTTCGCGGCCGCACTCCTCA GGTGCAG
Gene88 K176R Fwd	cccgtgatcctgatcagactgagcaacctgagcg
Gene88 K176R Rev	cgctcaggttgctcagtctgatcaggatcacggg
Gene88 P2	ctactaccggtgccgcCACTGTGTCCTCGTCCTCCTCC
Gene88 P27	actagctagcgccgccaccATGGCTGAGCTGATCAGCAGCG
Gene90 P9	gccgccaccATGGAAACAGCCGCCACAATGAC
Gene90 P10	actaggtacctaggccgcgccgccaccATGGAAACAGCCGCCACAATG
GFP P18	ggccgctcattaCTTGTACAGCTCGTCCATGCCGAG
GFP P20	actagctagcTCATTACTTGTACAGCTCGTCCATGC
OE P1	CTGTCTCATCATTTTGGCAAAGAATTCCC
OE P2	CTGCACCTGAGGAGTGCGGCCGCG
OE P13	CAGTGgcggcaccggtagtagcaGTGAGCAAGGGCGAGGAGA
OE P14	actaggtacctaggccgctcattaCTTGTACAGCTCGTCCATGCCG
OE P15	ACTAGCTAGCGCCGCCACCATGG
OE P16	ACTAGGTACCTAGGCCGCTCATTAC
tdTomato P1	ctgcaccggtagtagcaGTGAGTAAGGGCGAGGAAGTGATCAAAG
tdTomato P2	gagtgcggccgctttaCTTATACAGCTCATCCATGCCGTACAGAAAC

Supplementary Table 4 – Solutions used to characterize ion selectivity

Solution	[Na] (mM)	[K] (mM)	[Ca] (mM)	[H] (mM)	pH	Other (mM)
Intracellular	0	140	0	5.10E-05	7.40	5 EGTA, 2 $MgCl_2$, 10 HEPES
145 mM NaCl	145	5	1	5.10E-05	7.40	10 HEPES, 5 glucose, 2 $MgCl_2$
145 mM KCl	0	145	1	5.10E-05	7.40	10 HEPES, 5 glucose, 2 $MgCl_2$
90 mM $CaCl_2$	0	5	91	5.10E-05	7.40	10 HEPES, 5 glucose, 2 $MgCl_2$
5 mM NaCl	5	5	1	5.10E-04	6.40	135 NMDG, 10 HEPES, 5 glucose, 2 $MgCl_2$

Supplementary Video 1 – Experimental setup with a visual arena.

The fly was tethered and centered in the visual arena[50]. In this movie, a flowing random dot pattern is shown. The visual arena was removed from the setup in other conditions. Fly behavior was recorded using a camera with 850 nm IR illuminator.

Supplementary Video 2 – PER of a Gr64f X CsChrimson fly to 720 nm light in darkness.

A fly with CsChrimson expression in sugar receptors shows PER to deep red light stimulation.

Supplementary Video 3 – Startle response to 720 nm light in darkness

A control fly without CsChrimson expression shows clear startle response to deep red light.

Supplementary Video 4 – PER of a Gr64f X CsChrimson fly to 720 nm light in a blue random dot arena.

PER of a fly with CsChrimson expression in sugar receptors is not affected by visual distractors.

Nature Methods: doi:10.1038/nmeth.2836

Supplementary Video 5 – Inhibited startle response to 720 nm light in a blue random dot arena.

The startle response of a control fly without CsChrimson expression is effectively inhibited.

Supplementary Video 6 – Optogenetics in freely behaving intact flies.

Top: Light-induced CO_2 avoidance behavior (VT031497-Gal4 x UAS-CsChrimson in attP18). Bottom: A control group (WTB x UAS-CsChrimson in attP18). Circles show raw video images with false color red background indicating the illuminated quadrants. The effect of light is quantified (see Methods) and plotted as a single blue line corresponding to the presented examples and a plot representing the mean of all 9 sessions (±SEM error bars). Plots will be in red region if more than 50% of flies are in illuminated quadrants. Replay speed: 4x.

Nat. Methods **11**, 338–346 (2014)

Independent optical excitation of distinct neural populations

Nathan C Klapoetke, Yasunobu Murata, Sung Soo Kim, Stefan R Pulver, Amanda Birdsey-Benson, Yong Ku Cho, Tania K Morimoto, Amy S Chuong, Eric J Carpenter, Zhijian Tian, Jun Wang, Yinlong Xie, Zhixiang Yan, Yong Zhang, Brian Y Chow, Barbara Surek, Michael Melkonian, Vivek Jayaraman, Martha Constantine-Paton, Gane Ka-Shu Wong & Edward S Boyden

In the version of this supplementary file originally posted online, CsChrimson was incorrectly labeled as Chrimson. The error has been corrected in this file as of 28 August 2014.